ARISTOTLE UNIVERSITY OF THESSALONIKI
SCHOOL OF GEOLOGY
DEPARTMENT OF GEOPHYSICS

ANTERRIOTIS-KALPAKIDIS NIKOLAOS
Geologist

COMPARING PROBABILISTIC SEISMIC HAZARD MAPS WITH SHAKEMAP FOOTPRINTS AND STRONG MOTION RECORDS IN GREECE

MASTER THESIS

POSTGRADUATE STUDIES PROGRAMME: 'APPLIED AND ENVIRONMENTAL GEOLOGY'
DIRECTION: 'APPLIED GEOPHYSICS AND SEISMOLOGY'

THESSALONIKI
2024

ANTERRIOTIS-KALPAKIDIS NIKOLAOS
ΑΝΤΕΡΡΙΩΤΗΣ-ΚΑΛΠΑΚΙΔΗΣ ΝΙΚΟΛΑΟΣ
Πτυχιούχος Γεωλόγος

COMPARING PROBABILISTIC SEISMIC HAZARD MAPS WITH SHAKEMAP FOOTPRINTS AND STRONG MOTION RECORDS IN GREECE

ΣΥΓΚΡΙΣΗ ΠΙΘΑΝΟΛΟΓΙΚΩΝ ΧΑΡΤΩΝ ΣΕΙΣΜΙΚΗΣ ΕΠΙΚΙΝΔΥΝΟΤΗΤΑΣ, ΧΑΡΤΩΝ SHAKEMAP ΚΑΙ ΚΑΤΑΓΡΑΦΩΝ ΙΣΧΥΡΗΣ ΣΕΙΣΜΙΚΗΣ ΚΙΝΗΣΗΣ ΣΤΗΝ ΕΛΛΑΔΑ

Υποβλήθηκε στο Τμήμα Γεωλογίας στα πλαίσια του Προγράμματος Μεταπτυχιακών Σπουδών 'Εφαρμοσμένη και Περιβαλλοντική Γεωλογία', Κατεύθυνση 'Εφαρμοσμένη Γεωφυσική και Σεισμολογία'

Ημερομηνία Προφορικής Εξέτασης: 13/09/2024
Oral Examination Date: 13/09/2024

Three-member Examining Board

Professor Anastasia Kiratzi, Supervisor
Associate Professor Zafeiria Roumelioti, Member
Dr Odysseas Galanis, Member

Τριμελής Εξεταστική Επιτροπή

Καθηγήτρια Αναστασία Κυρατζή, Επιβλέπουσα
Αναπληρώτρια καθηγήτρια Ζαφειρία Ρουμελιώτη, Μέλος
ΕΔΙΠ Οδυσσέας Γαλάνης, Μέλος

Citation:

Anterriotis-Kalpakidis N., 2024. - Comparing probabilistic seismic hazard maps with ShakeMap footprints and strong motion records in Greece. Master Thesis, School of Geology, Aristotle University of Thessaloniki, 97 pp.
Αντερριώτης-Καλπακίδης Ν., 2024. - Συγκριση πιθανολογικων χαρτων σεισμικης επικινδυνοτητας, χαρτων ShakeMap και καταγραφων ισχυρης σεισμικης κινησης στην Ελλαδα. Μεταπτυχιακή Διπλωματική Εργασία, Τμήμα Γεωλογίας Α.Π.Θ., 97 σελ.

Acknowledgments

I would like to express my heartfelt gratitude to all those who supported me throughout my journey in completing this thesis. First and foremost, I would like to thank my supervisor, professor Anastasia Kiratzi, for their invaluable guidance, support, and encouragement.

I would also like to extend my thanks to my committee members, associate professor Zafeiria Roumelioti and Dr Odysseas Galanis, for their constructive feedback and help.

Finally, I would like to acknowledge the academic and laboratory teaching staff of the Department of Geophysics for the knowledge that helped me to acquire during the postgraduate studies program.

Abstract

Probabilistic Seismic Hazard Assessment (PSHA) maps provide estimates of the likelihood and intensity of ground shaking, usually expressed in terms of Peak Ground Acceleration (PGA) or Spectral Acceleration (Sa) at different periods, due to potential earthquakes, over a specific time. These maps are a vital tool for assessing earthquake engineering requirements.

This study evaluates the performance of four PSHA maps for Greece —ESHM20, ESHM13, GSHAP, and the national seismic hazard map of Greece (EAK2000)— all designed for a 10% probability of exceedance in 50 years. These maps are compared against observational data from ShakeMap footprints, strong-motion records, and historical macroseismic intensities to assess their reliability. We analyzed intensity measures (*IMs*) such as Peak Ground Acceleration (PGA) and spectral accelerations at 0.3s, 1.0s, and 3.0s, derived from ShakeMaps spanning January 1973 to January 2023. Sites where observed *IMs* exceeded those predicted by the PSHA maps were identified, and fractional exceedance areas were calculated to compare these exceedances with the 10% probability target. EAK2000 showed the closest fit to this target, with all maps displaying reasonable alignment overall.

In addition to general site comparisons, specific regions of interest, including urban areas in Greece, were analyzed and compared with results from Ground Motion Prediction Equations (GMPEs). Strong-motion data was further examined to determine how many seismic stations were expected to exceed the predicted thresholds and compared these results to observed station exceedances. Additionally, historical macroseismic data was used to estimate PGA through ground-motion intensity conversion equations (GMICEs), allowing for the identification of regions with higher-than-expected seismic activity.

Our findings highlight areas where the expected levels of ground motion were considerably exceeded during earthquakes and also provide insights into the strengths and weaknesses of PSHA models in Greece. These results contribute to the ongoing development of more accurate seismic hazard assessments and risk mitigation strategies specific to the region.

This thesis is structured in five chapters: In the first chapter, an introduction is provided to probabilistic seismic hazard maps, as well as a review of the four maps studied alongside, a review of the methodologies and results from similar studies.

In the second chapter, the data for each of the three methods is described. The completeness of the data is discussed, along with the uncertainties present in the ShakeMap charts, as well as in the calculation of macroseismic intensities from historical earthquakes.

In the third chapter, the methodology followed to retrieve the maximum ground acceleration values for the corresponding observation periods is described, as well as how the influence of local ground conditions was addressed and the calculation of the expected exceedance rates for the seismic hazard maps.

In the fourth chapter, the results for each method are presented, and limitations and uncertainties that may exist in the results are discussed, mainly due to the limited availability of data.

Finally, in the fifth chapter, the conclusions of the study are summarized.

Περίληψη

Οι Πιθανολογικοί Χάρτες Σεισμικής Επικινδυνότητας (PSHA) παρέχουν εκτιμήσεις σχετικά με την πιθανότητα και την ένταση της σεισμικής κίνησης, συνήθως εκφρασμένες σε όρους Μέγιστης Εδαφικής Επιτάχυνσης (PGA) ή Φασματικής Επιτάχυνσης (Sa) σε διαφορετικές περιόδους, λόγω πιθανών σεισμικών γεγονότων, για ένα συγκεκριμένο χρονικό διάστημα. Αυτοί οι χάρτες είναι ζωτικής σημασίας για την αξιολόγηση των απαιτήσεων της αντισεισμικής μηχανικής.

Η παρούσα μελέτη αξιολογεί την απόδοση τεσσάρων PSHA χαρτών για την Ελλάδα —ESHM20, ESHM13, GSHAP και τον εθνικό χάρτη σεισμικής επικινδυνότητας της Ελλάδας (ΕΑΚ2000)— οι οποίοι έχουν σχεδιαστεί για πιθανότητα υπέρβασης 10% σε 50 χρόνια. Τα προβλεπόμενα επίπεδα της σεισμικής κίνησης από αυτούς τους χάρτες PSHA συγκρίνονται με πραγματικές παρατηρήσεις από χάρτες ShakeMap, καταγραφές ισχυρής εδαφικής κίνησης και ιστορικές μακροσεισμικές εντάσεις για την αξιολόγηση της αξιοπιστίας τους.

Αναλύσαμε μέτρα έντασης (*IMs*), όπως η Μέγιστη Εδαφική Επιτάχυνση (PGA) και φασματικές επιταχύνσεις στα 0.3s, 1.0s και 3.0s, που προέρχονται από χάρτες ShakeMap για την περίοδο από τον Ιανουάριο 1973 έως τον Ιανουάριο 2023. Εντοπίστηκαν περιοχές όπου τα παρατηρούμενα *IMs* υπερέβαιναν τις προβλεπόμενες τιμές από τους χάρτες PSHA, και υπολογίστηκαν οι περιοχές υπέρβασης, ώστε αυτές οι υπερβάσεις να συκριθούν με τον στόχο του 10%. Ο χάρτης ΕΑΚ2000 εμφάνισε την πιο ακριβή προσέγγιση στον στόχο, ενώ όλοι οι χάρτες έδειξαν γενικά καλή προσαρμογή.

Επιπλέον, εφαρμόσαμε την ίδια διαδικασία για συγκεκριμένες περιοχές ενδιαφέροντος, συμπεριλαμβανομένων αστικών περιοχών στην Ελλάδα, και τα αποτελέσματα συγκρίθηκαν με αυτά που προέκυψαν από Εξισώσεις Πρόβλεψης Εδαφικής Κίνησης (GMPEs). Τα δεδομένα ισχυρής εδαφικής κίνησης εξετάστηκαν περαιτέρω για να προσδιοριστεί πόσοι σεισμολογικοί σταθμοί αναμένεται να υπερβούν τα προβλεπόμενα όρια και συγκρίθηκαν αυτά τα αποτελέσματα με τις παρατηρήσεις των σταθμών. Επιπλέον, χρησιμοποιήθηκαν ιστορικά μακροσεισμικά δεδομένα για την εκτίμηση της PGA μέσω εξισώσεων μετατροπής της έντασης (GMICEs), επιτρέποντας τον εντοπισμό περιοχών με υψηλότερη σεισμική δραστηριότητα από την αναμενόμενη.

Τα ευρήματά μας, καταρχάς αναδεικνύουν περιοχές για τις οποίες έχει παρατηρηθεί υπέρβαση των προβλέψεων των χαρτών και επιπρόσθετα αναδεικνύουν τις αβεβαιότητες που υπεισέρχονται στην εκτίμηση της σεισμικής επικινδυνότητας στην Ελλάδα από τα μέχρι σήμερα επικρατέστερα μοντέλα.

Η διατριβή έχει πέντε κεφάλαια: Στο πρώτο κεφάλαιο γίνεται μία εισαγωγή στους πιθανολογικούς χάρτες σεισμικής επικινδυνότητας, καθώς και μία ανασκόπηση των τεσσάρων χαρτών που μελετιούνται στην εργασία. Τέλος, γίνεται μια ανασκόπηση των μεθοδολογιών και των αποτελεσμάτων από παρόμοιες εργασίες.

Στο δεύτερο κεφάλαιο περιγράφονται τα δεδομένα για κάθε μία από τις τρείς μεθόδους. Σχολιάζεται η πληρότητα τους, καθώς οι αβεβαιότητες που υπάρχουν στους χάρτες ShakeMap, όπως και στον υπολογισμό των μακροσεισμικών εντάσεων

από τους ιστορικούς σεισμούς.

Στο τρίτο κεφάλαιο περιγράφεται η μεθοδολογία που ακολουθήθηκε ώστε να ανακτηθούν οι μέγιστες τιμές της εδαφικής επιτάχυνσης για τις αντίστοιχες περιόδους παρατήρησης, ο τρόπος που αντιμετωπίστηκε η επίδραση των τοπικών εδαφικών συνθηκών, καθώς και ο υπολογισμός των αναμενόμενων ποσοστών υπερβάσεων για τους χάρτες σεισμικής επικινδυνότητας.

Στο τέταρτο κεφάλαιο παρουσιάζονται τα αποτελέσματα για κάθε μέθοδο και συζητιούνται περιορισμοί και αβεβαιότητες που μπορεί να υπάρχουν στα αποτελέσματα κυρίως λόγω των περιορισμένων διαθέσιμων δεδομένων.

Τέλος, στο πέμπτο κεφάλαιο συνοψίζονται τα συμπεράσματα της εργασίας.

Contents

1. Introduction

1.1 Probabilistic seismic hazard assessment overview

In earthquake engineering, the main pursuit is to ensure that a building will withstand a given level of ground shaking during a potential earthquake. The level of potential ground shaking at a specific site is determined by the convolution of the size (magnitude of the potential earthquake), the location (distance to the earthquake, attenuation) of the site, and the site conditions. Probabilistic seismic hazard assessment (PSHA) aims to determine, quantify, and combine these factors in order to produce a description of the distribution of future shaking at a site. Baker (2008) has described the five steps that compose a PSHA:

1. Identify all earthquake sources capable of producing damaging ground motions.
2. Characterize the distribution of earthquake magnitudes.
3. Characterize the distribution of source-to-site distances associated with potential earthquakes.
4. Predict the resulting distribution of ground motion intensity as a function of earthquake magnitude, distance, etc.
5. Combine uncertainties in earthquake size, location and ground motion intensity, using a calculation known as the total probability theorem.

The final result of this process will be a map illustration of the distribution of potential ground shaking during an earthquake that is predicted to be observed at each site. This probabilistic approach to seismic hazard determination makes PSHA maps important tools that are utilized to determine seismic hazard levels for earthquake engineering, and they are a useful method to describe earthquake engineering demands for codes and standards.

A PSHA map can be provided for various ground-motion intensity measures (*IM*), like peak ground acceleration (PGA), peak ground velocity (PGV), or peak spectral acceleration (PSA), in diverse periods, and it is usually calculated at rock sites. This predicted level of ground shaking, represented by an *IM*, has a probability, p, of being exceeded in a given time interval or, equivalently, exceedance return period, *RP*. This probability that the *IM* values at each site may be exceeded at least once in the time interval (Δt). As Cito et al. (2024) described, each site of a hazard map can be assumed as a Bernoulli random variable with probability p this *IM* value exceeds a certain threshold and *1-p* if does not. For each site the probability p of exceedance can be calculated by the equation

$$p = 1 - e^{-\Delta t/RP} \tag{1}$$

where *RP* is the PSHA map return period. This equation premises that earthquakes are Poisson distributed, so the number of exceedances in a given time period follows Poisson process as well. Then, by modelling exceedance as a Bernouli random variable, the expected number of sites experiencing exceedance can be calculated. If each site within a hazard map has an independent probability p of experiencing exceedance, then on average, the fraction of sites with exceedance will be also p.

This idea of “trading time for space” allows us to estimate the expected fraction of sites with exceedance in a given time period using this temporal exceedance probability p. In other words, the "trading time for space" idea helps to simplify the interpretation of seismic hazard maps by shifting focus from individual site-specific probabilities to a regional or spatial perspective. For example, if a hazard map is designed for a 475-year return period, the probability of exceedance in 50 years can be used to predict the fraction of sites with exceedance using equation 1. Thus, for a 475-year return period, the probability of exceedance in 50 years will be 10%. One can infer that, on average, about 10% of the area will experience ground motions exceeding the specified threshold during that period.

1.2 Testing PSHA maps - Applying methods

In this study, we tested PSHA maps for Greece to identify their strengths and weaknesses and then to conclude which one is the most reliable for a given area. This study compares four different PSHA maps for Greece: the 2013 Euro-Mediterranean Seismic Hazard Model (ESHM13), which was developed within the SHARE Project (Woessner et al., 2015), the 2020 update of the European Seismic Hazard Model (ESHM20; Danciu et al., 2021, the Global Seismic Hazard Assessment Program (GSHAP; Giardini et al., 1999), and the national seismic hazard map of Greece (EAK2000). We tested all these PSHA maps for an exposure time $T = 50yr$ and a return period of 475 years. The ESHM20 is provided for a probability of exceedance of $p = 0.2103\%$ in 1 yr, which corresponds to an *RP* of 475 yr. Thus, it is equivalent with the other three maps.

Several studies have compared PSHA models with observed data (macroseismic or instrumental) worldwide (Albarello & D’Amico, 2008; Tasan et al., 2014; Manea et al., 2024; Rey et al., 2018). Testing PSHA models is a very challenging process, especially due to the length of the observation period available compared to the PSHA map return period. Using ShakeMaps, PGA values estimated by a ground-motion prediction equation (GMPE) on past earthquakes and converting historical macroseismic intensity into PGA values using a ground-motion intensity conversion equation (GMICE) are suggested methods to extend the length of the observation period (Allen et al., 2009; Tasan et al., 2014; Rey et al., 2018).

This research compared these four PSHA maps by applying three methods. First, we compared the PSHA maps results using *IMs* estimated from ShakeMap footprints (Allen et al., 2009; Pothon et al., 2020; Allen et al., 2023; Cito et al., 2024). We compared the estimated-by-ShakeMap *IM* to expected-by-PSHA, and we calculated the corresponding fractional exceedance area (Allen et al., 2023; Cito et al., 2024), taking into account the uncertainty in ground shaking estimation from the ShakeMaps and the lack of data —and their potential effect on the final result— for the chosen observational period (Pothon et al., 2020; Cito et al., 2024). Furthermore, we compared ShakeMap-to-PSHA results with those coming from the comparison of *IMs*, estimated by ground-motion prediction equation (GMPE) on past earthquakes, to those estimated from PSHA models for specific cities and areas of interest. Additionally, in the other two methods we tested the PSHA maps using ground-motion observations and macroseismic intensity data from historical earthquakes (Albarello & D'Amico, 2008; Tasan et al., 2014; Rey et al., 2018; Manea et al., 2024).

1.2.1 Comparative studies overview

The ShakeMap method was applied by Allen et al. (2009) to compare GSHAP with the maximum PGA estimated by ShakeMaps for past earthquakes from 1973 to 2007. The Allen et al. (2009) method was to count the number of spatial points for which the maximum PGA exceeded GSHAP thresholds. They found that 7.3% of the grid was exceeded and 3.8% when considering only the points in which the GSHAP gave an expected PGA above $0.8\,\mathrm{m/s^2}$.

Similarly, Pothon et al. (2020) compared PSHA maps for Indonesia with the maximum PGA estimated by ShakeMap footprints for earthquakes with a magnitude of M4.5 or more, occurring between 1968 and 2018. The methodology was to count the sites (spatial points) for which the independent maximum PGA exceeded the expected values from PSHA maps after identifying the sites that may be affected by an earthquake not modeled by a ShakeMap. To obtain the independent PGA value on rock sites, they developed a selection process and a comparison method, considering the uncertainty of ShakeMap estimates. They applied their method to the whole of Indonesia and to the western part only. The results show that the best fit model did not change for these two tests; however, the results for western Indonesia were significantly different, and all testing PSHA models were more comparable to past seismicity.

Allen et al. (2023) calculated ShakeMaps using observed seismicity of the Australian continent from January 1972 to December 2021 and generated a "composite ShakeMap" extracting the maximum PGA for each site. After that, they estimated the fractional exceedance area for four seismic hazard maps of Australia. They found that all PSHA models forecast a higher seismic hazard relative to the ground motion that is estimated to have occurred. They also tested the sensitivity of those results by adding a rare scenario earthquake with a recurrence interval of 8700 years, as based on historical observations, large-magnitude earthquakes can occur in locations with low seismicity. However, the results did not show that any of the PSHA models exceeded the expected target.

In another study, Cito et al. (2024) calculated the fractional exceedance area for Italy for three PSHA maps and four different return periods by comparing them to PGA -Sa(0.3s) and Sa(1.0s)- estimated by a completed 12-year ShakeMap catalog as well as a synthetic ShakeMap catalog of historical earthquakes. They found that in the cases of return period of 50, 475, and 975 years, the exceedance area is comparable across *IMs* and PSHA modes. Instead, for return period 2475, the exceedance area is equal to or close to zero, as the 12-year period is too short for these thresholds. Also, their results show that the exceedance area is approximately the same for all PSHA models, despite their apparent differences.

Tasan et al. (2014) tested PSHA maps for France and Turkey using ground motion records. They compared the distribution of the expected number of sites with exceedance with the observed number. They applied a similar method with Stirling and Gerstenberger (2010) to calculate the distribution of the expected number of sites, according to stations life times, which are different from each other. For Franch, they also used a synthetic data set calculated with a ground-motion prediction equation to increase the observation time window. They calculated the life times for the Turkish stations from the recording history, due to the lack of lifetime data for these stations. They also identify potential gaps in the recording history. To handle site conditions, they estimated accelerations at rock using a site-amplification model. For low acceleration levels or short return periods, they found the models for France overestimate the number of sites with exceedance. Instead, in Turkey the observed numbers of sites with exceedance are well within the bounds of the predicted distribution. However, for both countries, for larger acceleration levels, the observations were few or the predicted distribution lower bound was equal to zero. Thus, the PSHA models could not be rejected, or no conclusion could be drawn.

Manea et al. (2024) tested the ESHM20 model against observations for Romanian cities. The observations included ground shaking recordings and macroseismic observations, extending the observational time window to few hundred years. The found the number of exceedance for two peak ground acceleration thresholds, 0.1g and 0.2g, and they compared it with the expected probability distribution from the PSHA model. They found that the PSHA model overestimated the observations in the most seismic region in Romania and underestimated those at the far-field. However, the PSHA model shows close agreement for the cities located near the Vrancea intermediate-depth source.

1.3 Seismic hazard and PSHA models in Greece

1.3.1 Seismotectonics and seismic hazard in Greece

Greece is one of the most seismically active regions in Europe, as it is located on the most active part of the Africa-Eurasia collision zone, and more than 60% of the European seismicity is expected to occur in this region. Greece is crossed by large and complex tectonic structures almost along its entire extent, which are responsible for large earthquakes, exposing a large part of the population to potential ground motion due to a large earthquake. In Figure 1-1, the active faults of the Greek territory (Ganas et al., 2013) are shown, as the population distribution as well. The population concentration around large faults is an important factor in the study of seismic hazard and risk, as more people and infrastructure are exposed to significant potential ground shaking. A first look at Figure 1-1 shows that most big urban areas are located near large faults. For example, the cities of Athens and Thessaloniki, which gather approximately 47% of the population of Greece, are both located in close proximity to large active faults, responsible for large earthquakes (e.g., the 6.0M earthquake on 7-9-1999 in Athens and the 6.4M earthquake on 20-6-1978 in Thessaloniki).

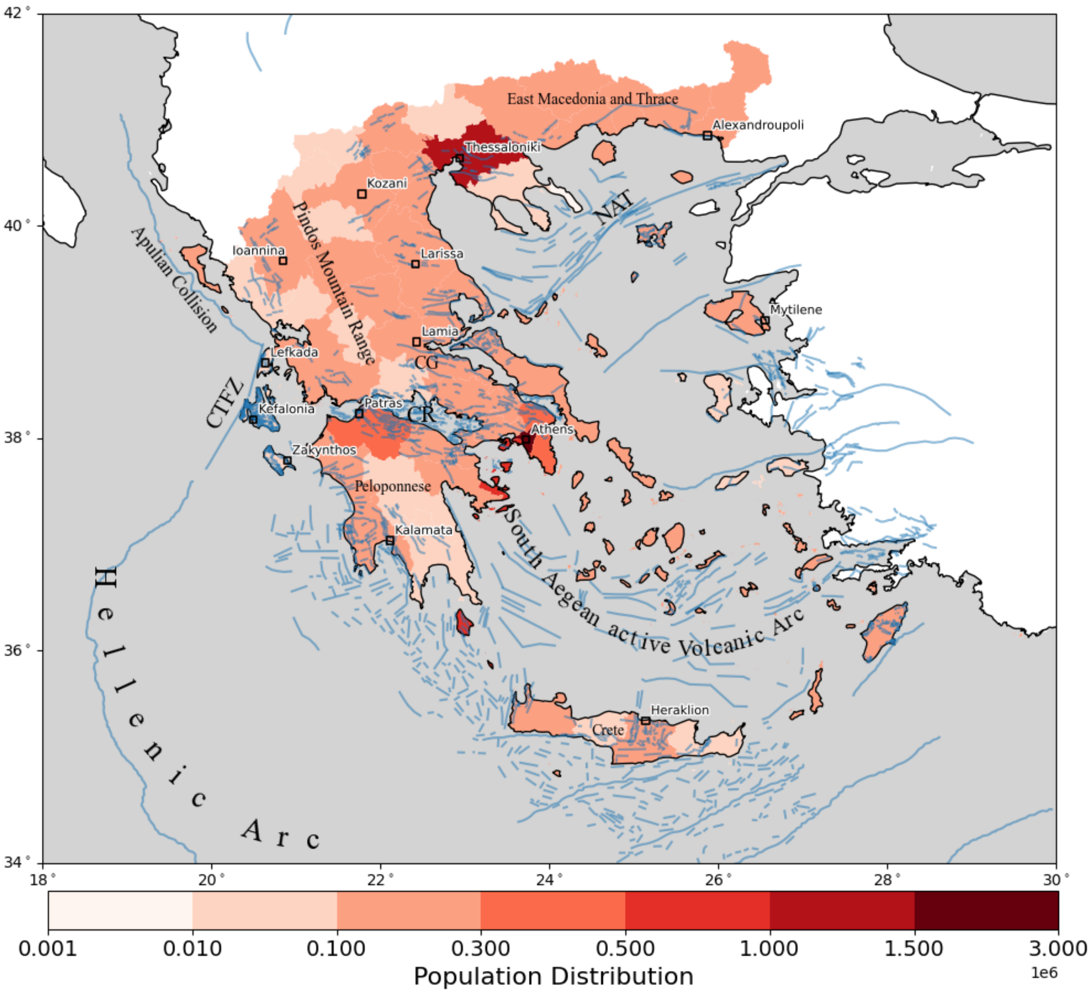

Figure 1-1. Summary map showing the main seismotectonic features and active faults of the Greek territory (Ganas et al., 2013). The color scale represents the distribution of population in Greece (source: Hellenic Statistical Authority). NAT: North Aegean trough, CR: Corinth rift, CTFZ: Kefalonia transform fault zone, CG: Central Greece.

Greece is mainly threatened by shallow crust earthquakes, however, subduction seismicity occurs across the Hellenic Arc (Fig. 1-1). Two areas that gather a significant percentage of the annual seismicity are Central Ionian and Gulf of Patras-Corinth (Fig. 1-1). The main tectonic structure in the Central Ionian Sea is the Kephalonia Transform Fault Zone (KTFZ), a dextral strike-slip fault with two main segments: the Lefkada Segment in the north and the Cephalonia Segment in the south (Benetatos et al., 2005). The Gulf of Patras-Corinth is an under-extension rift deforming by normal faults, with a significant strike-slip component in the western part (Gulf of Patras and western part of the Peloponnese), parallel in strike to KTFZ (Kiratzi & Louvari, 2003). The Hellenic Arc, together with KTFZ, gathers the highest seismicity rates (Kassaras et al., 2020). The inner part of the Hellenic Arc is deforming by normal faults, as is the back-arc Aegean area (Fig. 1-1). The area in the central and north Aegean Sea, extending from eastern coasts of Central Greece up to the coasts of Turkey, is deforming mainly by strike-slip faults showing the propagating tip of the North Anatolian Fault into the Aegean through North Aegean Trough (NAT) (Kiratzi & Louvari, 2003; Kassaras et al., 2020). The higher rates of crust deformation, which occurs in the area extending from Central-North Aegean Sea (NAT) to Central Greece, Gulf of Corith, Gulf of Patras, and Ionian Sea (KTFZ), are spatially well-correlated with large magnitude earthquakes (equal to M5.6 or higher), making the seismic hazard in these areas significantly high (Chousianitis et al., 2024).

1.3.2 Seismic hazard models in Greece

Several seismic hazard studies and PSHA models have been performed for Greece at a regional or local scale (Papazachos et al., 1990; Banitsiotou et al., 2004; Tsapanos et al., 2009; Tselentis & Danciu, 2010; Slejko et al., 2010; Stylianou et al., 2016; Vamvakaris et al., 2017; Vavlas et al., 2019; Slejko et al., 2021; Kaviris et al., 2022; Sotiriadis et al., 2023). Moreover, seismic hazard estimations for Greece are presented in the Global Seismic Hazard Assessment Program (GSHAP; Giardini et al., 1999) and the two European seismic hazard models, ESHM13 (Woessner et al., 2015) and ESHM20 (Danciu et al., 2021). In this study, we tested these three PSHA models (GSHAP, ESHM13, and ESHM20), as well as the latest national seismic hazard map (EAK2000).

Starting with the oldest, the Global Seismic Hazard Assessment Program (GSHAP; Giardini et al., 1999) was launched in 1992, and it depicts the seismic hazard as peak ground acceleration (PGA) with 10% probability of exceedence in 50 years, corresponding to a return period of 475 years. The GSHAP was based on the joining of all results for different GSHAP regions and test areas: the Americas (Shedlock & Tanner, 1999), Asia, Australia and Oceania (Zhang et al., 1999; McCue, 1999), Europe, Africa and the Middle East (Grünthal et al., 1999). The GSHAP results for Greece are provided in Figure 1-2d.

The EAK2000 is the latest national seismic hazard map of Greece, and it was published in 2000. It was revised in 2003 (Earthquake Planning and Protection Organization, 2003), without having been updated since then. EAK2000 is currently used for the seismic design of buildings and infrastructure in Greece. For this reason, this study focuses to the results for EAK2000 and its comparison with the other three PSHAs. The GSHAP, the ESHM13, and the ESHM20 present the ground shaking that is expected to be reached or exceeded over a return period for on-land sites equidistant per 10 kilometers. Instead, the EAK2000 divides Greece into three different seismic hazard zones (Fig. 1-2c) with a corresponding expected PGA (0.16g, 0.24g, and 0.36g, respectively) and a probability of exceedance for a return period of 475 years. For the following process, it is necessary to convert these three EAK2000 seismic hazard zones to on-land sites equally spaced every 10 kilometers, as the other three PSHA maps are. Because there is no available geospecial data online for EAK2000 (e.g., ShapeFile or geoJSON files), we created a 0.1 x 0.1 degree grid, which corresponds to 10 kilometers equidistant, and we received an expected PGA value with respect to EAK2000 seismic hazard zones.

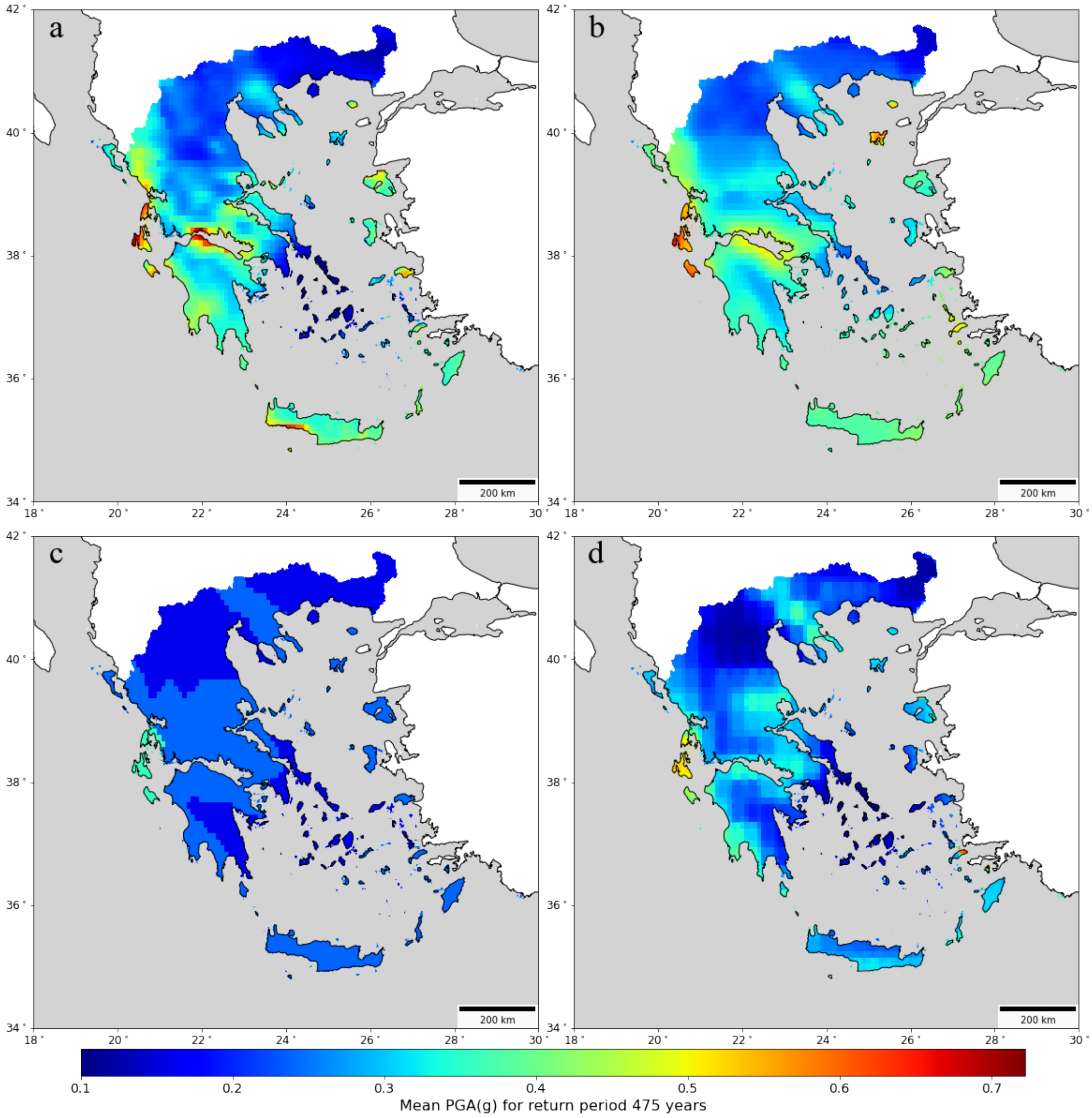

Figure 1-2. The four seismic hazard maps. The maps show the mean PGA for the return period of 475 years. (a) ESHM20, (b) ESHM13, (c) EAK2000, and (d) GSHAP.

Moving on to the most current seismic hazard models, the 2013 Euro-Mediterranean Seismic Hazard Model (ESHM13; Woessner et al., 2015) was developed within the Seismic Hazard Harmonization in Europe (SHARE) Project (Giardini et al., 2014) and provides a reference model of seismic hazard that contributed to the modulation of the current application of the European seismic regulations for building design, Eurocode 8 (CEN, 2004), which has been in effect since 2010. The ESHM13 provides the expected ground motion over return periods ranging from 70 to 5000 years, and it is produced for periods of ground acceleration from PGA to 4s. This period range covers all periods in which the built environment is vulnerable. Respectively, the 2020 European Seismic Hazard Model (ESHM20; Danciu et al., 2021) is an update of the ESHM13 and follows the same principles. It is produced in a greater range of periods than ESHM13, for periods of ground acceleration from PGA to 5s and return periods for 50 to 5000 years. Also, it is foreseen as an annex to the new generation of Eurocode 8. The ESHM20 utilizes updated seismogenic source parts (earthquake catalogues, active faults, sources), and it has revised the ESHM13 Ground Motion Prediction Equation (GMPE) logic tree with the newly ground motion data. The ESHM13 and ESHM20 results for Greece are provided in Figure 1-2a and Figure 1-2b, respectively. As mentioned, in contrast with EAK2000 and GSHAP, which are provided only for PGA, the ESHM20 and the ESHM13 are provided for a variety of periods. Thus, for these two PSHA maps, we performed the test not only for PGA but also for Sa(0.3s), Sa(1.0s), and Sa(3.0s). The results of the ESHM13 and the ESHM20 for Sa(0.3s), Sa(1.0s), and Sa(3.0s) for Greece are given in the appendix of this study (Fig. A-1).

1.3.3 Comparison of seismic hazard models of Greece

The maps in Figure 1-2 show the four seismic hazard models that will be utilized in this study. All of them show practically the same seismic hazard pattern, but with different expected PGA values. For all PSHA models, the higher seismic hazard is noticed in the region of the Ionian Islands, in western Greece. Instead, lower seismic hazard is noticed in northern Greece (regions of Macedonia and Thrace), Attica (Athens), and the Cyclades islands in the Aegean Sea. In the rest of Greece, a middle seismic hazard is noticed.

As it was mentioned before, EAK2000 is the current seismic hazard map, and in accordance it, all buildings and infrastructure in Greece are designed in terms of their resistance to the expected ground shaking. For this reason, we made a simple comparison between EAK2000 and the other three seismic hazard maps. Thus, we calculated the ratio of expected PGA values for EAK2000 versus the other PSHA maps. The comparison between EAK2000 and the other three seismic hazard models is illustrated in Figure 1-3. The three zones of EAK2000 correspond to the low hazard zone, with PGA equaling 0.16g (Zone I), the mibble hazard zone, with PGA equaling 0.24g (Zone II), and the high hazard zone, with PGA equaling 0.36g (Zone III). Generally, EAK2000 underestimates the hazard expected by the other three models. Starting with GSHAP, which is the oldest seismic hazard model, it seems that it overestimates the hazard of the greater part of EAK2000 Zone II and Zone III overall (middle and high seismic hazard zones) but not Zone I (low seismic hazard zone). Zone I displays higher expected PGA values (Cyclades Islands, Aegean Sea). However, GSHAP is the most comparable model to EAK2000. ESHM13, on the other hand, overestimates EAK2000 overall. The region of Thrace (Northern Greece) is an exception, as EAK2000 presents greater expected PGA values than ESHM13 there. Finally, the most recent model, the updated Euro-Mediterranean seismic hazard model, ESHM20, generally overestimates EAK2000, but as it was observed on the GSHAP map, there are areas that belong to EAK2000 Zone I where EAK2000 predicts higher seismic hazard, but these areas are not as many as those on the GSHAP map. In conclusion, excluding ESHM13, which forecasts greater PGA values than EAK2000 for the whole of Greece, EAK2000 has the tendency to overestimate its lower seismic hazard zones compared with the other two maps (GSHAP and ESHM20) and vice versa to underestimate its higher seismic hazard zones. As it was expected, the two most recent models (the ESHM13 and ESHM20) are less comparable to the EAK2000, as they include more recent input data.

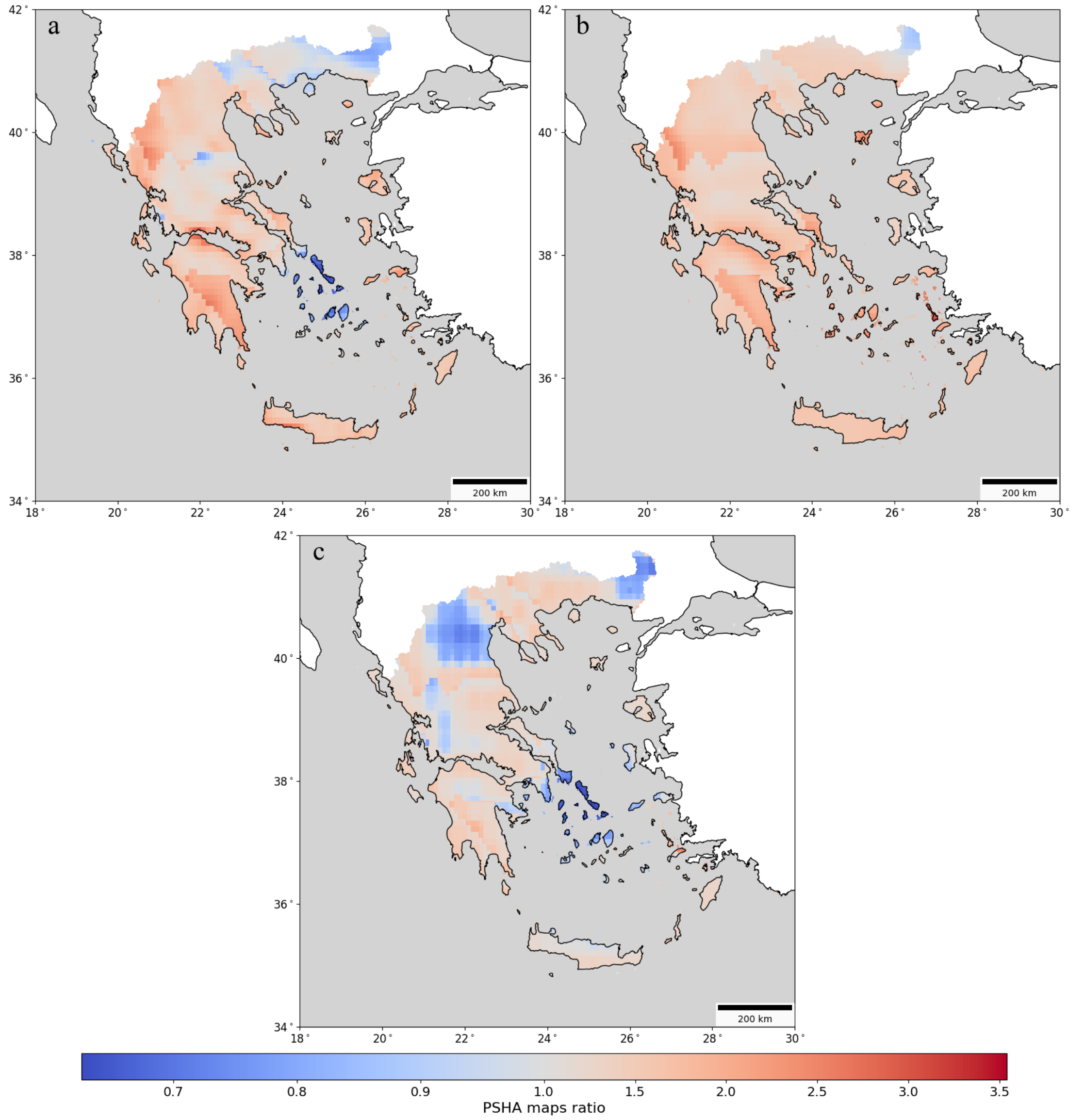

Figure 1-3. The ratio of (a) ESHM20, (b) ESHM13, and (c) GSHAP to EAK2000. Values over 1.0 show the sites at which the other three PSHA maps overestimate the hazard predicted by EAK2000.

Furthermore, a simple comparison was made between the ESHM13 and ESHM20. The PGA, Sa(0.3s), Sa(1.0s), and Sa(3.0s) values provided by the ESHM20 model are divided by the corresponding values from the ESHM13. The results of the differences between these two models are given in the appendix of this study (Fig. A-2). Generally, the ESHM13 and ESHM20 maps have a similar spatial pattern, with the ESHM20 map being overall lower in most of the areas. Nonetheless, increased PGA values are also present in some areas, such as the central Ionian Sea, the Patras and Corinth gulf, the Peloponnese, and the central Aegean Sea. The pattern of the differences is similar for Sa(0.3s), however, the areas at which the ESHM20 forecasts higher seismic hazard are more. Moving on to the longer periods (Sa(1.0s) and Sa(3.0s)), ESHM20 is overall lower in most areas. These differences are likely caused by the updated seismogenic sources, as these changes cause many of the local differences across the entire region (Danciu et al., 2021).

2. Data Set

2.1 ShakeMap data

2.1.1 A ShakeMap overview

A ShakeMap is produced after a real earthquake or based on a fictive scenario and provides a way to represent the distribution of ground shaking intensity across a geographic area affected by seismic activity. ShakeMap uses GMPEs to provide the initial estimates of ground motions. In addition to these individual GMPEs, ShakeMap allows for a weighted combination of two or more GMPEs (Worden et al., 2020). As Graizer and Kalkan (2016) have described, a GMPE can be analyzed into different components. A GMPE that calculates *IM* can be split as follows

$$\ln(IM) = \ln(G_1) + \ln(G_2) + \ln(G_3) + \ln(G_4) + \ln(G_5) + \sigma_{\ln(IM)} \tag{2}$$

in which *IM* is a ground motion intensity measure (PGA or SA), G_1 is the scaling function for magnitude and style of faulting, G_2 captures the path scaling, G_3 accounts for the regional inelastic attenuation, G_4 is the site amplification, G_5 represents the basing scaling function, and $\sigma_{\ln(IM)}$ is a centered Gaussian distribution capturing the total variability. This last term provides an uncertainty for each PGA and SA value, which will be taken into account later.

2.1.2 Building ShakeMap dataset

In this study, we used a total of 217 ShakeMap footprints from the U.S. Geological Survey (USGS) for the time period January 1973 to January 2023 (50 years) for earthquakes occurring in Greece and surrounding area with a magnitude of M4.5 or more. USGS ShakeMap program combines information from individual stations, site amplification characteristics, and ground-motion prediction equations (GMPE) for the distance to the hypocenter (or to the causative fault) to create the best composite map (Worden et al., 2020). Because these 217 ShakeMaps are few for this time period, we enhanced our dataset with 385 ShakeMap footprints from the National Observatory of Athens (NOA). Specifically, we retrieved 516 ShakeMaps from NOA for the time period 1973-2023. From these, we removed those that already exist in the USGS ShakeMap database. Thus, we ended up with 602 ShakeMap footprints (217 from USGA and 385 from NOA) that correspond to earthquakes that occurred in Greece and the 100-kilometer surrounding area. This process was performed because earthquakes

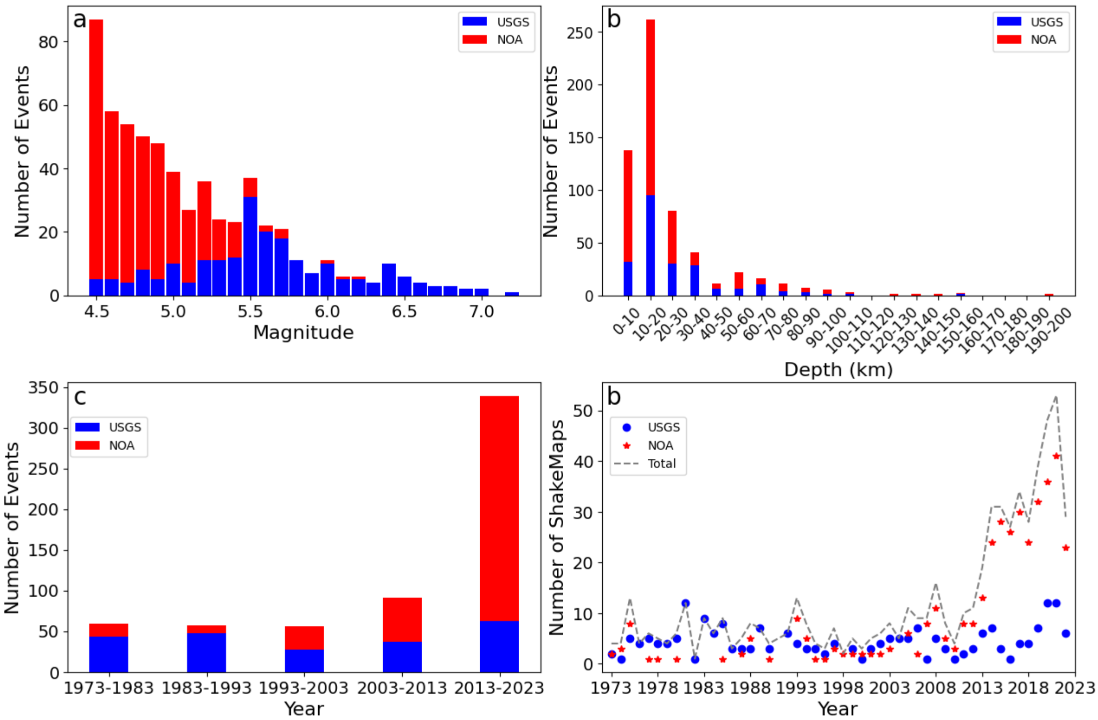

Figure 2-1. Distribution of (a) magnitude, (b) depth, and (c) origin year of the 602 ShakeMap footprints from 1973 to 2023 that constitute the dataset. (d) total number of ShakeMap footprints per year.

that occurred 100km away from Greece may have also affected the region of Greece. Instead, earthquakes at a distance of over 100km could not generate significant ground motion in the area of Greece due to the large distance to the hypocenter. A Table with these 602 events is given in the supplement of this study (Table S1).

Figure 2-1 shows the distribution of events in relation to magnitude, depth, and origin year. It is observed that NOA ShakeMaps have enhanced the database with earthquakes lower in magnitude (lower than M5.5), as USGS ShakeMap database includes all large-magnitude earthquakes as well. The large enrichment of the data with small- and medium-magnitude earthquakes (especially between M4.5 and M5.0) is not negligible, as these events could provide essential levels of ground shaking in the near-field. Additionally, NOA ShakeMaps seems to have enhanced the database with events that occurred between 2013 and 2023. Instead, USGS ShakeMaps are more uniformly distributed in time (Fig. 2-1c). The ShakeMap dataset covers the entire 50-year period with virtually no gaps. Also, the density of ShakeMap data was approximately constant until 2013, after which it significantly increased, especially for the NOA dataset (Fig. 2-1d). Finally, more events occurred in shallower depths (less than 30km), and intermediate-depth events are too few. The spatial distribution of the 602 ShakeMap events is illustrated in Figure 2-5a.

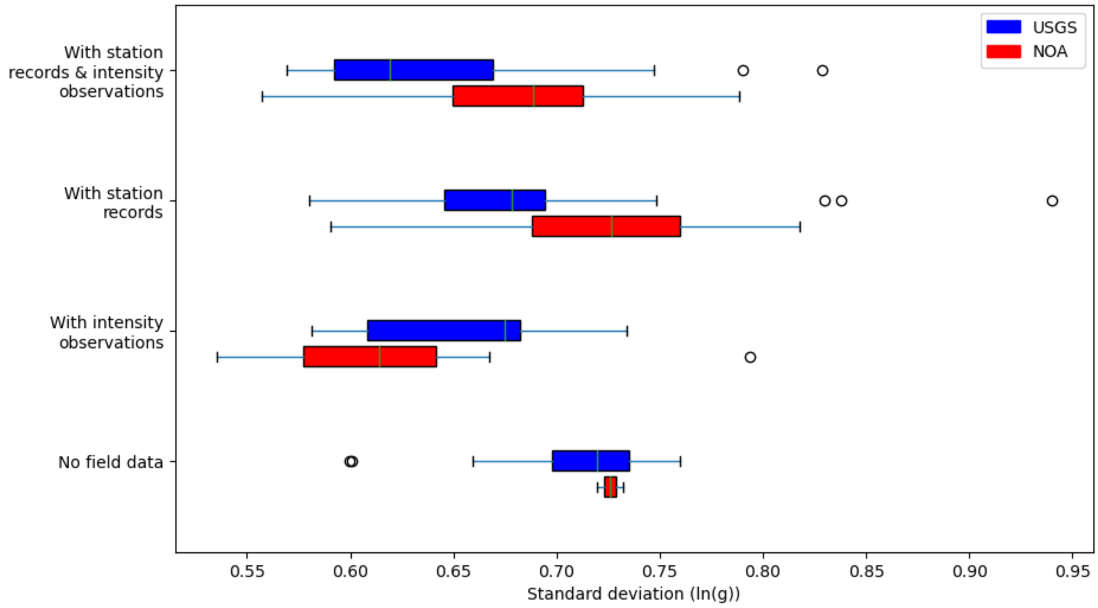

Figure 2-2. Distribution of the mean standard deviation for PGA for the 602 ShakeMap footprints, 217 and 385 from USGS and NOA ShakeMap catalogs, respectively. Distributions vary depending on whether ShakeMap used field data such as seismic records and/or intensity observation reports or not. Distributions of mean standard deviations are illustrated using boxplots.

2.1.3 ShakeMap uncertainty

As it was mentioned, ShakeMap footprints estimate *IM* values using a variety of GMPEs (equation 2). These GMPEs have a standard deviation of the Gaussian distribution (term σ in equation 2). Thus, the ShakeMap program utilizes information from station records and field intensity observations, like reports from the web application "Did you feel it?" (DYFI). DYFI is a questionnaire that collects information from people who felt the earthquakes and identifies this data to intensity measurements. This field data helps to reduce these uncertainties, as shown in Figure 2-2, where the mean uncertainty for PGA of each ShakeMap is illustrated. It is clear that ShakeMap footprints that have used field data have lower mean uncertainties.

The number of ShakeMap footprints that were built using DYFI reports or/and seismic station records is shown in Table 1. It is clearly observed that ShakeMap footprints, which were built using no field data or only DYFI reports, correspond to past events. Instead, the most contemporary events correspond to ShakeMap footprints that use seismic station records or both field intensity observations and instrumental data. We used the year 2011 as tipping point, as it was the year that the development of the Hellenic Unified Seismological Network (HUSN) had been completed, increasing the number of online seismic stations in Greece (Mignan & Chouliaras, 2014). From the 602 ShakeMap footprints, only 94 have been built without using field data; the majority of them belong to the USGS ShakeMap catalog, which includes the ShakeMap footprints for the oldest seismic events (Fig. 2-1c).

2.2 Strong-Motion Data

2.2.1 Building the Strong-Motion dataset

In the second method we tested the PSHA maps against strong-motion records. We used strong-motion records from the Engineering Strong Motion database (ESM) strong-motion flat-file 2018 (Lanzano et al., 2018). We retrieved 3902 strong-motion records coming from 809 earthquakes. These earthquakes cover a time-period between December 1977 and December 2016. To enhance our database in order to enlarge this time window, as well as add earthquakes that were not included in ESM flat-file, we added strong-motion data from the Engineering Strong Motion Database. The additional not-included-in-flatfile data was 21881 records from 2080 earthquakes for the time-period from June 1983 to December 2023. The final data set included 25784 records from 2331 earthquakes covering a time-period between December 1977 and December 2022, and a magnitude range from 2.54 to 7.02. There was no data available before 1977 for Greece, thus our dataset covers a 46-year time window and not a 50-year time window.

From these recordings, we utilized those coming from earthquake events with magnitude (moment Mw, local ML, or surface waves Ms) 4.5 or higher. Thus, the total number of strong-motion records utilized in this study was 7641, which corresponds to 650 earthquakes with magnitude 4.5 or higher and a time-period of 46 years (1977-2023). The time distribution of the records (filtered and raw) is given in Figure 2-3. Figure 2-3b shows the time distribution of the records coming from earthquakes with magnitudes equal to 4.5 or higher. A significant 7-year gap is identified in the dataset (from 2003 to 2010). After this gap, the data sharply increased. The raw data (Fig. 2-3a) has the same time distribution pattern, and the 7-year gap is identified as well. In Figure 2-5b, the spatial and magnitude distribution of the corresponding earthquakes with magnitude equal to M4.5 or higher that have produced the utilizing records is illustrated.

The VS30 (the average shear wave velocity of the top 30 meters) for each station, which is necessary for our analysis in order to describe site conditions, was included in the ESM strong-motion flat-file 2018 for the majority of the stations. For those that VS30 was not included, we used the Engineering Strong

Table 1. Number of ShakeMap Footprints Using “DYFI?” Reports or/and Seismic Station Records.

	Period	No Field Data	With DYFI? Reports	With Seismic Records	With Seismic Records and DYFI? Reports	Total
USGS	Before 2011	84	9	35	22	150
	After 2011	8	4	26	29	67
NOA	Before 2011	2	18	61	11	92
	After 2011	0	1	97	195	293
	Total	94	32	219	257	602

DYFI?: “Did You Feel It?”; USGS: U.S. Geological Survey; NOA: National Observatory of Athens

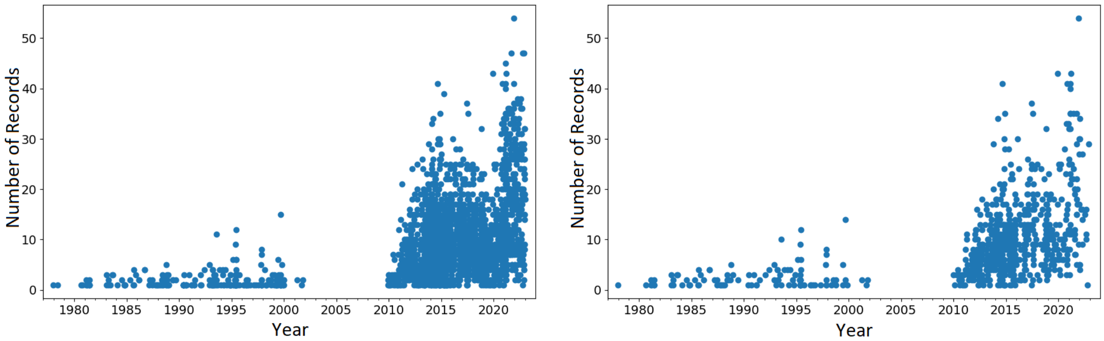

Figure 2-3. The time distribution and the density of the recordings correspond to magnitudes equal to M4.5 or higher.

Motion Database *masterstationlist*, a text file with VS30 inferred from slope for each available station. There were 38 stations for which we did not find VS30 information. For those, we used the slope-based VS30 database from the USGS. The origin of the data, the total number of recordings and the corresponding events, and the origin of the VS30 is given in Table 2.

2.2.2 Stations lifetime calculation - Detecting gaps in the data

To calculate the expected probability of exceedance, it is necessary to have knowledge about station lifetimes (i.e., the period in which the stations were active). We retrieved this information from the International Federation of Digital Seismograph Networks. We managed to recover lifetimes for 150 stations. For the other 102 stations, we calculated the lifetimes from their recording histories (Tasan et al., 2014). In particular, we assumed that the lifetime of the stations starts on the day of the first recording and ends on the day of the last recording. Also, we found 10 stations for which the recording history covered a longer period compared to the lifetimes retrieved from FDSN. For these stations, we re-calculated their lifetimes from their recording histories. The next step was to calculate potential gaps in recording history.

To identify gaps in stations recording histories, we applied a method based on average interevent times, as described from Tasan et al. (2014). First, we calculated the average time between records for each station. For this process, we used the raw data (i.e., no magnitude filter). Subsequently, interevent times greater than 10 times the average interevent time were considered as a gap. Finally, we corrected the stations lifetimes, removing the gaps. An example of this process is illustrated in Figure 2-4. Moreover, there were 30 stations with fewer than two records, so we were not able to calculate their lifetimes or gaps. For these stations, we assumed a minimum lifetime of one month. Furthermore, there were 13 stations that had slightly different coordinates during their lifetimes. These stations probably moved to slightly different positions; however, because the spatial differences between the old and new locations were too small, we could not consider the new location as an independent station, so we assumed these stations as one. A Table with the total stations (location,

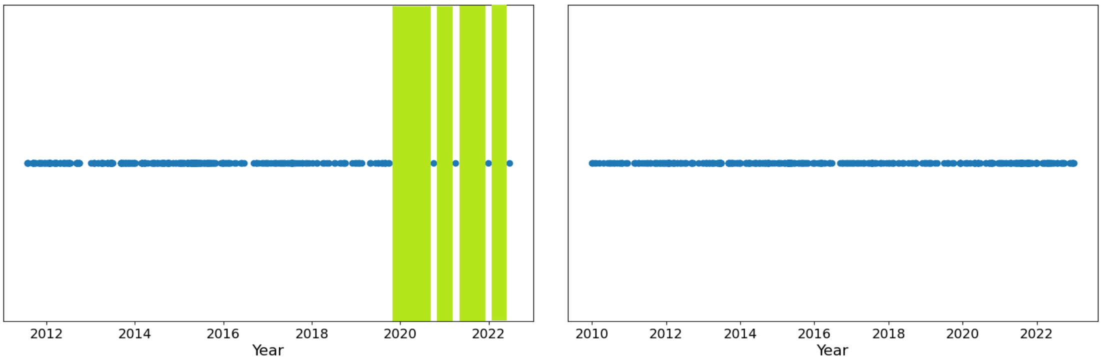

Figure 2-4. An example of the identification of gaps using average interevent times. (a) The time history at ZKR station (lifetime 19.31 years). Characteristic gaps are marked in green frames. The total gap identified was 10.83 years (corrected lifetime 8.48 years). (b) The time history at IACM station (lifetime 13 years). No gaps were identified.

network, VS30, lifetime, corrected lifetime, and the maximum *IMs*) is given in the supplement of this study (Table S2).

2.3 Macroseismic Intensity Data

The macroseismic intensity data from historical earthquakes are coming from the European Archive of Historical Earthquake Data (AHEAD; Albini et al., 2013). AHEAD inventory and make available multiple sets of data dealing with the earthquake history of Europe between 1000 and 1899. AHEAD provides the results of historical earthquake investigation, identifying the lists of parameters representing the earthquake location and energy.

We found 450 earthquakes with magnitude 4.5 or higher, which occurred in Greece and the 100-kilometer surrounding area, in AHEAD. For these events only for 339 there are macroseismic intensity data available based on the European Pre-instrumental Earthquake Catalogue (EPICA; Rovida & Antonucci, 2021; Rovida et al., 2022), which is based on AHEAD. Macroseismic intensity data

Table 2. Number of Strong-Motion record used in this study and the number of testing sites (stations).

	Events	Records	Stations With Measured VS30	Stations With Slope-Inferred VS30	Total Stations
Flat-File	372	2099	34	106	140
Additional Data	453	5542	2	154	154
Total*	650	7641	34	218	252

VS30: average shear wave velocity in the top 30 meters; Flat-File: Engineering Strong Motion database (ESM) strong-motion flat-file 2018 (Lanzano et. al., 2018); Additional Data: 2017-2022 not included in the flat-file 2018 strong-motion records from ESM database.
* Total events and stations might not be the sum of these presented in Flat-File and Additional Data, as some events and stations exist in both datasets. "Total" field shows the unique events and stations of the final dataset.

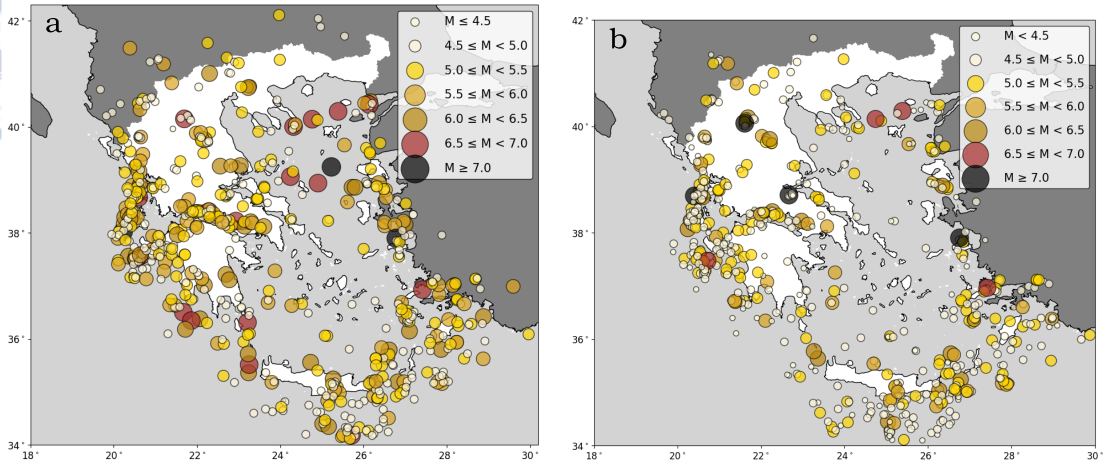

Figure 2-5. (a) The spatial distribution of the 602 ShakeMap events from 1973 to 2023. (b) The spatial distribution of the 650 Strong-motion events from 1977 to 2023.

are provided as Macroseismic Data Points (MDP), which are locations, such as cities or villages, where seismic intensity has been determined. These 339 earthquakes correspond to 1829 MDPs based on EPICA. However, we managed to retrieve data only for 800 MDPs, which correspond to 56 earthquakes between 1040 and 1897. The availability of MDPs depends on whether they are provided online, and they do not have *NaN* or questioned intensity values. Because some of the earthquakes, occurred in Greece and the 100-kilometer surrounding area, had MDPs in regions outside the area of Greece, we removed these MDPs. Finally, we ended up with 688 MDPs, which correspond to 48 earthquakes for the time-period 1204-1897.

The intensities of these MDPs were measured in different scales, such as European Macroseismic Scale (EMS) and EMS-98, Medvedev-Sponheuer-Karnik (MSK) scale and Mercalli–Cancani–Sieberg (MCS) scale. We made the assumption that the intensity scales are approximately equivalent, as the differences between scales are not significant enough (Musson et al., 2009; Caprio et al., 2015).

In Figure 2-6a the spatial distribution of the MDPs used in this study and the corresponding earthquakes are given. Also, in Figure 2-6b the MDPs distribution in time is given. Figure 2-6a shows that MDPs are not well distributed, as the majority of them are congregated in the cental Greece and Peloponnese. Also, Lefkada island (Ionian Sea) is well covered. Also, the data is poorly distributed in time (Fig. 2-6b), and an important gap between 1600 and 1700 (a century) is identified. However, these events correspond to high-magnitude earthquakes (Fig. 2-6a), with the minimum magnitude being 5.36 and the maximum being 8.26. Thus, it is reasonable for high-magnitude events like these to be more rare in time (i.e., the time between events is longer). Moreover, Figure 2-6b shows that more earthquake events correspond to a small number of MDPs (1 to 25) and only 7 have more than 25 MDPs. The two earthquakes with the most MDPs are the 7.17Mw on 1886-08-27 (Sakellariou et al., 2010) with 187 MDPs and the 6.77Mw on 1894-04-20 (Albini & Pantosti, 2004) with 96 MDPs.

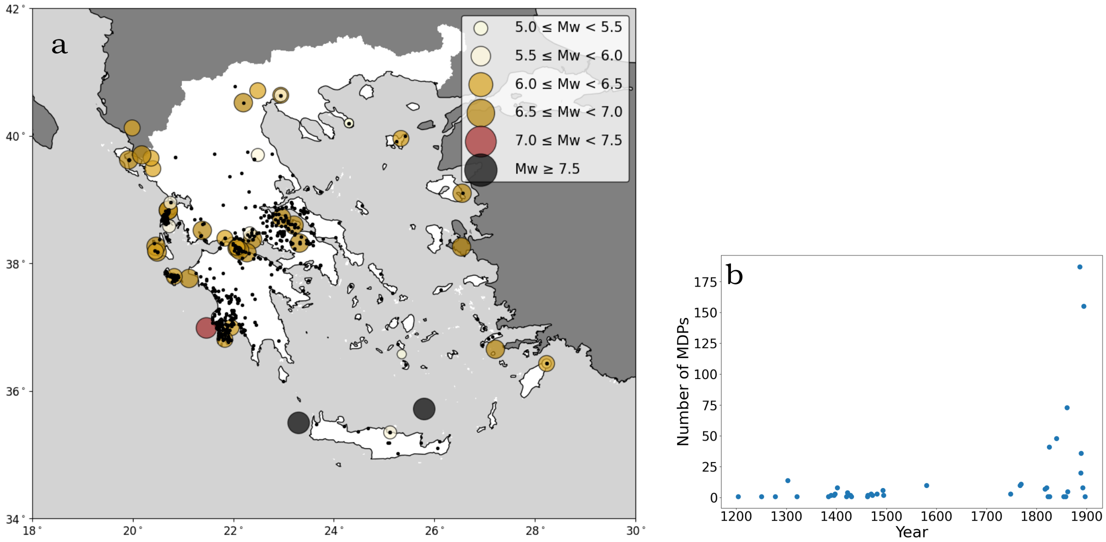

Figure 2-6. (a) spatial distribution of the MDPs and the corresponding earthquakes. (b) time distribution of the MDPs and their density.

3. Data Processing

3.1 ShakeMap data processing

3.1.1 Retrieval of the maximum intensity measure

From the total 602 ShakeMap footprints, which were released between January 1973 and January 2023 for earthquakes occurring in Greece and the 100-kilometer surrounding area with a magnitude of M 4.5 or more (Fig. 2-5a), we looked at PGA, Sa(0.3s), Sa(1.0s), and Sa(3.0s), which correspond to the maximum value in each spatial grid point. Because the 602 ShakeMap footprints were not computed on the same grid and all these grids have differences in size and resolution, we created a new base 0.01°x0.01° grid (see. 3.1.4). Subsequently, we retrieved the maximum *IM* ever estimated at each spatial grid cell over the observational period (Pothon et al., 2020). The density of the data for each grid cell is given in Figure 3-1. Data density is higher in central Greece, the Ionian Sea, and the Patras-Corinth Gulf, as in these regions most seismicity is observed (2-5a). In Figure 3-2a, the maximum PGA from 1973 to 2023 is illustrated. The maximum Sa(0.3s), Sa(1.0s), and Sa(3.0s) for the same time-period are illustrated in Figure 3-3a, 3-3b, and 3-3c, respectively. Of the 602 ShakeMaps, only 143 have contributed to the maximum PGA, 149 to the maximum Sa(0.3s), 98 to the maximum Sa(1.0s), and 77 to the maximum Sa(3.0s). These 143, 149, 98, and 77 ShakeMap footprints, respectively, cover the whole of Greece (Fig. 3-1, Fig. 3-2, and Fig. 3-3), and there are no sites that do not correspond to a ground motion intensity measure. All these PGA (and SA) values correspond to mean values when the uncertainty, $\sigma_{\ln(IM)}$, of the estimated value in equation 2 is equal to zero.

3.1.2 Retrieval of the site conditions

The PSHA maps provide the expected levels of ground shaking at rock sites. Thus, the comparison between estimated by ShakeMaps and expected by PSHA maps PGA (and SA) is sensible only at rock sites. We utilized the U.S. Geological Survey global slope-based VS30 database (Allen & Wald, 2007) to count the rock sites, assuming that a rock site verifies $VS30 \geq 800m/s$, according to the classification of EuroCode 8 (CEN, 2004). Thus, we retrieved a VS30 value for each base-grid cell. Due to the smaller grid size of slope-based VS30 (USGS), if a base-grid cell corresponded to more than one slope-based VS30 (USGS) grid cell, we used the average value (see. 3.1.4). As the VS30 points (located in the same

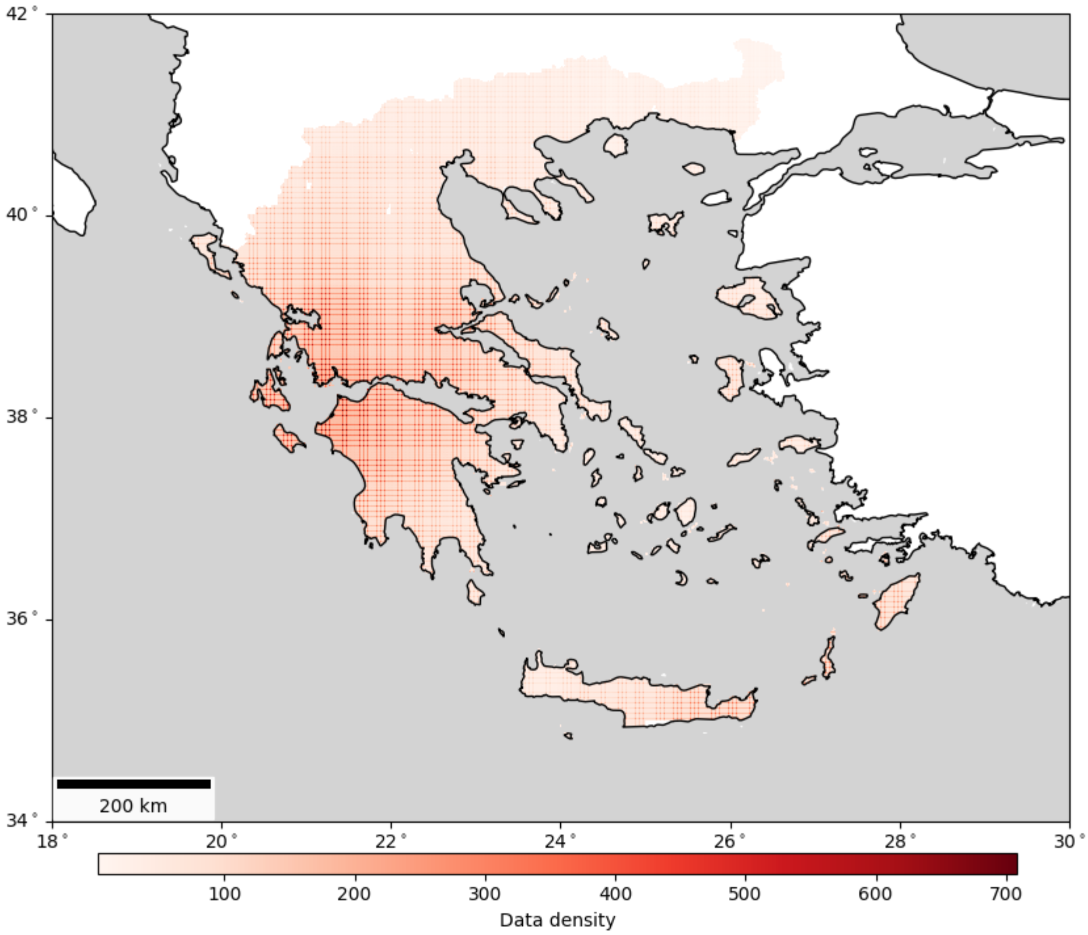

Figure 3-1. The number of the data from the 602 ShakeMap footprints (PGA and SA values) corresponds to each 0.01x0.01 base-grid cell. Due to the differences in ShakeMap equidistant there are base-grid cells that store more than one value for the same ShakeMap.

base-grid cell) are in close proximity, there is not much variation in their values, so the average value is representative of a base-grid cell.

We found only 32 sites with VS30 equal to or higher than 800m/s, which are too few for the process to have credibility, as they cover a small part of Greece with poor spatial distribution (Fig. 3-4a). Also, they correspond to sites in mountainous areas (such as the Pindos mountain range), away from cities and, by extension, from infrastructure. In order to manage this situation, we applied two different approaches: a) we made the comparison not for rock sites but for average-rock sites, assuming that correspond to $VS30 \geq 400m/s$, using Pitilakis et al. (2016) classification, and b) we de-amplified the ShakeMap footprints PGA and SA values, using Borcherdt (1994) amplification factors to convert them to rock-site PGA and SA.

In the average-rock sites approach, we filtered 123,050 average-rock sites, which cover the greater part of Greece (Fig. 3-4b). Instead, in de-amplification approach, we used all 142,050 sites, which were contained in our base-grid. The distribution of average-rock sites and total sites among the ShakeMaps is given

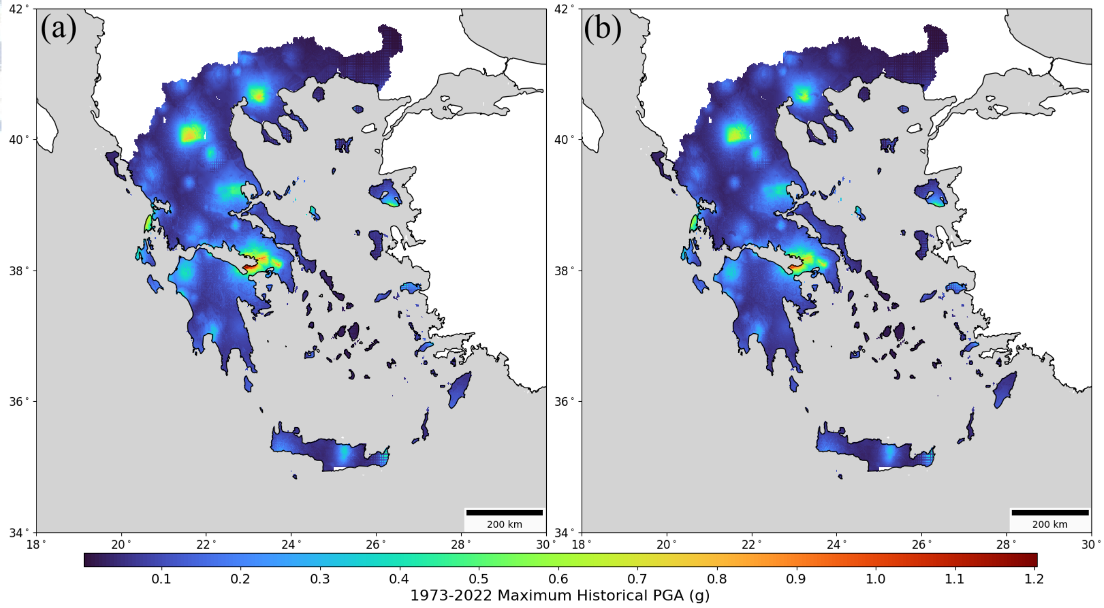

Figure 3-2. Maximum historical PGA ever estimated from the 602 ShakeMap footprints from January 1973 to January 2023. (a) PGA values as they have been produced by the 602 ShakeMap footprints, (b) PGA values after de-amplification using Borcherdt (1994) amplification factors.

in Table 3. To de-amplify the maximum PGA at each site, we used Borcherdt's low-period factors. The de-amplified maximum PGA is shown in Figure 3-2b. For de-amplification of SA at 0.3, 1.0, and 3.0 seconds, we used Borcherdt's short-, mid-, and long-period amplification factors, respectively (Fig. 3-3d, 3-3e, 3-3f). An amplification factor, a, is given by:

$$a = \frac{\mathrm{IM_{soil}}}{\mathrm{IM_{rock}}} \tag{3}$$

where $\mathrm{IM_{soil}}$ is the *IM* recorded in a site and $\mathrm{IM_{rock}}$ the *IM* recorded in the same site bedrock. Thus, knowing the $\mathrm{IM_{soil}}$ (from ShakeMap footprints) and the amplification factor, a, we calculated the $\mathrm{IM_{rock}}$ from 3.

Table 3. Distribution of ShakeMap footprints by number of points with the maximum PGA estimates at Average-rock sites and at Total sites.

Average-rock Sites per ShakeMap	Number of ShakeMaps	Total Sites per ShakeMap	Number of ShakeMaps
0-1	0	0-1	0
2-10	17	2-10	17
11-50	20	11-50	19
51-100	15	51-100	17
101-1000	62	101-1000	60
>1000	27	>1000	30

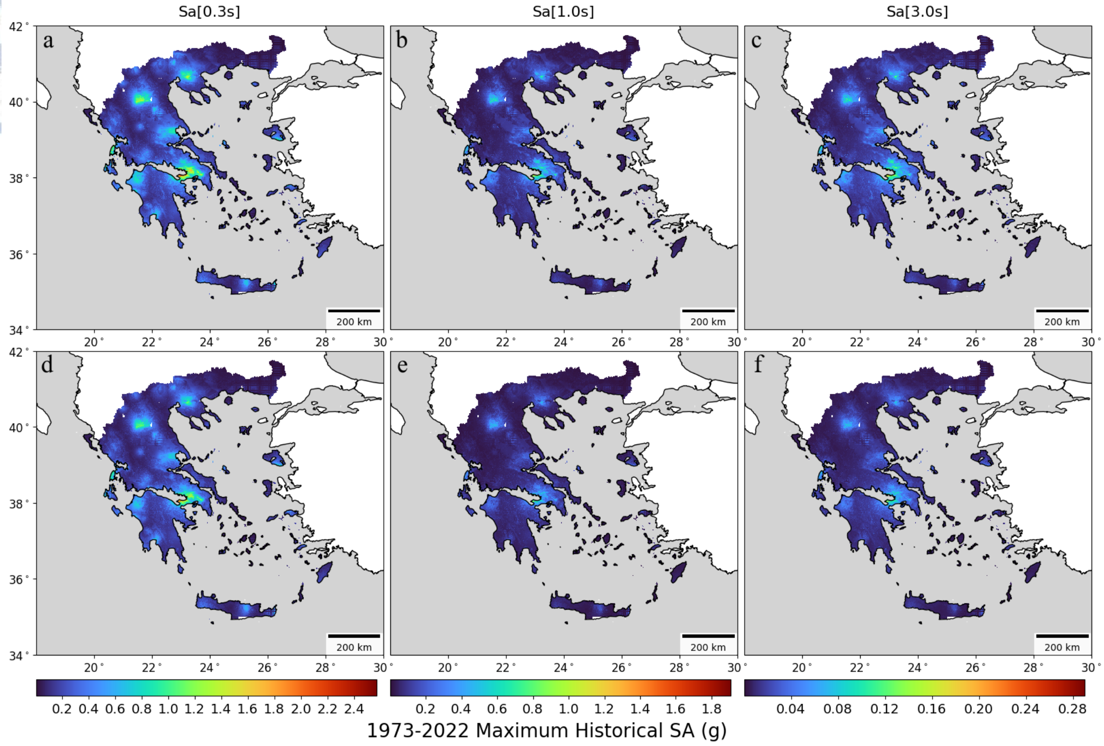

Figure 3-3. Maximum historical SA for periods 0.1s, 1.0s, and 3.0s ever estimated from the 602 ShakeMap footprints from January 1973 to January 2023. (a,b,c) SA values as they have been produced by the 602 ShakeMap footprints, (d,e,f) SA values after de-amplification using Borcherdt (1994) amplification factors.

3.1.3 Retrieval of the expected from the PSHA maps *IM* values

The last step was to retrieve the corresponding expected *IM* that the four PSHA maps provide for each base-grid cell, and combine it with the maximum *IM* for the same site (base-grid cell). For EAK2000 and GSHAP, the comparison was made only for PGA, as they provided only this intensity measure. Due to differences in PSHA maps grid size, if a base-grid cell overlays more than one PSHA map grid cell, we used this with the maximum expected value, operating more conservatively (see. 3.1.4). Finally, for each base-grid cell, we stored the maximum *IM*, the maximum IM_{rock} (after de-amplification), the site VS30, and the expected *IM* from the four PSHA maps. The base-grid is given in the supplement of this study (Table S3).

3.1.4 Spatial processing of the data

In order to make the comparison that was described above, we had to retrieve the *IM* provided from ShakeMap footprints, the VS30, and the expected PSHA threshold for each site. However, all these grids did not have the same type, size, and resolution. For example, the 602 ShakeMap footprints were usually computed at 0.083 degree resolution; however, some ShakeMap footprints were computed at 0.016 degree resolution. In order to have a uniform spatial

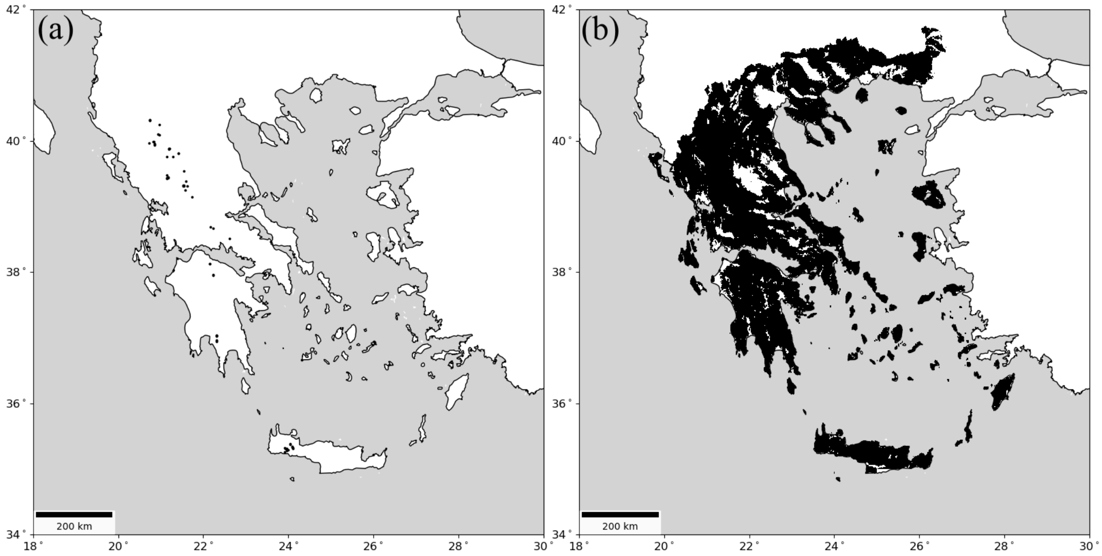

Figure 3-4. Rock sites according to the U.S. Geological Survey (USGS) global slope-based VS30 database (Allen & Wald, 2007). Black dots represent (a) rock sites for $VS30 \geq 800m/s$, and (b) average-rock sites for $VS30 \geq 400m/s$.

information, we created a base 0.01°x0.01° rectangle grid (polygon geometry), which comprises 142,050 grid cells that correspond to a rectangle region with an area of 1 square kilometer.

The base procedure to retrieve this spatial information to the base-grid was spatial overlay. In Figure 3-5a, an example of a spatial overlay between the base-grid and two ShakeMap footprints with different resolutions is illustrated. As it is seen, for a ShakeMap footprint with 0.083 degree spacing, more than one point could correspond to a base-grid cell (in particular, 1, 2, or 4 may correspond). Instead, for a ShakeMap with 0.0166667 degree spacing, there are base-grid cells with no corresponding ShakeMap grid. Thus, it leads to differences in the density of the data and the creation of strange patterns like those seen in Figure 3-1. Finally, for each base-grid cell, we kept only the maximum *IM*. It is worth noting that there might be some *IM* values very close to the maximum value (if not equal to); however, PSHA maps are calculated with the probability of certain sites exceeding their thresholds at least once. So, the maximum value is sufficient for this comparison.

The PSHA maps are given in 0.1-degree resolution. Thus, during the spatial overlay, there are base-grid cells that match on the boundary of two PSHA cells, as illustrated in the example of Figure 3-5b. In this case, we choose to keep the PSHA threshold that corresponds to the PSHA cell with the highest expected value. We did not choose to keep an average value, as we did not want to interfere arbitrarily with the PSHA model, changing the expected values. Instead, we choose the highest expected value as a more conservative approach. Also, the expected values for neighboring PSHA cells are close enough, and thus exceeding the threshold of one cell probably means exceeding the other neighboring cell (or cells) as well.

Finally, the USGS slope-inferred VS30 grid is given in 0.0083-degree resolution. Thus, multiple VS30 grid cells might fit into the same base-grid cell, as in Figure 3-5c. In this case, we kept an average value for these VS30 cells. Due to resolution differences between the two grids (VS30 and base-grid), usually four or six VS30 cells fit in one base-grid cell. We believe that the average value of these VS30 cells is the most reliable for the 1 square kilometer site, which a base-grid cell represents. The maximum or minimum value would represent a small part of the base-grid cell (e.g., 1/4) that might be different enough for the rest of the cell. Instead, the average value takes into account the VS30 values of all corresponding VS30 cells and offers a more complete view of VS30 variability in a base-grid cell.

The spatial overlay process was done using the *GeoPandas* library (Jordahl et al., 2020) in Python. Also, the EAK2000 map was created by digitizing its three hazard zones using QGIS software and is given in the supplement of this study.

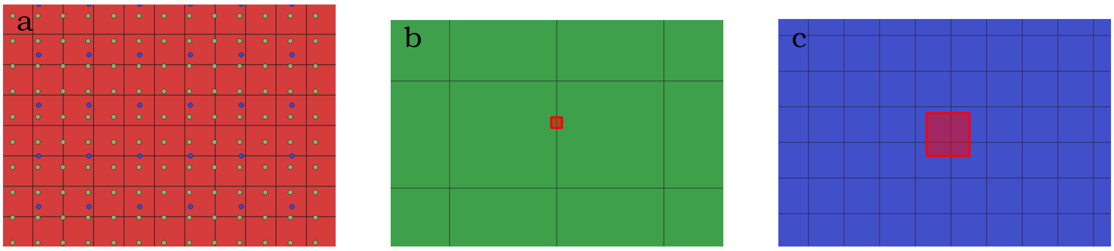

Figure 3-5. Examples of difficulties during the spatial overlap process. (a) Example of a spatial overlay of the 0.01x0.01 degree rectangle base-grid (red) with a 0.0083x0.0083 degree point ShakeMap grid (green) and a 0.0166667x0.0166667 degree point ShakeMap grid (blue). (b) Example of a spatial overlay of the 0.01x0.01 degree rectangle base-grid (red) with a 0.1x0.1 degree rectangle PSHA grid. (c) Example of a spatial overlay of the 0.01x0.01 degree rectangle base-grid (red) with the 0.0083x0.0083 degree rectangle USGS slope-inferred Vs30 grid.

3.1.5 Calculation of the fractional exceedance area

The comparison of the ShakeMap footprints with the thresholds from the PSHA maps enables quantifying the estimated fraction of the country that has been subjected to exceedance at least once. The fractional exceedance area of each PSHA model relative to the maximum *IM* is calculated. To calculate the fractional exceedance area, first we counted the sites (base-grid cells) where the maximum *IM* exceeded the expected PSHA threshold. Subsequently, we divided the number of exceeded sites by the total number of sites. For the average-rock method, the divisor was the total number of average-rock sites (sites with VS30 equal to 400m/s or higher). The fractional exceedance area was calculated for each *IM* and PSHA map. We have the expectation that the latest models should have a fractional exceedance area closest to the target value, as they utilize the most complete datasets and the most recent scientific knowledge.

3.1.6 Specific areas of interest: processing and comparison with GMPEs

We repeated the process described above for four urban areas: Athens (Attica), Thessaloniki, Patras, and Heraklion, and three areas of interest: Lefkada, Kefalonia, and Kozani (see locations in Figure 1-1). The base-grid was formatted to include these cities and their surrounding area. Also, we compared the results to those provided by two GMPEs, Boore et al. (2021) and Kotha et al. (2020).

To compare the results produced by the ShakeMap footprints with those produced by the two GMPEs (Boore et al., 2021 and Kotha et al., 2020), we used all earthquakes from the ANSS catalog (USGS) that occurred between January 1973 and January 2023 in a 100-km radius for each area of interest, assuming that earthquake events occurring over a distance of 100km would not provide significant ground motion in these specific regions. From these events, we used only those that occurred at a depth of 50km or less, as both GMPEs are for shallow crustal earthquakes (see 4.1.2). The total earthquake events stored for each area of interest and those that were finally used are presented in Table 4.

For each earthquake, an *IM* was calculated for each site (modified base-grid cell), and finally, the maximum value was stored. Then, this maximum *IM* calculated from the two GMPEs was compared with the PSHA maps thresholds. Boore et al. (2021) required parameters are described in subsection 4.1.2. In this subsection, the way we calculated these parameters is described as well. For Kotha et al. (2020), the only required parameter is the Joyner-Boore distance (R_{JB}), and we handled it as an approximate epicentral distance (Kaklamanos et al., 2011).

As it mentioned, for this test, the base-grid was formatted to include these areas. However, instead of the islands of Lefkada and Kefalonia, which are bounded by their coastline, for the other areas (in mainland Greece), the selection of the spatial rectangular is relatively arbitrary. For each area, the spatial rectangular (formatted base-grid) includes the urban area (city and suburbs) as well as important infrastructure, such as airports, ports, industrial areas, etc. Thus, the calculation of the fractional exceedance area will have different results if a different (in size or location) spatial rectangular is utilized. However, in this part of the study, the main purpose is to illustrate the extent of the exceedance area (if it exists) in relation to cities and their infrastructure, not to calculate the exact fractional exceedance area of each specific area. The fractional exceedance area of each specific area on the mainland corresponds to the specific spatial rectangular as it is described by its coordinate window. The coordinate windows of each spatial rectangular for each mainland-specific area are given in the appendix of the study (Table A-1).

3.2 Strong-motion data processing

Similarly, for the strong-motion data, we retrieved the maximum *IM* from the ESM Flat-file and the ESM database at each station (site) for the period 1977-

Table 4. Earthquakes occurred between 1973 and 2023 within a 100km radius of each region of interest, according to the ANSS catalog (USGS).

Regions	Athens	Thessaloniki	Patras	Heraklion	Lefkada	Kefalonia	Kozani
Events	82	44	278	129	329	526	118
Events above 50km depth	72	44	255	98	315	507	117

ANSS: Advanced National Seismic System; USGS: U.S. Geological Survey

2022. From the 252 stations, only 28 have VS30 above 800m/s (measured or inferred). For these 28 stations (11.1%), there are no *IMs* that exceed the PSHA maps thresholds. We applied the same approach that we used in the ShakeMap footprints method, utilizing stations with $VS30 \geq 400m/s$ (average rock). These stations are 181 ($\approx 71\%$ of the total number of stations). Additionally, we applied the de-amplification approach, using all 252 stations after de-amplifying the strong-motion records using Borcherdt's amplification factors, depending on sites VS30 (measured or inferred). Finally, we stored the PSHA maps thresholds and compared them with the observed *IM* at each site (station). In Table S2, the stations information (location, network, Vs30, lifetime, etc.), the recorded maximum PGA and SA, and the corresponding PSHA maps thresholds are given.

3.2.1 Calculation of the expected exceedance

Unlike the ShakeMap footprints method, in this method, the observation period (term Δt in equation 1) is not uniform as it corresponds to stations lifetimes, which vary from a few hours to few decades. Thus, the test must be able to handle varying lifetimes. We followed the Stirling and Gerstenberger (2010) approach as described in Tasan et al. (2014). At each site, the PSHA maps give a *IM* threshold with a probability of exceedance for a specific time interval, Δt, and return period. If this time interval is one year, this probability is called annual probability of exceedance, λi. The mean expected number of exceedances is obtained by multiplying the rate λi by the duration of the observation time window Δt. Assuming that ground shaking for a time interval, Δt, at a site occurs according to a stationary Poisson process, the Poisson distribution, which is fully defined by its mean, provides the probability of observing a given number n of *IMs* above the PSHA threshold and is given by the equation

$$P(n) = \frac{(\lambda_i \Delta_t)^n e^{-\lambda_i \Delta_t}}{n!} \tag{4}$$

where λi is the annual probability of exceedance at site i given by the PSHA model in a time interval Δt. Stirling and Gerstenberger (2010) defined that a PSHA model is considered consistent with the observations if the number of exceeded sites falls within the bounds of the distribution, defined by the percentiles 2.5 and 97.5 per cent.

We applied the Monte Carlo method to sample the Poisson distributions for the 252 sites (eq. 4), characterized by their means ($\lambda i \Delta t$), and generate numbers of ground shaking exceedances for all sites, corresponding to the time interval Δt (Tasan et al., 2014). The annual rate of exceedance for the four testing PSHA maps with a return period equal to 475 years is 0.2103%. For each run, one set of 252 numbers of exceedance is generated (if the number of exceedance is higher than 0, the site exceeds PSHA thresholds). Sampling the Poisson distributions many times, many sets of numbers of exceedances are generated, reducing the randomness of the results. For each run, the total number of sites with exceedance is counted. After many runs, a probability distribution can be built. This distribution describes the expected number of sites with at least one exceedance, and it is very close to a binomial distribution. If stations lifetimes were equal, then this distribution should be binomial (Albarello & D'Amico, 2008). We applied 10,000 runs, as they are enough to provide stable results (Tasan et al., 2014).

3.3 Macroseismic Intensity Data Processing

3.3.1 Conversion of macroseismic intensities to PGAs

The first and most important step in macroseismic intensity data processing is the conversion of macroseismic intensities from historical earthquakes to PGA values. Thus, we calculated the expected PGA from the intensities that have been assessed in the 688 MDPs in Greece for the time-period 1204-1897. We used three different ground-motion intensity conversion equations (GMICEs) to do the conversion: Tselentis and Danciu (2008), Worden et al. (2012), and Caprio et al. (2015). To avoid significant errors in the conversion from intensity to PGAs, we applied each GMICE to the same range of intensities used by each author. Specifically, we applied Tselentis and Danciu (2008) GMICE only for intensities between 4.0 and 8.0. Correspondingly, we used Worden et al. (2012) and Caprio et al. (2015) GMICEs for intensities between 2.0 and 8.6 and between 2.0 and 9.0, respectively (Table 5). A Table with the 688 MDPs (location, intensity, VS30, earthquake) and the PGAs, which are estimated from the three GMICEs is given in the supplement of the study (Table S4).

The total number of MDPs for which a PGA has been estimated is 611, for a total intensity range of 2.0-9.0. Of these MDPs, 430 PGAs have been estimated by all three GMICEs and 65 only by Caprio et al. (2015). The results of the intensity-to-PGA conversion for each GMICE, with the corresponding uncertainties, and the distribution of the intensity-inferred PGAs with the epicenter distance are provided in Figure 3-6. As expected, the values of the intensity-inferred PGAs increase proportionally to the increase in intensity and are also correlated to the increase of the epicentral distance.

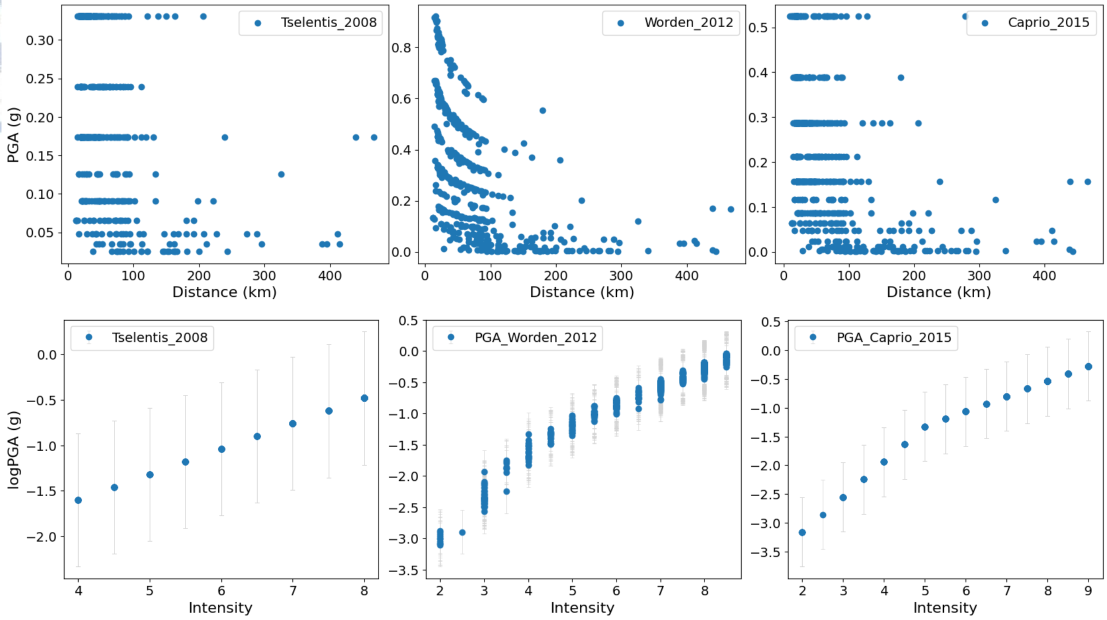

Figure 3-6. Distribution of the intensity-estimated PGA with the epicentral distance (top figures) and distribution of the logarithm of the intensity-estimated PGA with the corresponding intensity (bottom figures).

Table 5. The number of MDPs for which a PGA has been evaluated for each GMICE in a specific intensity range.

GMICE	Intensity range of application	Number of MDPs
Dancieu and Tselentis (2008)	4.0 - 8.0	430
Worden et al. (2012)	2.0 - 8.6	546
Caprio et al. (2015)	2.0 - 9.0	611

GMICE: ground-motion intensity conversion equation; MDP: macroseismic data point.

3.3.2 Estimation of hypocentral distance for the historical earthquakes

Worden et al. (2012) GMICE takes into account the effect of distance from the rupture to site as well as the effect of the earthquake magnitude. We used the hypocentral distance instead of the distance-to-rapture (Worden et al., 2012) because we did not have finite fault models for the earthquakes to calculate it. Following Worden et al. (2012) processing, we excluded from the analysis data points for which the rupture length exceeded 20% of the hypocentral distance. We estimated the rupture length using the Karakaisis et al. (2010) relation for the faults in the Aegean area. The AHEAD database does not provide depth estimations for the events, which are necessary to calculate hypocentral distances. Thus, we inferred the depth of each earthquake from the tectonic environment (Chiou & Youngs, 2008), so that we were able to determine the hypocentral distance.

To achieve this, we used all available data from the ANSS comprehensive earthquake catalog (U.S. Geological Survey). We retrieved 3931 earthquakes with magnitudes equal to 4.5 or higher from 1904 to 2024. For each historical event, we found the closest (distance < 35km) events from the ANSS catalog, and we set its depth as the average depth of these ANSS events, considering that these close-distance earthquakes occurred in the same tectonic environment. We used the events from the ANSS catalog, which have a magnitude equal to 4.5 or higher, so that they have the same magnitude range as the historical earthquakes, because only for close-in-magnitude earthquakes is it safe to make the above assumption. Figure 3-6a shows the intensity-estimated PGAs versus hypocentral distance. Worden et al. (2012) results (fig. 3-6), which have considered the effect of distance, show a more expected PGA-to-distance distribution compared with the other two GMICEs.

4. Results and Discussions

4.1 ShakeMap test

The regions where the maximum PGA from ShakeMap footprints, due to earthquake events that occurred from January 1973 to January 2023, exceeds the thresholds from PSHA maps have been estimated. The hazard ratios for PGA are illustrated in Figure 4-1 for both applied approaches. Hazard ratios have been calculated by dividing the maximum *IM* from the ShakeMaps by PSHA thresholds. Values over 1.0 represent the exceedance regions; moreover, from the color scale, it is easily understood the differences between the observed (PGA from ShakeMaps) and the expected (PGA from PSHA maps) values. Similarly, in Figure 4-2, the hazard ratios for Sa(0.3s), Sa(1.0s), and Sa(3.0s) for both approaches are given for the ESHM20 map. The SA results for the ESHM13 are given in the appendix (Fig. A-3).

The fractional exceedance areas (sites with exceedance / total sites) are given in Table 6 for each PSHA map and approach. ESHM20 and ESHM13 have considerably smaller fractional exceedance areas compared with EAK2000 and GSHAP (approximately half values). Also, ESHM13 has a significantly smaller exceedance area compared to ESHM20 for Sa(1.0s) and Sa(3.0s), instead, for Sa(0.3s) the exceedance area is almost the same. The differences between PSHA maps (i.e., which one has the smaller fractional exceedance area and hazard ratio) might be differentiated for a specific region in relation to the results for the whole of Greece, as we will discuss below.

Figure 4-1 shows clearly that for all PSHA models, despite their differences, and for both approaches, the fractional exceedance areas have approximately the same spatial distribution. These areas appear to be limited to the regions closest to the epicenter area. A plot of exceeded PGA values for the ESHM20 and EAK2000 versus epicentral distance is created (Fig. 4-3). This plot confirms this finding, as the majority of the exceeded sites are in an epicentral distance lower than 35km, especially for the significant high PGA values. Similarly, the exceedance areas tend to follow the same pattern for both the ESHM20 and ESHM13 maps for all SA periods. Thus, the differences between the PSHA models seem to have a limited effect on the area where at least one exceedance has possibly occurred from 1973 to 2023, but not in the total number of exceeded sites or in the hazard ratios.

Table 6. Estimated fractional exceedance area for Greece, according to the four PSHA models for the two different approaches.

	Approach	Fract. Exceedance Area(%) / Exceeded Events			
		ESHM20	**ESHM13**	**EAK2000**	**GSHAP**
PGA	**Average-rock**	7.22 / 20	5.86 / 19	13.32 / 53	10.13 / 38
	de-Amplification	4.98 / 16	3.98 / 13	10.02 / 43	7.33 / 28
Sa(0.3s)	**Average-rock**	6.68 / 29	6.60 / 31	-	-
	de-Amplification	4.56 / 22	4.48 / 24	-	-
Sa(1.0s)	**Average-rock**	13.37 / 34	9.63 / 31	-	-
	de-Amplification	8.05 / 24	5.48 / 22	-	-
Sa(3.0s)	**Average-rock**	8.29 / 25	3.02 / 17	-	-
	de-Amplification	4.42 / 21	1.30 / 12	-	-

ESHM20: European Seismic Hazard Model 2020; ESHM13: European Seismic Hazard Model 2013; EAK2000: National seismic hazard map of Greece; GSHAP: Global Seismic Hazard Assessment Program; PGA: Peak ground acceleration; SA: Spectral acceleration

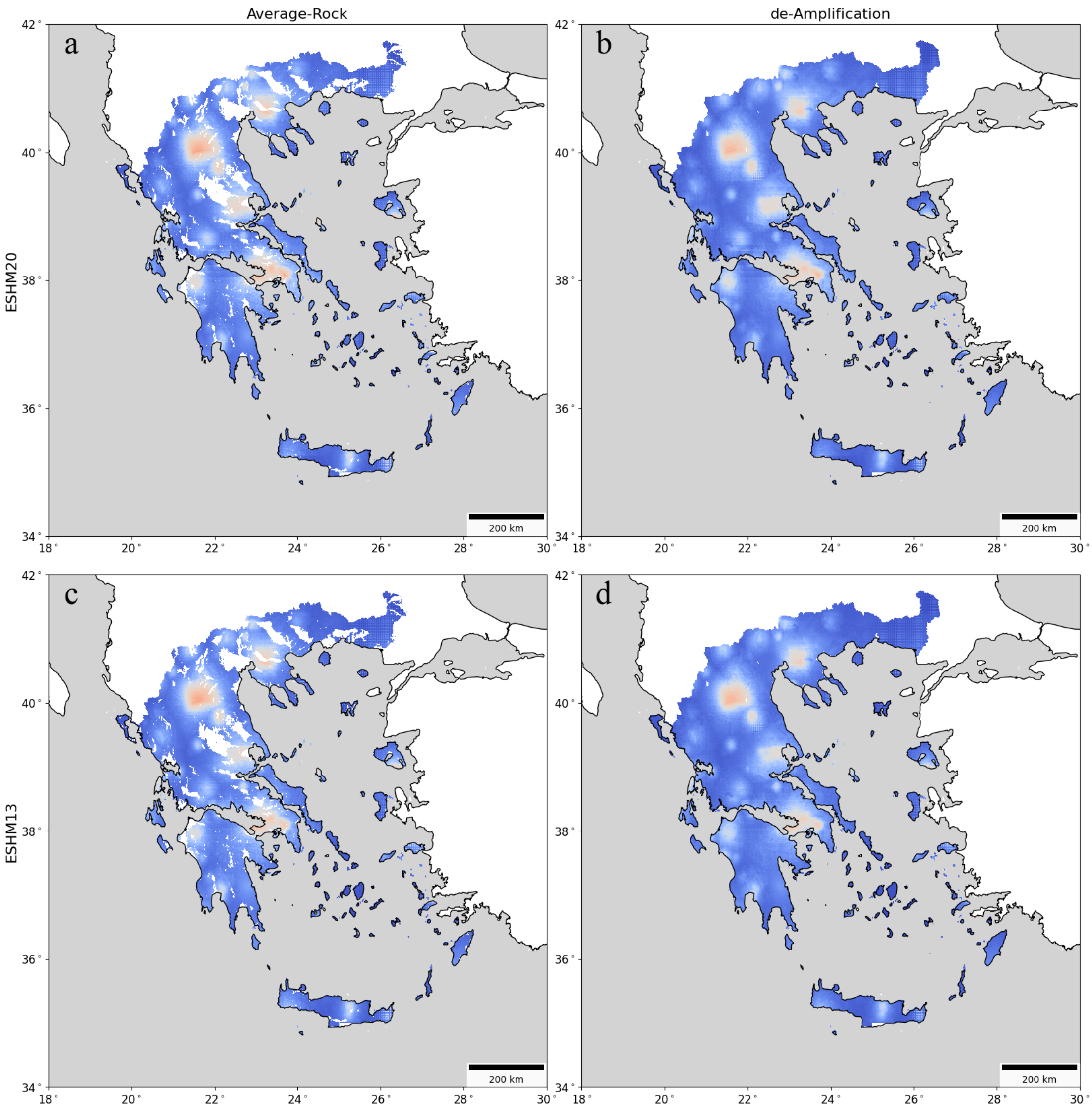

(Continued)

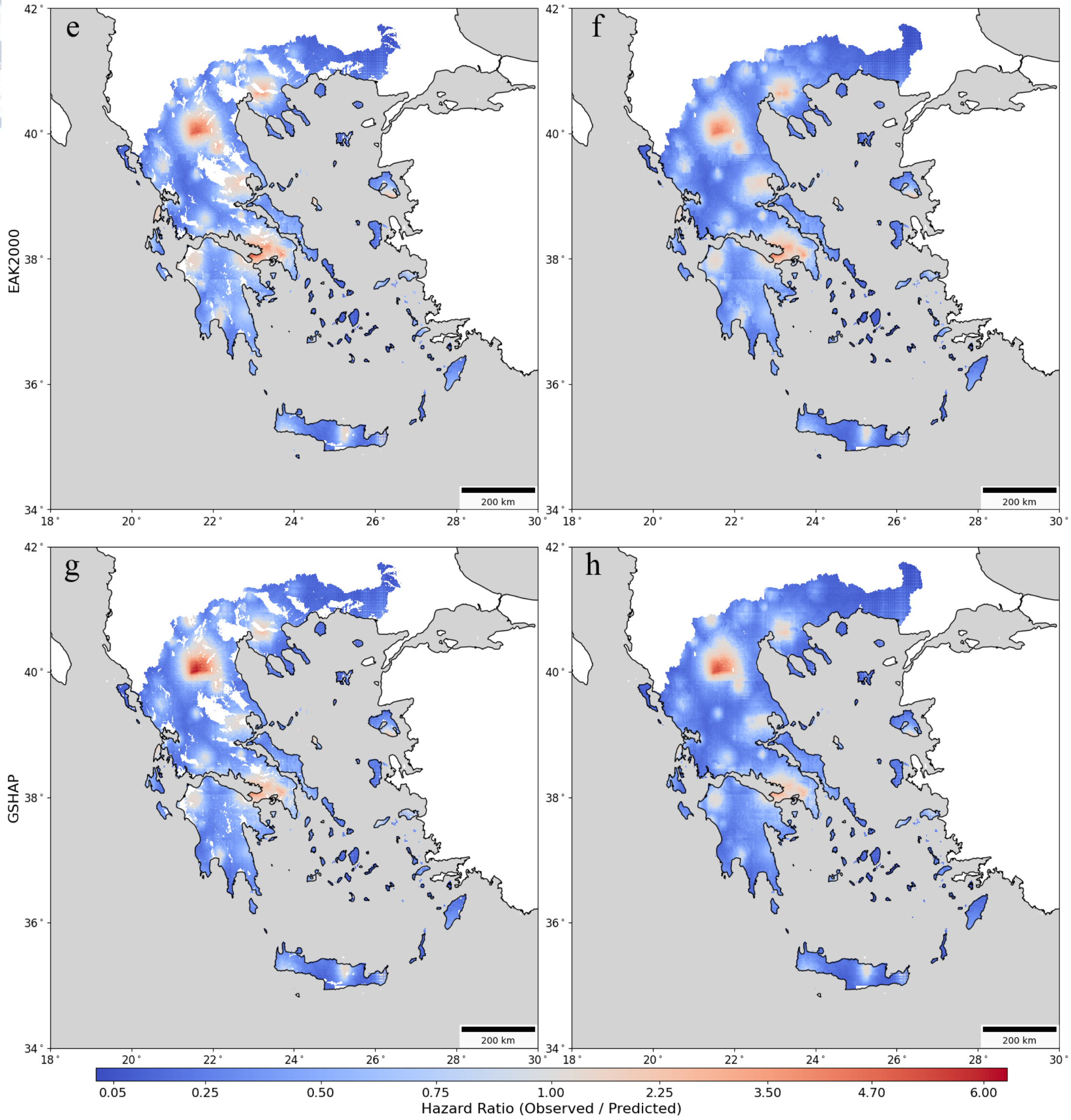

Figure 4-1. Hazard ratio of the 1973-2023 ShakeMap footprints PGA to the estimated PGA for 10% probability of exceedance in 50 years. Ratio maps are plotted for (a,b) ESHM20, (c,d) ESHM13, (e,f) EAK2000, and (g,h) GSHAP. (a,c,e,g) illustrate the results of the average-rock method, and (b,d,f,h) illustrate the results of the de-amplification method. Values greater than 1.00 show where the ShakeMap footprint PGA exceeds the correspond estimated from the PSHA map PGA.

The earthquake events that have provided the maximum PGA for the period 1973-2023 are 143 out of 602, which make up the data set (Fig. 4-4a). The total earthquake events that have produced a PGA greater than this that is estimated from the PSHA models for both approaches are 54 (out of 143; Fig. 4-4b). The maximum magnitude of them is 7.2M (1981-12-19, 61km west of Eresos), and the maximum depth is 33km. The number of events and their corresponding magnitude and depth are shown in Figure 4-5. Additionally, the total earthquake events that have produced a Sa(0.3s), Sa(1.0s), and Sa(3.0s) greater than PSHA models thresholds for both approaches are 28, 34, and 27, respectively, and

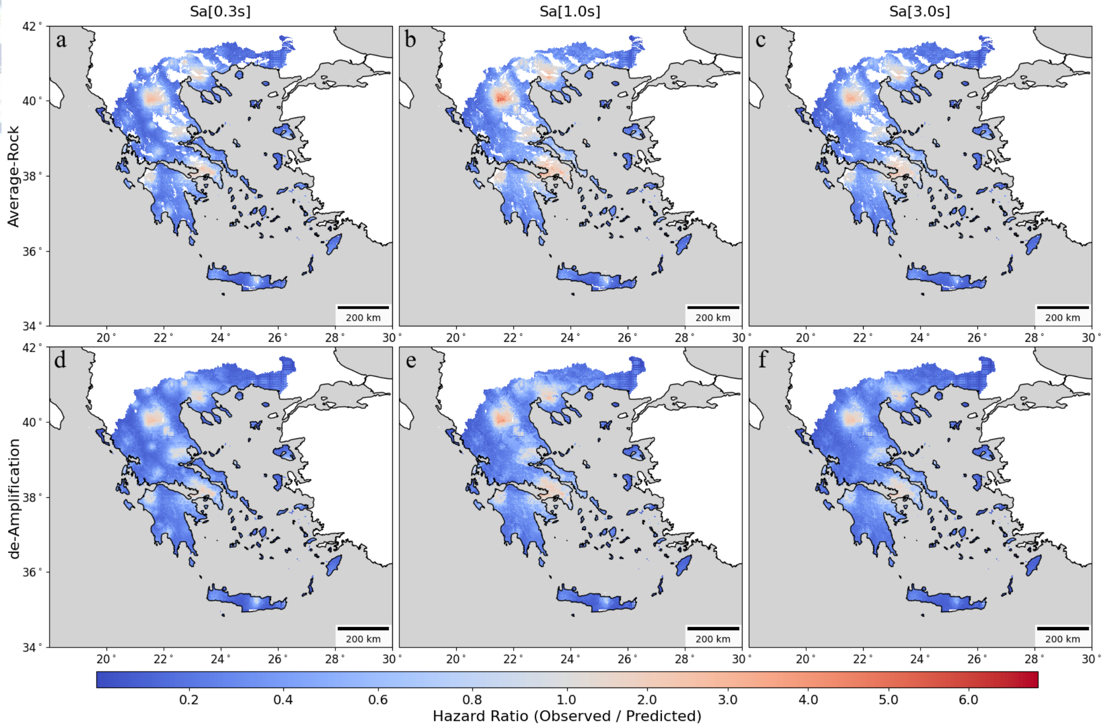

Figure 4-2. Hazard ratio of the 1973-2023 ShakeMap footprints SA to the estimated SA for 10% probability of exceedance in 50 years. Ratio maps are plotted for ESHM20. (a,d) Sa(0.3s), (b,e) Sa(1.0s), (c,f) Sa(3.0s). (a,b,c) illustrate the results of the average-rock method, and (d,e,f) illustrate the results of the de-amplification method. Values greater than 1.00 show where the ShakeMap footprint SA exceeds the PSHA thresholds.

spatial distribution is given in Appendix (Fig. A-4, Fig. A-5, and Fig. A-6).

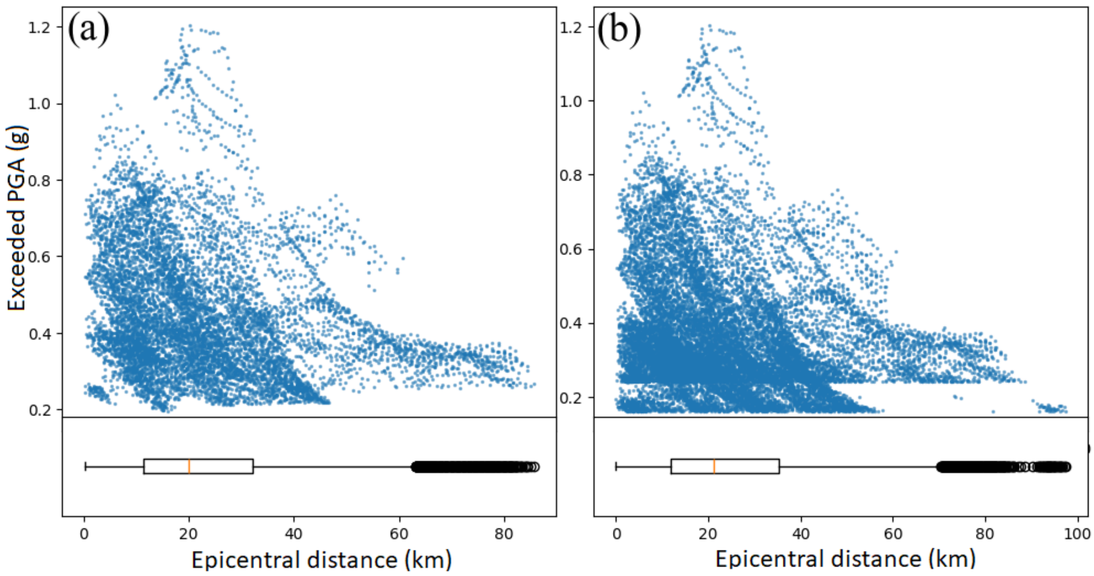

Figure 4-3. Distribution of exceeded sites PGA to the corresponding epicentral distance. The boxplots of exceeded PGA to epicentral distance are plotted as well. (a) results for the ESHM20, (b) results for the EAK2000.

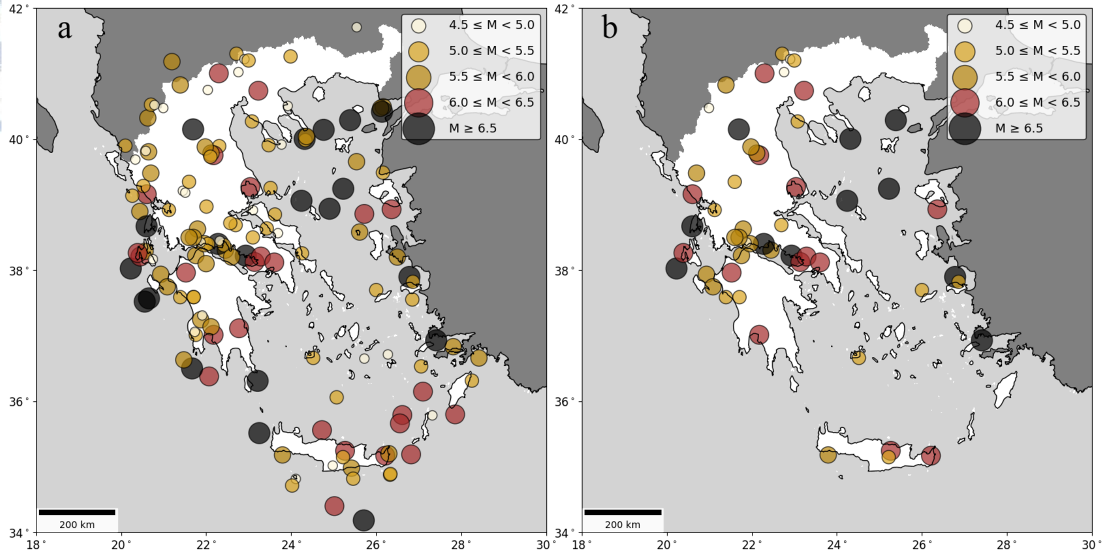

Figure 4-4. (a) Location and magnitude of all earthquake events for Greece and the 100-kilometer surrounding area processed by ShakeMap from 1973 to 2023, and they have produced the maximum historical PGAs. (b) Location and magnitude of earthquake events that have produced a PGA greater than PSHA maps thresholds for both approaches (average-rock or de-amplification).

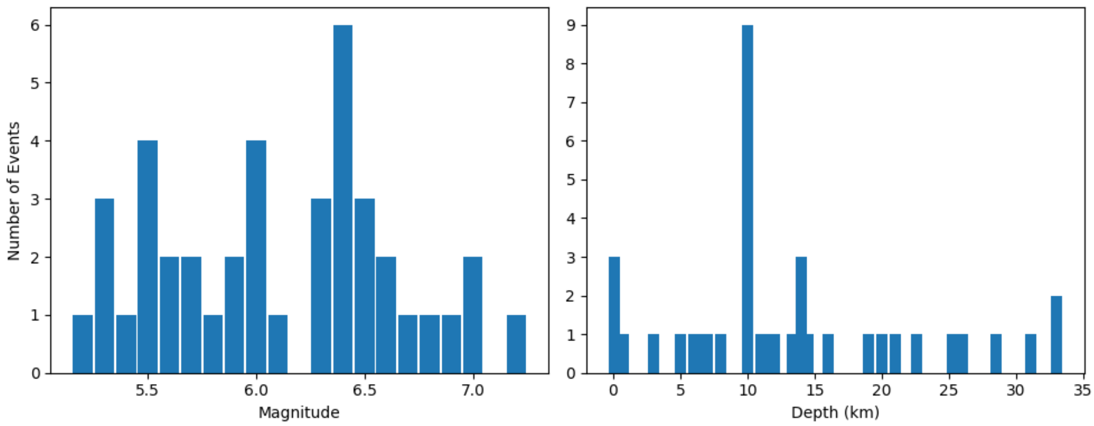

Figure 4-5. Number of earthquake events that have provided a PGA greater that was predicted from the PSHA models per magnitude and depth. These events are the total exceeded earthquake events for all PSHA models and approaches (average-rock or de-amplification).

4.1.1 Difference between the two approaches

Comparing the results for the two approaches, the de-amplification approach always has smaller fractional exceedance areas, with non-negligible differences (Table 6). We could say that the average-rock approach provides a relatively satisfactory view; however, the differences between the strong ground-motion recorded at site conditions with VS30 equal to 400m/s, might be crucial compared to those recorded at rock sites with VS30 equal to 800m/s.

The differences between the two approaches are bigger for the ESHM20 and

ESHM13, as the average-rock approach has approximately double values (Table 6). However, for the EAK2000 and GSHAP, the differences are not so significant. This happens because the EAK2000 and GSHAP have lower predicted hazard (Fig. 4-1) than the ESHM20 and ESHM13; thus, *IM* values after de-amplification were still above their thresholds. However, the fact that the EAK2000 and GSHAP have lower thresholds makes the differences in the number of events that have provided the exceeded PGA values higher, as small PGA reductions after de-amplification could reduce the number of exceeded events significantly, as it seems in Table 6.

Therefore, we consider the de-amplification approach results to be more valid and reliable than average-rock, as in this approach the comparison between the "observed" and predicted value is more close to rock-to-rock comparison, taking into account that the de-amplification approach contains some uncertainty as the determination of the amplification factors is a very complex process. Thus, henceforth, the processing that will be done in this study will be done with the de-amplification approach. The average-rock approach results must be treated with caution, and they can only provide a view of the patterns of exceedance areas without being able to approximate the exceedance area fraction or the hazard ratio with sufficient accuracy.

4.1.2 Fractional exceedance area determination and Limitations

In Figure 4-1 and Table 6, the hazard ratios and the fractional exceedance for all PSHA models and approaches are given. However, to determine precisely the fractional exceedance area and compare it with what is expected from the PSHA models with a return period of 475 years, our dataset should have all earthquakes with a magnitude ≥ 4.5. To handle this situation, we determined the sites (base-grid cells) that might have been affected by another earthquake, which were not included in our data set. Following the Pothon et al. (2020) process, we used the Advanced National Seismic System (ANSS) catalog (USGS) to store all earthquake events with a magnitude 4.5 or higher that occurred in Greece and the 100-kilometer surrounding area for the period 1973-2023. We found 2637 events, and we removed those that had been modeled by a ShakeMap. We used the Gardner and Knopoff (1974) algorithm to identify aftershocks and foreshocks, as we assumed that they had produced lower *IMs* than the associated mainshock because they occurred in the same area and at lower magnitude (Båth, 1965). We classified 147 earthquakes as foreshocks and 711 as aftershocks, and we removed them from the catalog. Finally, we ended up with 1215 earthquakes not modeled by a ShakeMap, identified as mainshocks according to the Gardner and Knopoff (1974) algorithm.

Sites that do not have a modeled-by-ShakeMap event at a closer distance and in higher magnitude could be affected by these not-modeled-by-ShakeMap events. We found that 95% of the base-grid does not satisfy this condition and could theoretically be affected by an earthquake not modeled by a ShakeMap. Thus, we estimated the *IM* produced by these 1215 not-modeled-by-ShakeMap events using Boore et al. (2021) GMPE for shallow crustal earthquakes in Greece, and we stored the maximum *IM* for each site (base-grid cell). Boore et al. (2021) GMPE was selected as it is one of the most reliable for Greece (Sotiriadis & Margaris, 2023).

Boore et al. (2021) GMPE requires input parameters like depth to the top of the rupture, Z_{TOR}, the slant distance to the closest point on the rupture plane, R_{RUP}, the horizontal distance to the surface projection of the rupture (the Joyner-Boore distance), R_{JB}, and the horizontal distance to the surface projection of the top edge of the rupture measured perpendicular to the fault strike, R_X. We calculated these parameters based on Kaklamanos et al. (2011), and we handled the Joyner-Boore distance (R_{JB}) as an approximate epicentral distance (Kaklamanos et al., 2011). To calculate these parameters, focal mechanism solutions are necessary, and only 450 out of 1215 events were available in the ANSS catalog (USGS). For the other 765 earthquake events, we estimated fault strikes, dips, and rakes following the procedure developed by Chiou and Youngs (2008).

The missing values were estimated from other associated events or from the tectonic environment. To associate events with each other, we utilized all 2637 events from the ANSS catalog with a magnitude 4.5 or higher that occurred in Greece and the 100-kilometer surrounding area for the period 1973-2023. First, we applied Gardner and Knopoff (1974) algorithm to associate mainshocks with aftershocks or foreshocks. If an earthquake with no focal mechanism solutions has been determined as an aftershock or foreshock of an earthquake with focal mechanism solutions, we used the same strike, dip, and rake. For those earthquakes unassociated with other events, fault dips were assigned as follows: 90º for strike-slip, 40º for reverse, and 55º for normal (Chiou & Youngs, 2008). The fault strike was assumed to be random (Chiou & Youngs, 2008). The fault type was estimated using the rake of the nearest event with focal mechanism solutions, assuming that close-to-distance events occur in the same tectonic environment. 25% of the faults with no focal mechanism solutions had the nearest event (with a focal mechanism solution) at a maximum distance equal to 3.23km, 50% at 6.02km, 75% at 11.08km, and 90% at 19.35km. We considered that a distance of up to 50Km is relatively safe to assume that these earthquakes with magnitude 4.5 or higher occurred in the same tectonic environment. 16 earthquakes were at a distance above 50km from the nearest event with a focal mechanism solution. We did not include these events in the process. The choice of the 50-kilometer maximum distance is arbitrary, but we consider it appropriate to limit the total error.

To avoid errors in this *IMs* calculation, we applied Boore et al. (2021) GMPE only for shallow crustal earthquakes; thus, based on the location of the subducting plate, a maximum depth of 50km was used to avoid including subduction earthquakes in the dataset. Also, 90% of the earthquakes modeled by a ShakeMap that produced a maximum PGA have a depth lower than 33km, and exceeded earthquake events have a maximum depth of 33km as well. Thus, we also assumed that earthquakes at depths greater than 50km could not produce a higher *IM* than this already stored from the ShakeMap footprints.

Finally, we stored the maximum *IM* calculated by Boore et al. (2021)

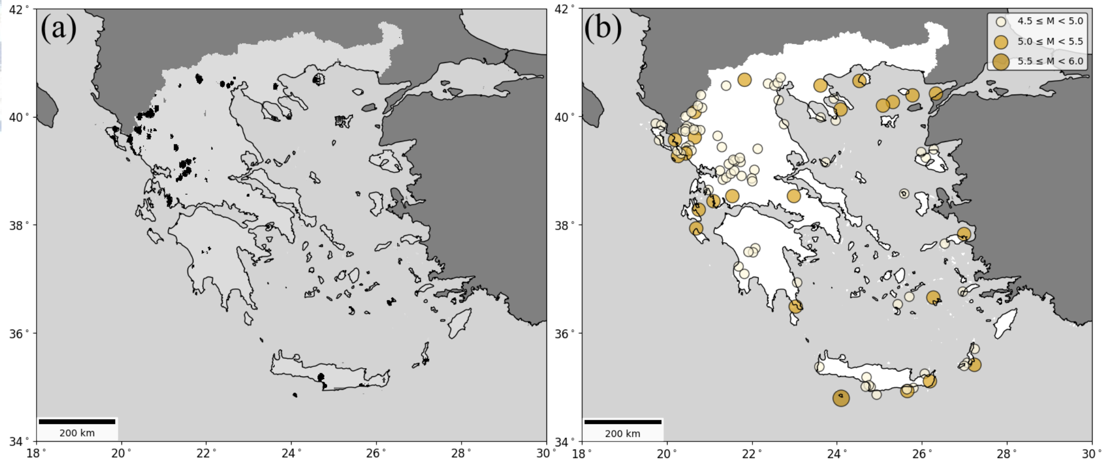

Figure 4-6. (a) The total area is illustrated with grey color. The areas with PGA estimated by Boore et al. (2021) GMPE higher than the maximum historical PGA from ShakeMap footprints are illustrated with black color (affected sites). (b) The location and magnitude of earthquake events, which are not modeled by a ShakeMap footprint, producing the PGA estimated by Boore et al. (2021) GMPE higher than the maximum historical PGA.

GMPE for the 1021 not-modeled-by-ShakeMap earthquakes that occurred in Greece and the 100-kilometer surrounding area at a depth of 50km or lower. Subsequently, we compared the maximum GMPE-calculated *IM* (calculated for rock with VS30=800m/s) with the maximum *IM* from the de-amplification approach as a more reliable approach and because its values correspond to rock sites as well. We identified 5,273 sites where the maximum GMPE-calculated PGA was higher than the maximum PGA (3.71% of the total sites), and they are illustrated in Figure 4-6, alongside the location and magnitude of the correspond earthquakes. The potential affected by a non-modeled-by-ShakeMap earthquake sites for Sa(0.3s), Sa(1.0s), and Sa(3.0s) were also identified, and the results are given in the appendix (Fig. A-7, Fig. A-8, and Fig. A-9). The affected sites are approximately located in the same areas for both PGA and SA, and they were reduced for longer periods.

From Figure 4-4 and Figure 4-6, it is clear that the magnitudes of the earthquake events that have produced the greater-than-expected PGA values are fairly higher than those that have produced the calculated-from-BooreEtAl2021 PGA, which is higher than estimated from ShakeMap footprints maximum PGA at affected sites. Furthermore, the distribution of affected sites also extends around the nearby area at the epicenter.

In order to estimate the exceedance area with greater precision, without sites that might be affected by earthquakes not modeled by a ShakeMap, we removed these sites (Fig. 4-4a) from base-grid and re-estimated the fractional exceedance area, comparing it with the expected exceedance from the PSHA maps for observation period 50 years and return period 457 years. The probability of a PSHA map being exceeded at least once is calculated from equation 1, and it is equal to 10%. Furthermore, because ShakeMaps have an uncertainty for the provided ground motion, as we mentioned before (see 2), we took into account this error term to have a measure of the variability of the fractional exceedance area (Cito et al., 2024). Thus, we calculated the exceedance area first by taking the maximum *IM* after adding one standard deviation and second by subtracting one standard deviation (these operations were done in logarithmic space). The results of the re-estimation of the exceedance area without the potentially affected sites by a non-modeled-by-ShakeMap earthquake and its one-sigma variability due to ShakeMap uncertainties are given in Table 7.

Additionally, the binomial distribution of the exceedance sites (empirical), including the "worst" and "best" scenarios (+1 std and -1 std, respectively), in comparison with the expected binomial distribution of the PSHA maps for 10% probability of exceedance for a 50-year observation period with a 475-year return period (theoretical), has been calculated and given in Figure 4-7. Generally, all PSHA models have a good fit with the data. The ESHM20, ESHM13, and GSHAP maps have estimated a higher seismic hazard. The ESHM20 and ESHM13 have an empirical fractional exceedance area approximately half that expected. Also, although EAK2000 has the greater fractional exceedance area (10.41%), compared to the other three PSHA models, it is the best fit to the expected 10% target (Fig. 4-7). Similarly, the results for Sa(0.3s), Sa(1.0s), and Sa(3.0s) are given in Figure 4-8 for ESHM20 and for ESHM13 in the appendix (Fig. A-10). Similarly to PGA, the hazard ratio has the same pattern for both the ESHM20 and ESHM13, and also, the fractional exceedance areas are close for Sa(0.3s); instead, for Sa(1.0s) and Sa(3.0s), the ESHM13 has quite smaller exceedance areas. Generally, the model that is closest to the 10% target is the ESHM20, especially for Sa(1.0s).

Finally, one could say that the ESHM20, ESHM13, and GSHAP are overly conservative. However, large-magnitude earthquakes might occur, even in low-seismicity regions (such as Thrace), with a return period that does not allow them to be on the earthquake or historical earthquake catalogs. When those rare large-magnitude earthquakes did occur, large areas would be exceeded. Thus, a PSHA model has to take into account the likelihood that these large earthquakes occur for a return period. Thus, small overestimates of the objective exceedance rate should not be considered to invalidate a PSHA model, especially when the interval time window is too small. For a different or larger observation time window, the result might be different. Thus, we believed that tests like this have to utilize different -and longer- time windows so that they end up to the most reliable model. We know that this study can provide information about the PSHA models accuracy and reliability only for the testing observational period and not in general.

4.1.3 Specific areas of interest and comparison with GMPEs results

The results for the whole of Greece have been presented above; however, fractional exceedance area and hazard ratio, or the best-fit PSHA model, might differ if a specific area is studied. The results for Athens, Thessaloniki, Lefkada, and Kefalonia are given in Table 8 and Table 9 for the ESHM20 and EAK2000, respectively, for PGA. Additionally, in Figures 4-9, 4-10, 4-11, 4-12, the fractional

Table 7. Estimated fractional exceedance area for Greece and the effect of ShakeMap uncertainty, according to four PSHA models for the de-amplification approach, without potentially affected sites by a non-modeled by a ShakeMap earthquake.

		ESHM20	ESHM13	EAK2000	GSHAP
	Expect. fractional area (%)	10	10	10	10
PGA	**Empirical fractional area (%)**	5.17	4.14	10.41	7.62
	"Worst scenario" (+one std)	17.04	14.58	31.97	23.81
	"Best scenario" (-one std)	1.11	0.96	3.15	2.45
Sa(0.3s)	**Empirical fractional area (%)**	4.68	4.61	-	-
	"Worst scenario" (+one std)	20.14	20.03	-	-
	"Best scenario" (-one std)	0.58	0.74	-	-
Sa(1.0s)	**Empirical fractional area (%)**	8.12	5.52	-	-
	"Worst scenario" (+one std)	27.06	21.48	-	-
	"Best scenario" (-one std)	1.61	1.11	-	-
Sa(3.0s)	**Empirical fractional area (%)**	4.44	1.31	-	-
	"Worst scenario" (+one std)	18.12	7.75	-	-
	"Best scenario" (-one std)	0.54	0.03	-	-

PSHA: Probabilistic seismic hazard assessment; ESHM20: European Seismic Hazard Model 2020; ESHM13: European Seismic Hazard Model 2013; EAK2000: National seismic hazard map of Greece; GSHAP: Global Seismic Hazard Assessment Program; std: Standard deviation; PGA: Peak ground acceleration; SA: Spectral acceleration

exceedance area for these regions for the ESHM20 and EAK2000 is presented. The results for ESHM13 and GSHAP are given in the supplement (hazard ratio figures and fractional exceedance area; Table S5). Also, Patras, Heraklion, and Kozani results for all PSHA maps and *IM* are given in the supplement (hazard ratio figures and fractional exceedance area; Table S5). The results for SA are given in the supplement (hazard ratio figures and fractional exceedance area; Table S6) for all specific areas.

Starting with capital Athens, both the ESHM20 and EAK2000 have approximately the same fractional exceedance area, despite their differences in ratio values (ESHM20 has a lower hazard ratio of approximately 1 value), 30.20% for ESHM20 and 38.96% for EAK2000 for Athens and surrounding area (Table 8 and Table 9), with the exceeded sites concentrated in the biggest part of the city. Exceedance areas have the same pattern for both PSHA maps and come from two earthquake events: the 6.0M earthquake on 7/9/1999 and the 6.4M earthquake on 4/3/1981. Also, a smaller part of the EAK2000 exceedance area comes from the 6.7M earthquake on 24/2/1981. Although the 6.0M earthquake on 7/9/1999 is the smallest in magnitude, it provides the highest hazard ratio and the largest area of exceedance, as it is the closest event in distance. The results for Boore et al. (2021) GMPE show a much smaller exceedance area for both PSHA maps (0.09% for ESHM20 and 1.36% for EAK2000), which corresponds to the 6.0M earthquake on 7/9/1999. Additionally, Kotha et al. (2020) GMPE shows no exceedance sites; however, both GMPEs provide the same hazard pattern (Fig. 4-9) with the ShakeMap results. The significant difference between ShakeMap and GMPEs results lies in the different way of calculating PGA, as ShakeMap

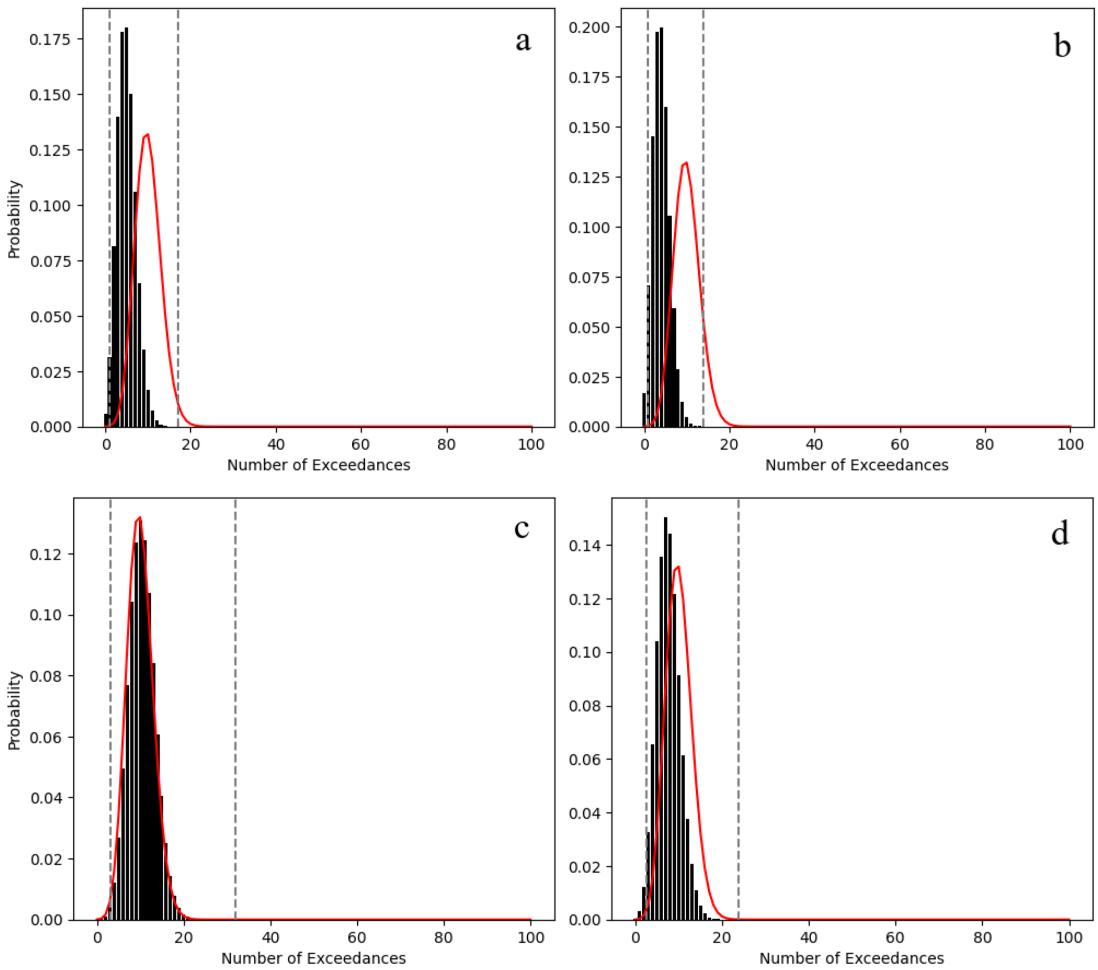

Figure 4-7. Binomial distribution of empirical exceedance area for PGA (black bars) and theoretical exceedance area (red line). The effect of ShakeMap uncertainty is given for ± one standard deviation (grey dashed line). (a) ESHM20, (b) ESHM13, (c) EAK2000, and (d) GSHAP.

software does not use a simple GMPE to calculate ground motion values but more than one, taking into account observation data as well. For ESHM13 and GSHAP, the exceedance was 22.20% and 37.52%, respectively.

Despite the different way of calculating *IMs*, the differences between ShakeMap and GMPEs results might be an effect of the way that site conditions are handled. The GMPEs estimate an *IM* at rock (VS30 = 800m/s), Instead, the ShakeMaps estimate an *IM* taking into account the site-amplification, and then they are de-amplified at rock. Thus, this variability has to be investigated in the future using different amplification factors or other approaches to handle site conditions.

Another difference is that ShakeMaps use finite rupture models or use point-source to finite-rupture equations if it is not specified (Worden et al., 2020). The use of a rupture model leads to important differences between the results. Finally, we have to mention that ShakeMaps provide the maximum value of the two horizontal components of motion (Worden et al., 2020). Instead, the

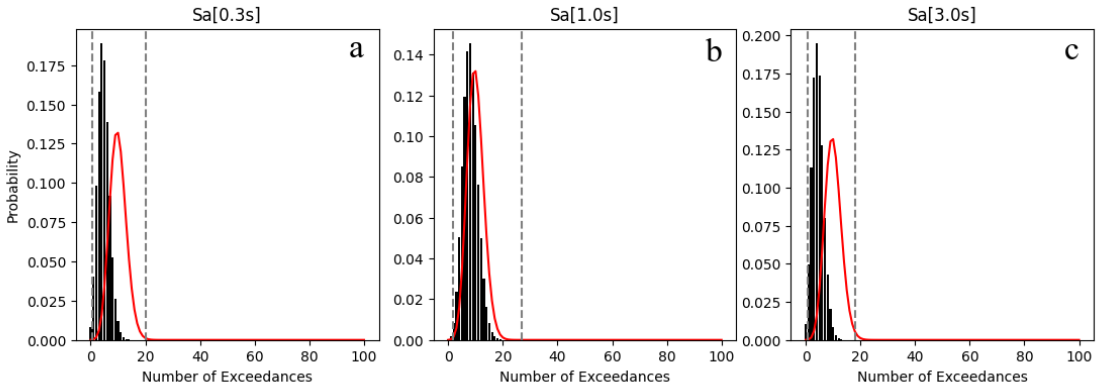

Figure 4-8. Binomial distribution of empirical exceedance area for spectral acceleration (black bars) and theoretical exceedance area fro the ESHM20 (red line). The affection of ShakeMap uncertainty is given for ± one standard deviation (grey dashed line). (a) Sa(0.3s), (b) Sa(1.0s), and (c) Sa(3.0s).

two GMPEs that we used provide the RotD50 of the horizontal components (Boore, 2006; Boore, 2010). Thus, it is reasonable for ShakeMaps to have greater exceedance area. This difference is discussed in more detail in Section 4.1.4.

In the second-largest city in Greece, Thessaloniki, ShakeMap results are not as similar for the ESHM20 and EAK2000 as they were in Athens. Instead, the ESHM20 fractional exceedance area is 14.31%, with the exceeded sites concentrated mainly in city suburbs, and EAK2000 is 53.58% (Table 8 and Table 9), with the exceeded sites spread across the city (Fig. 4-10). Also, the hazard ratio is higher for the EAK2000. For both PSHA maps, exceeded sites come from the 6.4M earthquake on 20/6/1978, occurring approximately 25km from the city. Similar to Athens, GMPEs results show no exceeded sites for both using GMPEs. For the ESHM13 and GSHAP, the exceedance was 14.15% and 16.06%, respectively.

Kefalonia and Lefkada are two islands in the Ionian Sea and have been chosen as they are located in the Kefalonia transform fault zone (Fig. 1-1), one of the most seismically active areas in Greece. The fractional exceedance area (Table 8 and Table 9) and the hazard ratio for Lefkada (Fig. 4-11) are significantly different for the ESHM20 and EAK2000. For the ESHM20, the fractional exceedance area is 4.28% (Fig. 4-11a) and limited to individual sites. Also, the hazard ratio for the exceeded sites is close to 1 (1.08 maximum value), concluding that the predicted from the ESHM20 values are close enough to the maximum PGA from ShakeMap footprints. Instead, for the EAK2000, approximately the whole island is exceeded, as the fractional exceedance area is 81.11%. Also, the hazard ratio shows that the exceeded sites are 0.5 to 1 value higher-than-predicted (Fig. 4-11d). Comparing to GMPEs results, only the EAK2000 test with Boore et al. (2021) estimated PGA provided exceeded sites (Table 9 and Fig. 4-11e). The exceedance area for both PSHA maps comes from the 6.4M earthquake on 14/8/2003. Instead, the exceedance area for Boore et al. (2021) results comes from the 6.5M earthquake on 17/11/2015. This could have many explanations, as these two GMPEs do not take into account

Table 8. Estimated fractional exceedance area for Athens, Thessaloniki, Lefkada, and Kefalonia, using ShakeMap maximum PGA from 1973 to 2023, and estimated PGA for Boore et al. (2021) and Kotha et al. (2020) GMPE for 1973-2023 earthquakes (ANSS catalog, USGS) occurred in 100km radius from each region, according to the ESHM20. The effect of ShakeMap and GMPEs uncertainty on the estimation of exceedance area is also given.

Regions	Athens			Thessaloniki			Lefkada			Kefalonia		
	S	B	K	S	B	K	S	B	K	S	B	K
Fract. exceedance area (%)	30.20	0.09	0.00	14.31	0.00	0.00	4.28	0.00	0.00	0.00	0.00	0.00
"Worst scenario" (+one std)	56.74	8.93	8.55	53.26	0.00	0.00	86.90	32.49	0.00	4.11	2.52	6.63
"Best scenario" (-one std)	9.66	0.00	0.00	0.00	0.00	0.00	0.00	0.00	0.00	0.00	0.00	0.00

S: ShakeMap; B: Boore et al., 2021; K: Kotha et al., 2020; PGA: Peak ground acceleration; ANSS: Advanced National Seismic System; USGS: U.S. Geological Survey; ESHM20: European Seismic Hazard Model 2020; GMPEs: Ground motion predicted equations; std: Standard deviation

parameters, such as directivity, that affect a site. For the ESHM13 and GSHAP, the exceedance was 22.42% and 45.59%, respectively.

The results for Kefalonia, given in Table 8, Table 9, and Figure 4-12, show no exceedance area for the ESHM20 and 0.65% for the EAK2000 for ShakeMap testing. Similarly, the results for comparison to PGA estimated from Boore et al. (2021) and Kotha et al. (2020) GMPEs show no exceedance area for the ESHM20 as well. Instead, GMPEs results for EAK2000 gave a fractional exceedance area equal to 0.84% for Boore et al. (2021) and 3.92% for Kotha et al. (2020). However, the uncertainty variability is significant, as the "worst scenario" has 53.87% exceedance area for ShakeMap and similar high values for GMPEs results. This means that the "observed" and the predicted from the EAK2000 expected values are close enough, and small changes to them significantly affect the final result. The exceedance area for the EAK2000 comes from the 7M earthquake on 17/1/1983, the 6M earthquake on 3/2/2014, and the 6.3M earthquake on 14/8/2003. On the other hand, the exceedance area for the EAK2000 from GMPEs results comes from the 6M earthquake on 3/2/2014 and from the 6.1M earthquake on 26/1/2014. For the ESHM13 and GSHAP, the exceedance was zero for both maps.

Testing for Patras and Heraklion, two large urban areas (Fig. 1-1), shows no exceedance area for Patras for all PSHA maps. Subsequently, for Heraklion, for the ESHM20 and ESHM13, there is no exceedance area as well. For the EAK2000 and GSHAP, a fractional exceedance area of 4.44% and 5.56% was identified, respectively, with low hazard ratios (below 1.1). The results from the GMPEs tasting show no exceedance area for both cities. The last area to which we applied this test was Kozani and the surrounding area (Fig. 1-1). The reason we chose this area as well was because it was there that the higher hazard ratio (difference between "observed" and predicted ground motion) appeared (Fig. 4-1). For the ESHM20, the fractional exceedance area was 51.04%; for the ESHM13, it was 52.67%; for the EAK2000, it was 93.84%; and for the GSHAP, it was 84.35%.

Table 9. Estimated fractional exceedance area for Athens, Thessaloniki, Lefkada, and Kefalonia, using ShakeMap maximum PGA from 1973 to 2023, and estimated PGA for Boore et al. (2021) and Kotha et al. (2020) GMPE for 1973-2023 earthquakes (ANSS catalog, USGS) occurred in 100km radius from each region, according to the EAK2000. The effect of ShakeMap and GMPEs uncertainty on the estimation of exceedance area is also given.

Regions	**Athens**			**Thessaloniki**			**Lefkada**			**Kefalonia**		
	S	B	K	S	B	K	S	B	K	S	B	K
Fract. exceedance area (%)	38.96	1.36	0.00	53.58	0.00	0.00	81.11	12.34	0.00	0.65	0.84	3.92
“Worst scenario” (+one std)	83.33	16.89	15.48	89.83	21.62	0.00	100.0	67.76	34.26	53.87	30.72	27.54
“Best scenario” (-one std)	19.95	0.00	0.00	9.86	0.00	0.00	10.83	0.00	0.00	0.00	0.00	0.00

S: ShakeMap; B: Boore et al., 2021; K: Kotha et al., 2020; PGA: Peak ground acceleration; ANSS: Advanced National Seismic System; USGS: U.S. Geological Survey; EAK2000: National seismic hazard map of Greece; GMPEs: Ground motion predicted equations; std: Standard deviation

The exceedance area comes from the 6.6M earthquake on 13/5/1995 and the maximum hazard ratio reach 5.44 for the GSHAP, 4.42 for the EAK2000, 2.91 for the ESHM20, and 2.86 for the ESHM13. Boore et al. (2021) GMPE results provided exceedance area for all PSHA maps but significantly smaller, and Kotha et al. (2020) GMPE results provided exceedance area only for the EAK2000 and GSHAP maps.

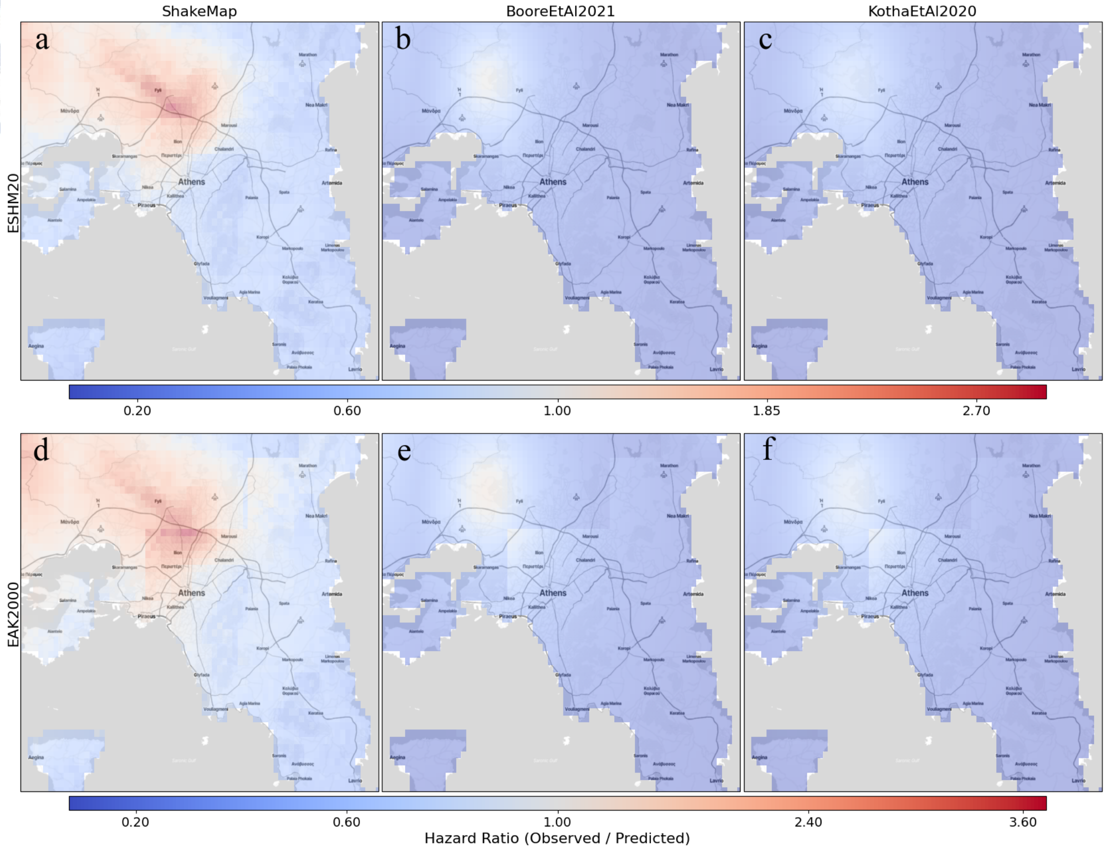

Figure 4-9. Hazard Ratio for Athens of the 1973-2023 ShakeMap footprints PGA (a,d), Boore et al. (2021) (b,e) and Kotha et al. (2020) estimated PGA from 1973-2023 ANSS catalog (USGS) earthquakes for 100km radius from the city, to the estimated PGA for 10% probability of exceedance in 50 years. Ratio maps are plotted for (a,b,c) ESHM20 (Danciu et al., 2021), (d,e,f) EAK2000. Values greater than 1.00 show where the PGA from ShakeMap footprints or GMPEs exceeds the correspond estimated from the PSHA maps.

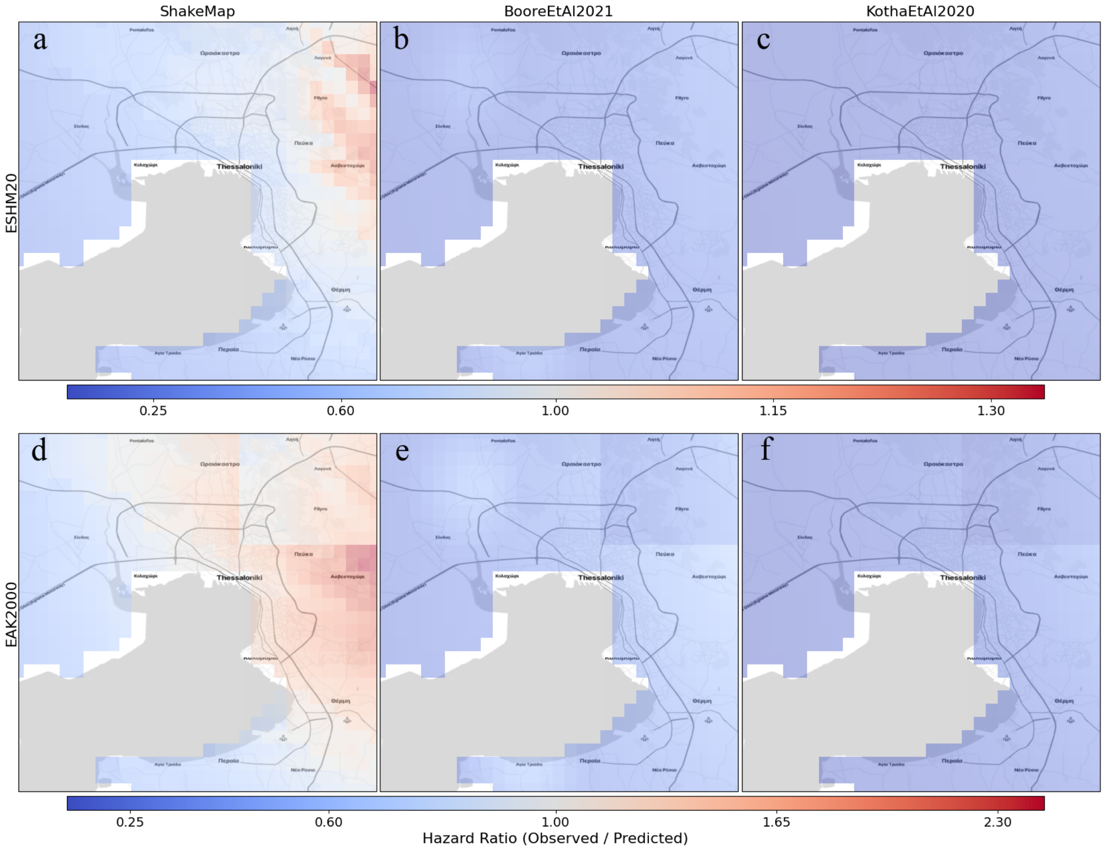

Figure 4-10. Hazard Ratio for Thessaloniki of the 1973-2023 ShakeMap footprints PGA (a,d), Boore et al. (2021) (b,e) and Kotha et al. (2020) estimated PGA from 1973-2023 ANSS catalog (USGS) earthquakes for 100km radius from the city, to the estimated PGA for 10% probability of exceedance in 50 years. Ratio maps are plotted for (a,b,c) ESHM20 (Danciu et al., 2021), (d,e,f) EAK2000. Values greater than 1.00 show where the PGA from ShakeMap footprints or GMPEs exceeds the correspond estimated from the PSHA maps.

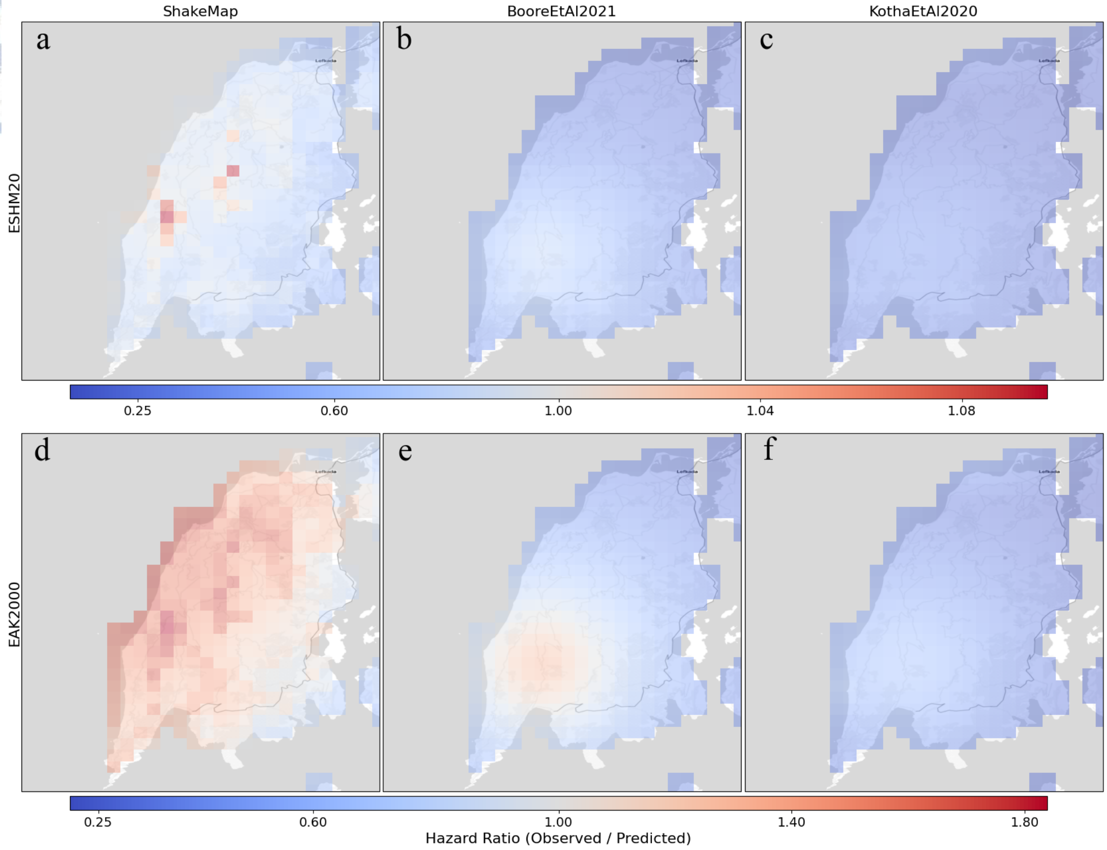

Figure 4-11. Hazard Ratio for Lefkada of the 1973-2023 ShakeMap footprints PGA (a,d), Boore et al. (2021) (b,e) and Kotha et al. (2020) estimated PGA from 1973-2023 ANSS catalog (USGS) earthquakes for 100km radius from the island, to the estimated PGA for 10% probability of exceedance in 50 years. Ratio maps are plotted for (a,b,c) ESHM20 (Danciu et al., 2021), (d,e,f) EAK2000. Values greater than 1.00 show where the PGA from ShakeMap footprints or GMPEs exceeds the correspond estimated from the PSHA maps.

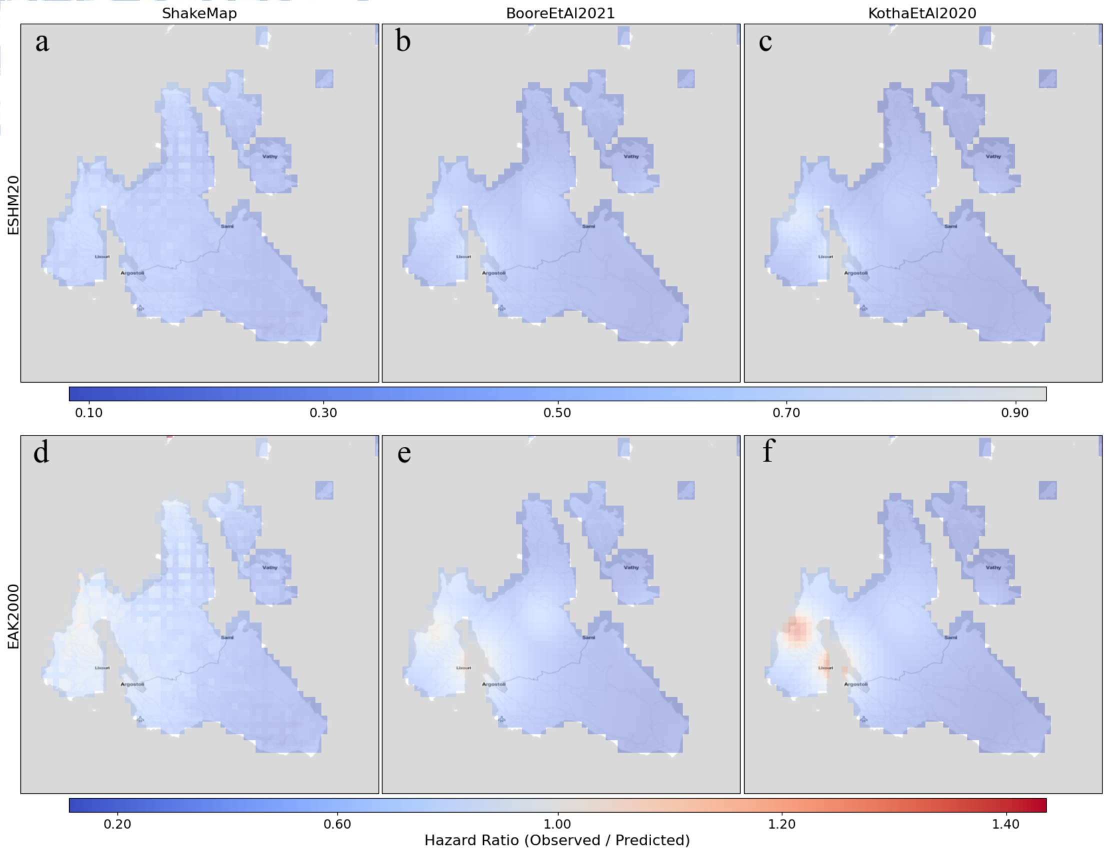

Figure 4-12. Hazard Ratio for Kefalonia of the 1973-2023 ShakeMap footprints PGA (a,d), Boore et al. (2021) (b,e) and Kotha et al. (2020) estimated PGA from 1973-2023 ANSS catalog (USGS) earthquakes for 100km radius from the island, to the estimated PGA for 10% probability of exceedance in 50 years. Ratio maps are plotted for (a,b,c) ESHM20 (Danciu et al., 2021), (d,e,f) EAK2000. Values greater than 1.00 show where the PGA from ShakeMap footprints or GMPEs exceeds the correspond estimated from the PSHA maps.

4.1.4 Using the RotD50 instead of maximum value of the two horizontal components

The ESHM20 results are valid for RotD50 of the horizontal components (Danciu et al., 2021). Likewise, the ESHM13. RotD50 is a rotation-independent measure and is described by Boore (2010) as the median (50th percentile) value of the response spectra over an azimuth given by an increment of rotation angle using the equation

$$a_{ROT}(\partial) = a_1 cos(\partial) + a_2 sin(\partial) \tag{5}$$

where a_1 and a_2 are the horizontal components, and ∂ is the rotation angle, the range of it is from 0° to less than 180°. Instead, the ShakeMap software represents peak ground motion as recorded using the larger of the two horizontal components (Worden et al., 2020).

To achieve a more accurate comparison between the results of the ShakeMaps and the PSHA maps, we use the period-dependent but magnitude- and distance-independent equation of Boore and Kishida (2017), which provides the statistical

Table 10. Estimated fractional exceedance area for Greece using the larger and the RotD50 of the two horizontal components, according to the ESHM20 and ESHM13 for the de-amplification approach, without potentially affected sites by a non-modeled by a ShakeMap earthquake. The effect of ShakeMap uncertainty is given.

		ESHM20		ESHM13	
		Large	**RotD50**	**Large**	**RotD50**
	Expect. fractional area (%)	10	10	10	10
PGA	**Empirical fractional area (%)**	5.17	3.95	4.14	3.14
	“Worst scenario” (+one std)	17.04	13.67	14.58	11.70
	“Best scenario” (-one std)	1.11	0.68	0.96	0.67
Sa(0.3s)	**Empirical fractional area (%)**	4.68	3.30	4.61	3.39
	“Worst scenario” (+one std)	20.14	16.08	20.03	15.95
	“Best scenario” (-one std)	0.58	0.32	0.74	0.45
Sa(1.0s)	**Empirical fractional area (%)**	8.12	5.94	5.52	3.98
	“Worst scenario” (+one std)	27.06	21.88	21.48	16.70
	“Best scenario” (-one std)	1.61	1.09	1.11	0.75
Sa(3.0s)	**Empirical fractional area (%)**	4.44	3.02	1.31	0.76
	“Worst scenario” (+one std)	18.12	13.80	7.75	5.54
	“Best scenario” (-one std)	0.54	0.27	0.03	0.00

PSHA: Probabilistic seismic hazard assessment; ESHM20: European Seismic Hazard Model 2020; ESHM13: European Seismic Hazard Model 2013; std: Standard deviation; PGA: Peak ground acceleration; SA: Spectral acceleration

relationships to convert among median and peak parameters and between aleatory variability for different definitions of the horizontal component of motion. Thus, we estimated the ratio between the larger of the two horizontal components to RotD50. This ratio was 1.126 for PGA and Sa(0.3s), 1.139 for Sa(1.0s), and 1.146 for Sa(3.0s). Using these ratios, we estimated the corresponding RotD50 values for the ShakeMaps.

Subsequently, we estimated the sites that are affected by an earthquake not modeled by a ShakeMap using the adjusted to RotD50 values. These sites correspond to 5.09% of the total grid for PGA. 3.60%, 1.24%, and 0.74% for Sa(0.3s), Sa(1.0s), and Sa(3.0s), respectively. The fractional exceedance area according to adjusted-to-RotD50 ShakeMaps for the ESHM20 and ESHM13 is given in Table 10. Also, the hazard ratio is given in Figure 4-13a for the ESHM20 and in Figure 4-13b for the ESHM13. The results show smaller fractional exceedance areas for both maps. Thus, the models fend off the 10% target, as the Figure 4-13c and Figure 4-13d show as well. However, the patterns of the exceedance area are still the same. This shows that the use of the larger, or RotD50, of the two horizontal components does not play a significant role in the spatial distribution of the exceedance area.

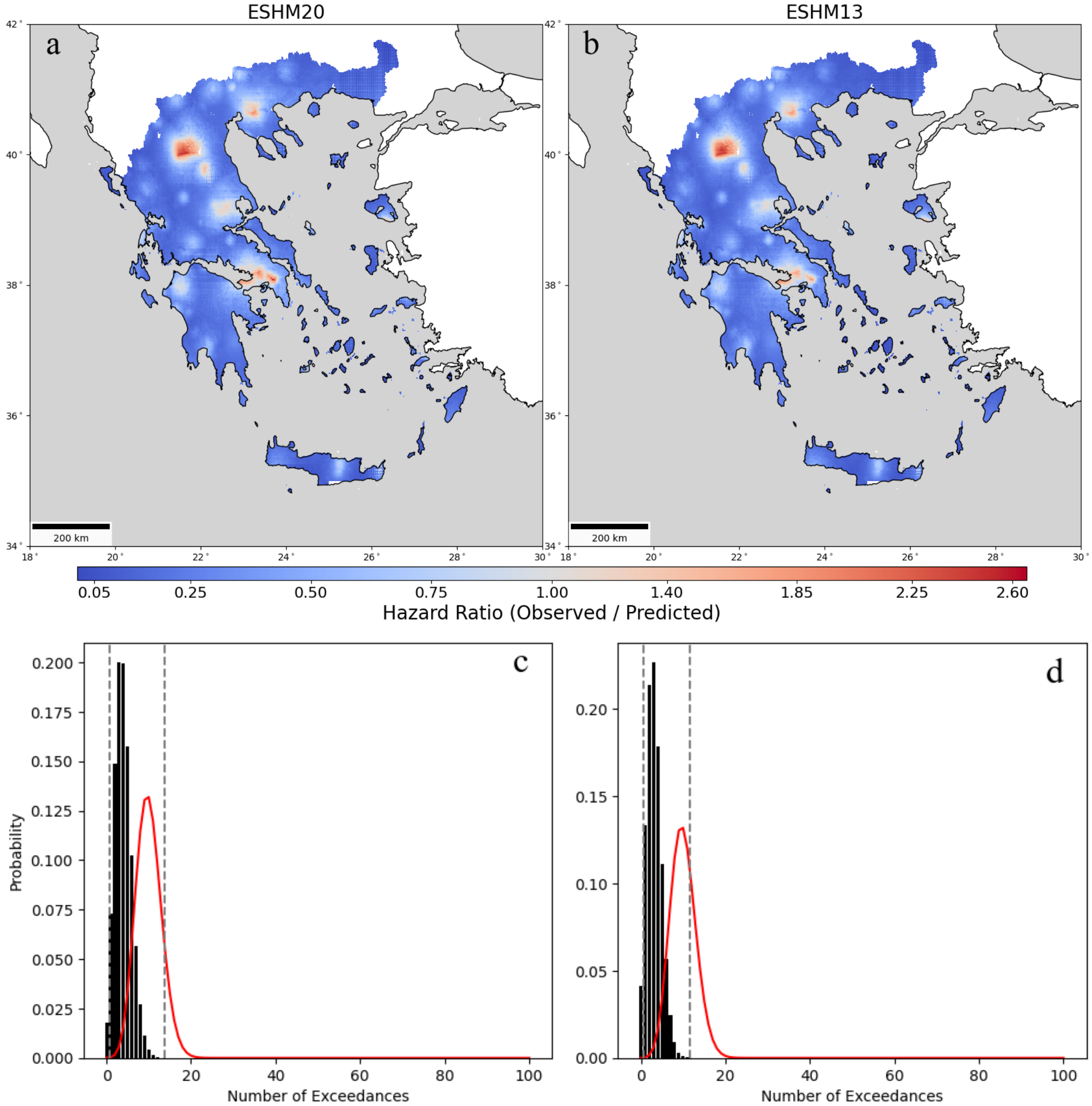

Figure 4-13. Hazard ratio of the 1973-2023 ShakeMap footprints PGA to the estimated PGA for 10% probability of exceedance in 50 years. Ratio maps are plotted for (a) ESHM20, (b) ESHM13 using the de-amplification approach. Values greater than 1.00 show where the ShakeMap footprint PGA exceeds the correspond estimated from the PSHA map PGA. ShakeMaps are adjusted to RotD50. (c, d) the Binomial distribution of empirical exceedance area for PGA (black bars) and theoretical exceedance area (red line). The effect of ShakeMap uncertainty is given for ± one standard deviation (grey dashed line). (c) ESHM20, (d) ESHM13. ShakeMaps are adjusted to RotD50.

The results for Sa(0.3s), Sa(1.0s), and Sa(3.0s) are given in Table 10, Figure 4-14, and Figure 4-15. Similar, the fractional exceedance area is smaller for adjusted-to-RotD50 ShakeMaps. However, as we mentioned for PGA, the patterns of exceedance area for SA in these three periods are still the same.

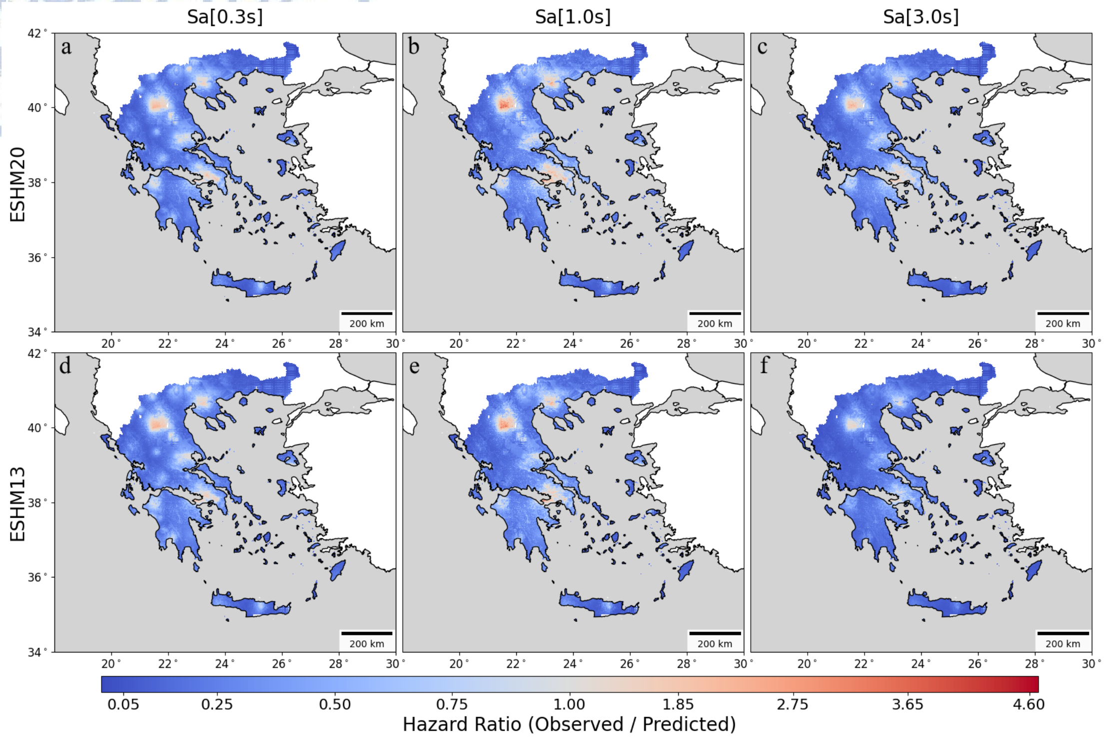

Figure 4-14. Hazard ratio of the 1973-2023 ShakeMap footprints SA to the estimated SA for 10% probability of exceedance in 50 years. (a,b,c) ESHM20. (d,e,f) ESHM13. Values greater than 1.00 show where the ShakeMaps SA exceeds the PSHA thresholds. De-amplification approach is used. The ShakeMaps are adjusted to RotD50.

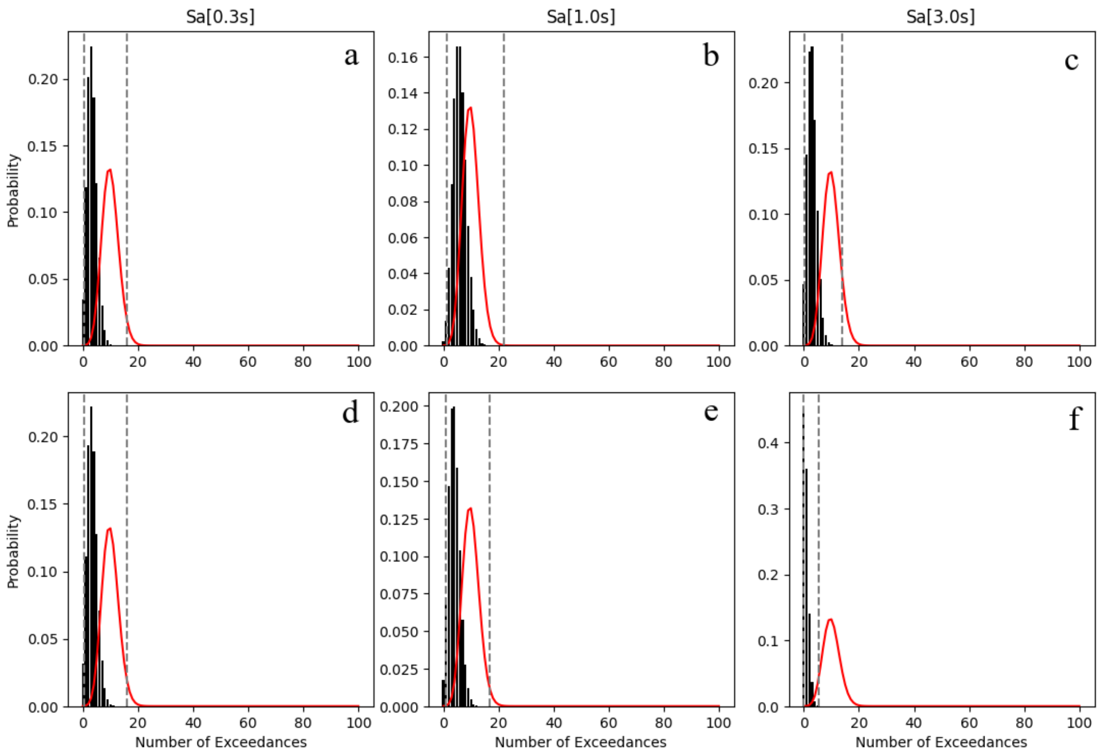

Figure 4-15. Binomial distribution of empirical exceedance area for SA (black bars) and theoretical exceedance area (red line). The effect of ShakeMap uncertainty is given for $\pm$ one standard deviation (grey dashed line). (a,b,c) ESHM20, (d,e,f) ESHM13. ShakeMaps are adjusted to RotD50.

The same process was applied for the specific areas. The results are given in the supplement of this study (Table S5 and Table S6, Figures S22-S35). As expected, the fractional exceedance areas were smaller. Also, the results from the adjusted-to-RotD50 ShakeMaps are closer to those coming from the two GMPEs. However, important differences still exist, showing that the variation between ShakeMaps and GMPEs results is more complex, as we discussed in Section 4.1.3.

4.2 Strong-motion records test

The stations (sites) with recorded *IM* from 1977 to 2023 that is above the PSHA maps thresholds are given in Table 11 for both approaches. Also, these sites and the maximum PGA recorded there are illustrated in Figure 4-16 for the average-rock approach and in Figure 4-17 for the de-amplification approach. Similarly, the results for SA are given in Figure 4-18 and Figure 4-19 for the average-rock and the de-amplification approach, respectively.

In Table 12, the number of earthquakes that have produced these above-the-thresholds *IMs* is given. The earthquakes that have produced an *IM*, which have been recorded in one of the 252 stations in Greece from 1977 to 2023, are 17 for all *IMs* and approaches. The spatial and magnitude distributions are given in Figure 4-20. Of these earthquakes, some of the *IMs* produced by them have exceeded most of the PSHA maps thresholds for both methods. Such as the 5.9Mw earthquake on 13/9/1986, the 5.4Mw earthquake on 26/3/1993, the 6.6Mw earthquake on 13/5/1995, and the 5.9Mw earthquake on 7/9/1999. All these 17 earthquakes are included in the ShakeMaps method except for two, and ten of them have produced an exceeded value in that method as well.

Table 11. Number of sites with exceeded strong-motion records for Greece for 1977 to 2023, according to four PSHA models for the two different approaches.

	Approach	**Exceeded Sites (*N*) / Exceeded Sites (%)**			
		ESHM20	**ESHM13**	**EAK2000**	**GSHAP**
PGA	**Average-rock**	3 / 1.66	3 / 1.66	12 / 6.63	7 / 3.87
	de-Amplification	3 / 1.19	1 / 0.4	11 / 4.37	9 / 3.57
Sa(0.3s)	**Average-rock**	7 / 3.87	11 / 6.08	-	-
	de-Amplification	5 / 1.98	9 / 3.57	-	-
Sa(1.0s)	**Average-rock**	3 / 1.67	5 / 2.78	-	-
	de-Amplification	4 / 1.59	4 / 1.59	-	-
Sa(3.0s)	**Average-rock**	3 / 1.68	2 / 1.12	-	-
	de-Amplification	2 / 0.79	0 / 0	-	-

ESHM20: European Seismic Hazard Model 2020; ESHM13: European Seismic Hazard Model 2013; EAK2000: National seismic hazard map of Greece; GSHAP: Global Seismic Hazard Assessment Program; PGA: Peak ground acceleration; SA: Spectral acceleration

The expected exceeded sites for the four PSHA maps with a return period of 475 years and an annual probability of exceedance of 0.2103% is calculated as described in Section 3.2.1. The distribution of the sites with exceedance is

Table 12. Number of earthquake events that have produced a maximum *IM*, according to the strong-motion record from 1977 to 2023, above the PSHA maps thresholds for the two different approaches.

	Approach	Exceeded Events (*N*)			
		ESHM20	ESHM13	EAK2000	GSHAP
PGA	Average-rock	3	3	10	7
	de-Amplification	2	1	9	7
Sa(0.3s)	Average-rock	6	10	-	-
	de-Amplification	3	7	-	-
Sa(1.0s)	Average-rock	3	4	-	-
	de-Amplification	4	4	-	-
Sa(3.0s)	Average-rock	2	1	-	-
	de-Amplification	2	0	-	-

ESHM20: European Seismic Hazard Model 2020; ESHM13: European Seismic Hazard Model 2013; EAK2000: National seismic hazard map of Greece; GSHAP: Global Seismic Hazard Assessment Program; PGA: Peak ground acceleration; SA: Spectral acceleration

presented in Figure 4-21 in comparison with the observed number of exceeded sites, according to the strong-motion records from 1977 to 2023 in Greece and the four PSHA maps. The Figure 4-21 shows the results for PGA. The results for SA are given in Figure 4-23 for the ESHM20 and in the appendix for the ESHM13 (Fig. A-11). As Table 11, Table 12, Figure 4-16, and 4-17 show, there are exceeded sites (stations) close in distance (located in the same city). These sites could not be assumed to be independent of each other (Tasan et al., 2014). Thus, if these close-in-distance sites have been exceeded by *IMs* produced by the same earthquake, we handled them as one site. Finally, we compared the number of independent exceeded sites with the expected from the PSHA maps, as it is calculated in Section 3.2.1 and presented in Figure 4-21 for PGA and Figure 4-23 for SA.

Figure 4-21 and shows that the observations are considered consistent with the PSHA maps as they are in the 2.5 and 97.5 percentile bounds (Stirling & Gerstenberger, 2010). Exception is the EAK2000, which exceeds the 97.5 percentile bound for both approaches. Also, the GSHAP exceeds the 97.5 percentile bound for the average-rock approach (Fig. 4-22). However, the number of exceeded sites is close to the 97.5 percentile bound for the de-amplification approach (9 for the de-amplification approach), which means it is not far from the observations. In Section 4.1.2, we saw that the most close-to-target PSHA map for the ShakeMap method was the EAK2000. In this method the opposite happens.

Factors affecting these results are the lack of data as the observation periods are too short for tests like this. More complete data sets could provide higher numbers of exceeded sites. Also, the limited access to stations lifetimes might lead to uncertainties in the expected distribution of the exceeded sites. However, it is a fact that, regardless of the comparison with the expected results, the EAK2000 has the biggest exceeded areas for both methods.

The results for SA are given in Figure 4-23 and Figure 4-24 for the ESHM20 and for ESHM13 in the appendix (Fig. A-11 and Fig. A-12). The results of the de-amplification approach for SA show that for Sa(1.0s) the observations are more consistent for both PSHA maps. For Sa(0.3s) and Sa(3.0s), the observations fit better to the ESHM20. Moreover, the ESHM13 is outside of the 97.5 percentile bound for Sa(0.3s), and for Sa(3.0s), it is equal to zero, according to the de-amplification approach. Thus, the ESHM20 model is the best fit for the SA strong-motion observations from 1977 to 2023. For the average-rock approach, the ESHM20 is in the bounds for the Sa(1.0s) and Sa(3.0s) and exceeds for Sa(0.3s). The ESHM13 has similar results.

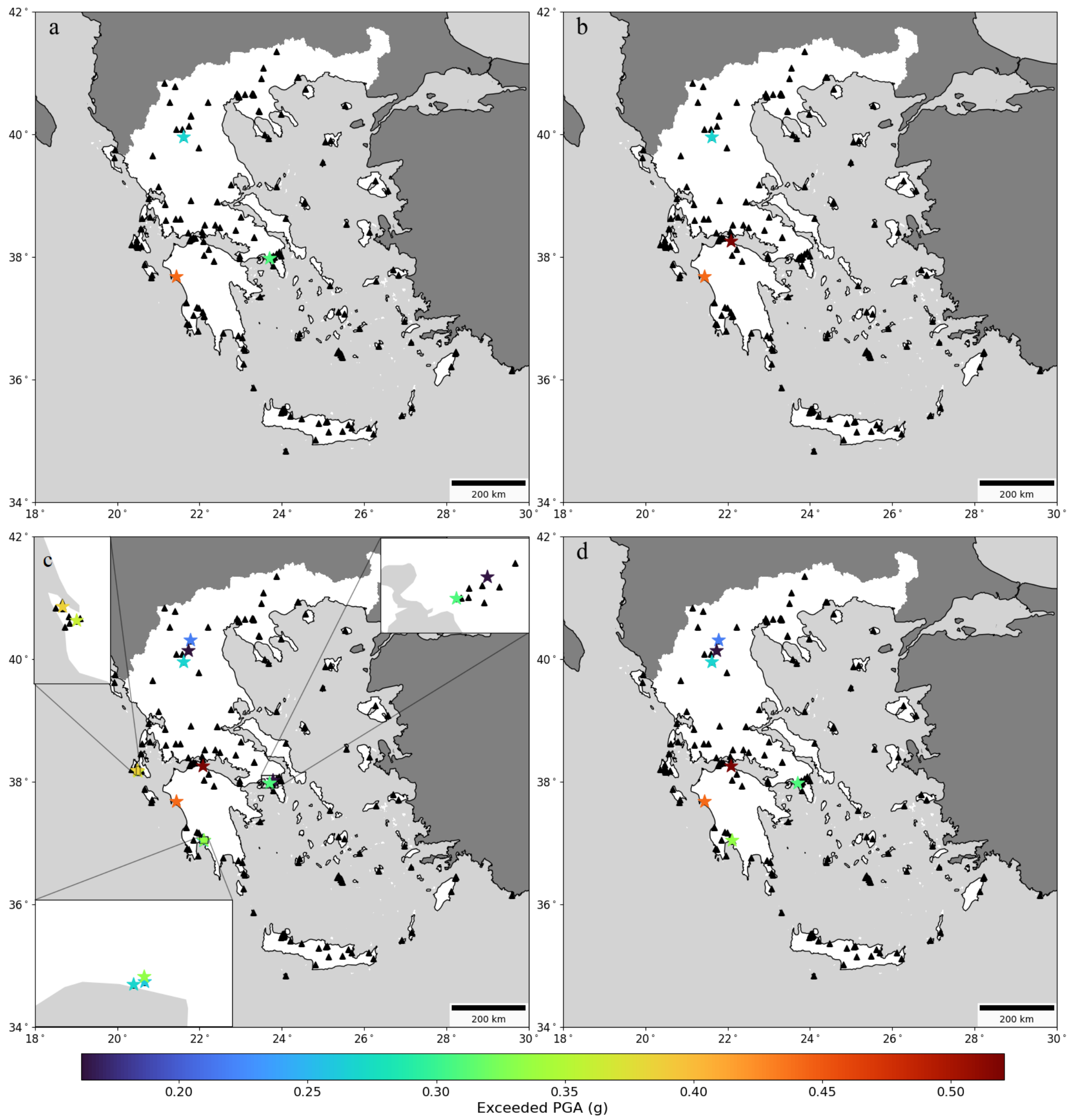

Figure 4-16. Stations (sites) with a maximum recorded PGA for the period 1977-2023 that exceeds (a) ESHM20, (b) ESHM13, (c) EAK2000, and (d) GSHAP map thresholds (stars) applying the Average-rock approach. The whole set of stations used in this study are presented as black triangles. The color scale refers to PGA levels.

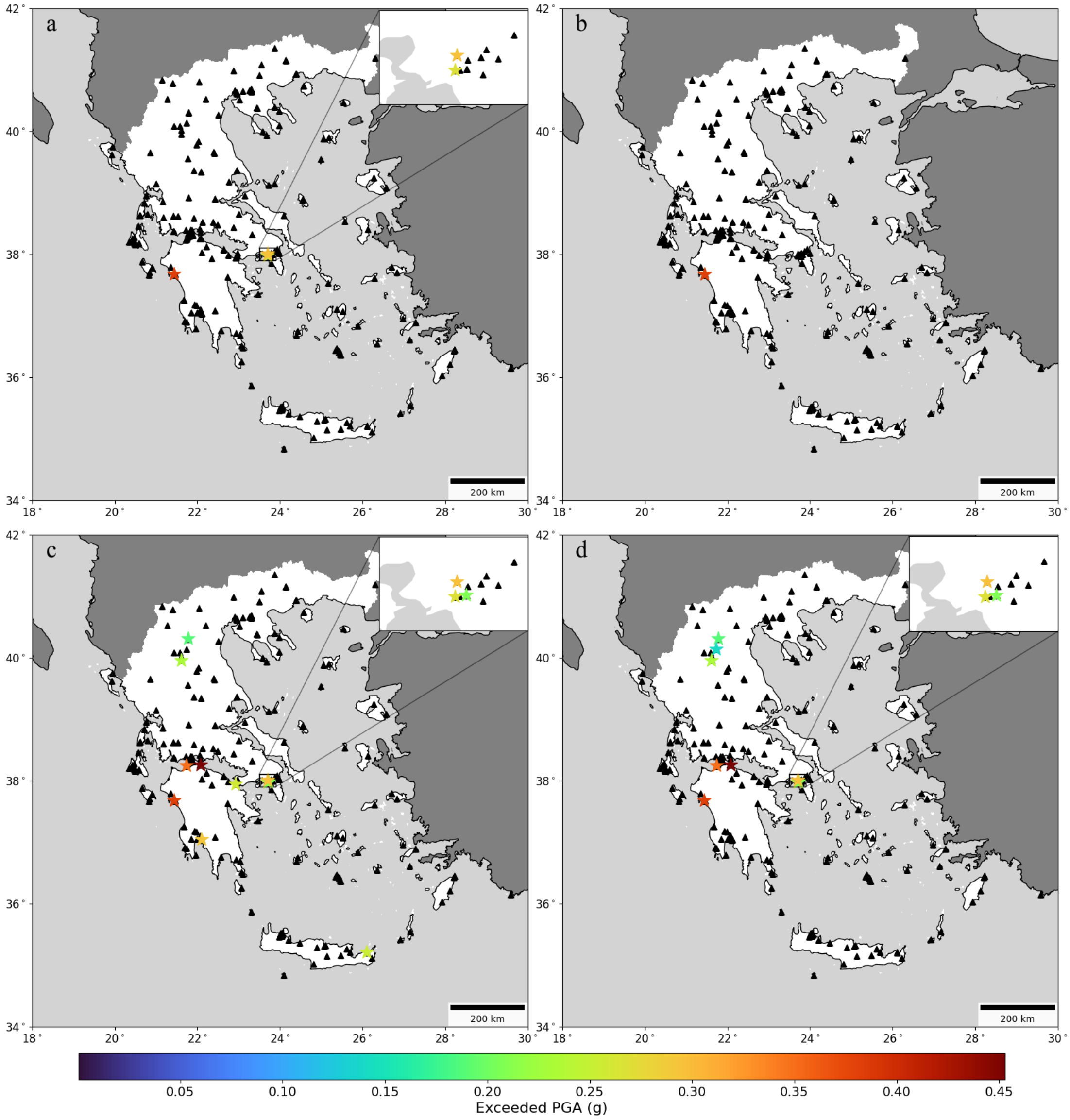

Figure 4-17. Stations (sites) with a maximum recorded PGA for the period 1977-2023 that exceeds (a) ESHM20, (b) ESHM13, (c) EAK2000, and (d) GSHAP map thresholds (stars) applying the De-Amplification approach. The whole set of stations used in this study are presented as black triangles. The color scale refers to PGA levels.

Finally, the distribution of the sites with exceedance that has been built according to the stations lifetimes has the 2.5 percentile equal to zero. This is expected for a large return period, such as 475 years, with respect to the total length of the observation time window (Tasan et al., 2014). In the case of Sa(3.0s) for the ESHM13 map, the number of exceeded sites is zero as well (de-amplification approach). In this case, no conclusions can be drawn.

Similar to the ShakeMap data, we tested the ESHM20 and ESHM13 using the RotD50. For the record that the RotD50 is not available, we calculated it using the equation 5. The results are given in Figure 4-25 for PGA. The observed number of sites with exceedance was reduced. However, the ESHM20 is in the bounds. Instead, the observed number of exceedance for the ESHM13 is zero, so no conclusions can be drawn. The results for SA are given in Figure A-15 and Figure A-16. Similar, the observed number of exceedance was reduced; however, the fit of the models in the expected distribution of sites with exceedance is the same as the results of the larger horizontal component.

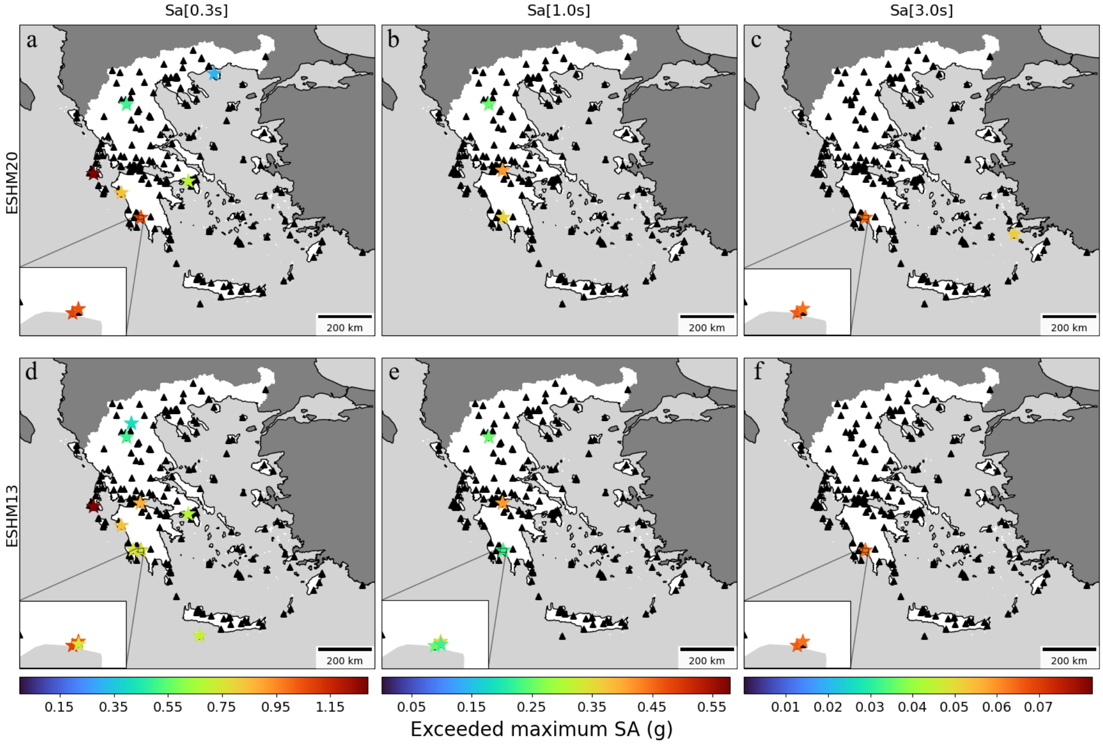

Figure 4-18. Stations (sites) with a maximum recorded SA for the period 1977-2023 that exceeds (a,b,c) ESHM20, (d,e,f) ESHM13 map thresholds (stars) applying the Average-rock approach. The whole set of station used in this study are presented as black triangles. The color scale refers to SA levels.

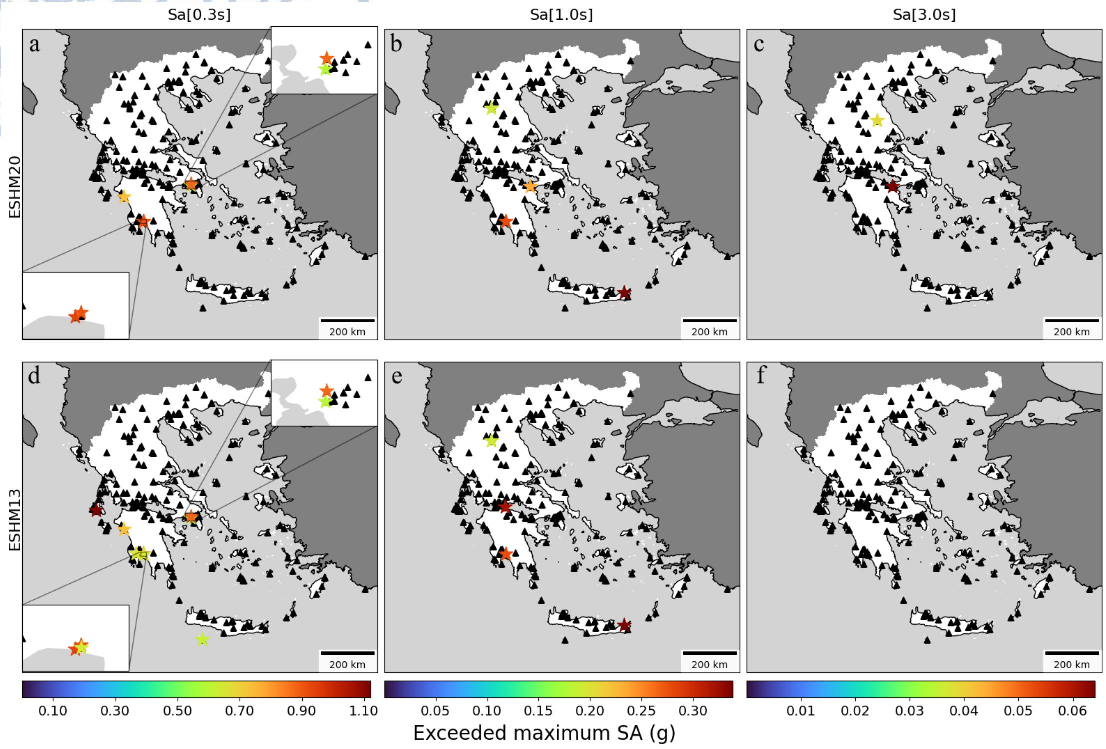

Figure 4-19. Stations (sites) with a maximum recorded SA for the period 1977-2023 that exceeds (a,b,c) ESHM20, (d,e,f) ESHM13 map thresholds (stars) applying the De-Amplification approach. The whole set of stations used in this study are presented as black triangles. The color scale refers to SA levels.

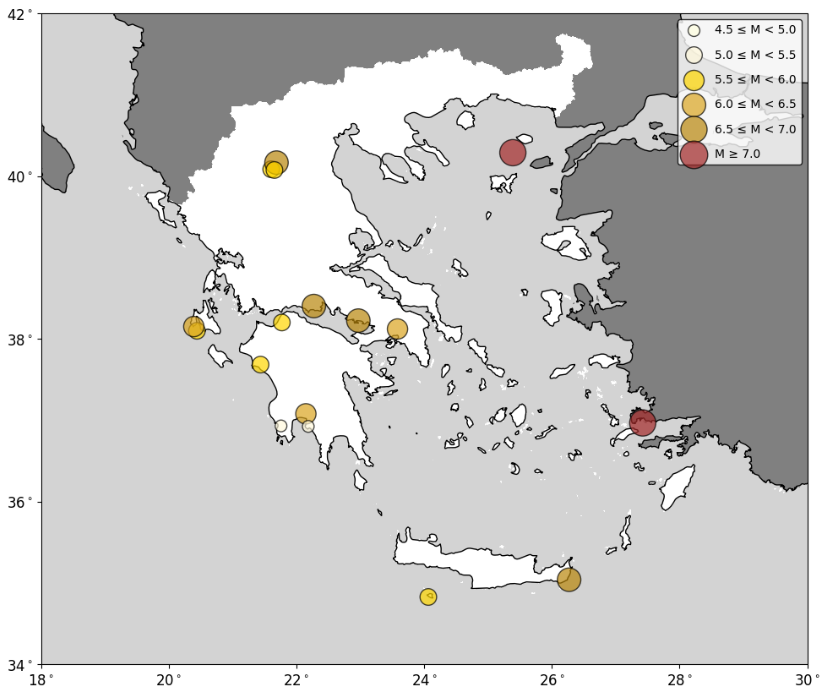

Figure 4-20. The 17 earthquake events from 1977 to 2023 that have produced strong-motion observations that exceed the PSHA maps thresholds, according to both average-rock and de-amplification approaches.

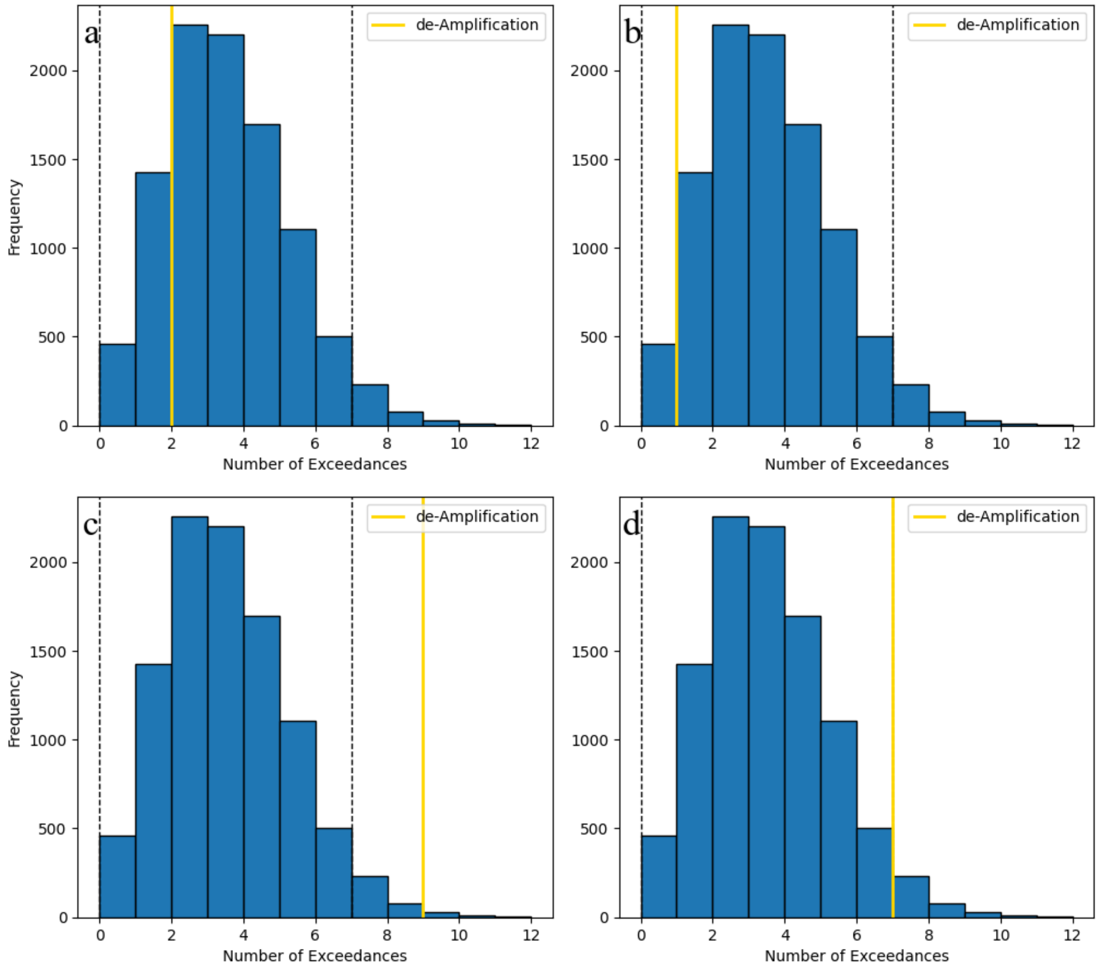

Figure 4-21. The distribution of expected exceeded sites, according to stations lifetimes and the PSHA maps annual probability of exceedance (blue bars). Lower and upper bounds, which correspond to 2.5 and 97.5 percentiles are plotted as black dashed lines. The number of observed exceeded sites due to strong-motion records for PGA from 1977 to 2023 is plotted and as yellow lines (de-amplification approach). (a) ESHM20, (b) ESHM13, (c) EAK2000, and (d) GSHAP.

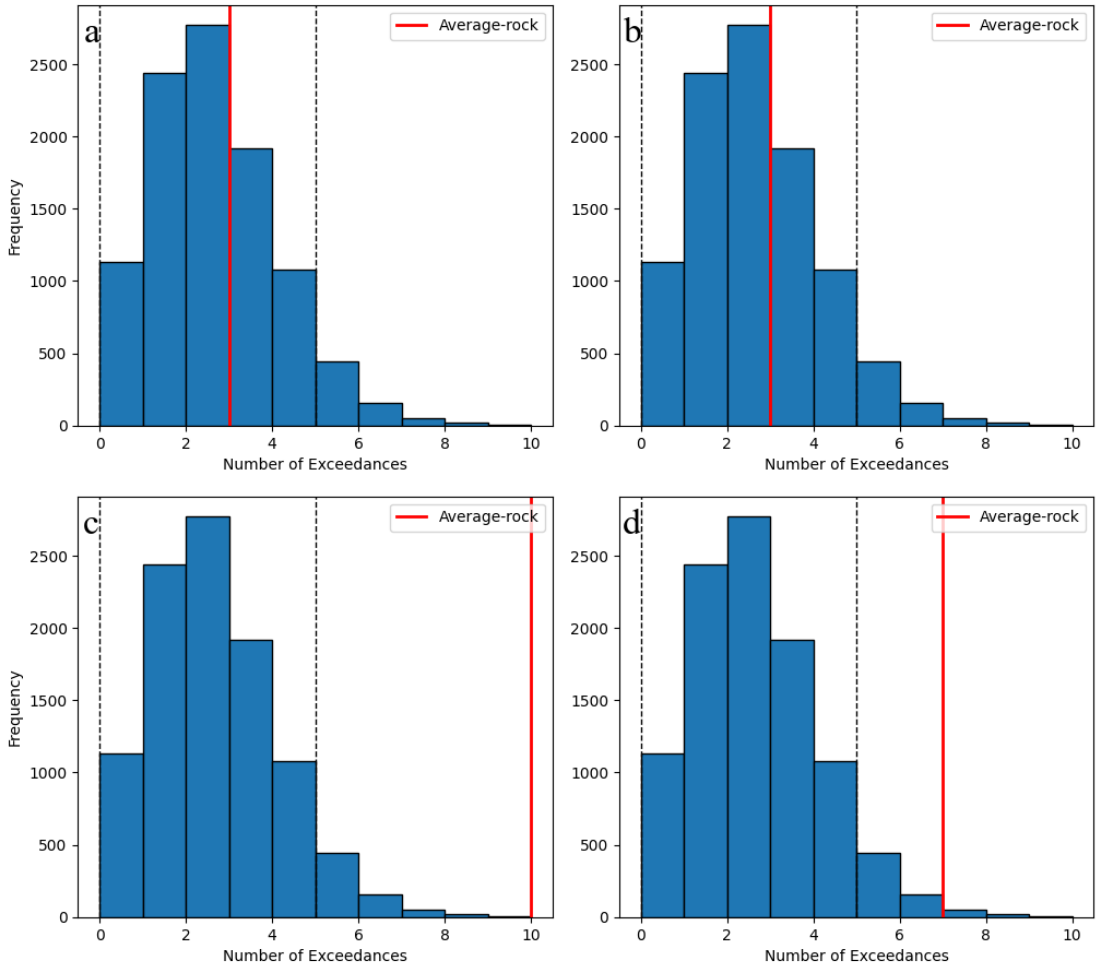

Figure 4-22. The distribution of expected exceeded sites, according to stations lifetimes and the PSHA maps annual probability of exceedance (blue bars). Lower and upper bounds, which correspond to 2.5 and 97.5 percentiles are plotted as black dashed lines. The number of observed exceeded sites due to strong-motion records for PGA from 1977 to 2023 is plotted as red lines (average-rock approach). (a) ESHM20, (b) ESHM13, (c) EAK2000, and (d) GSHAP.

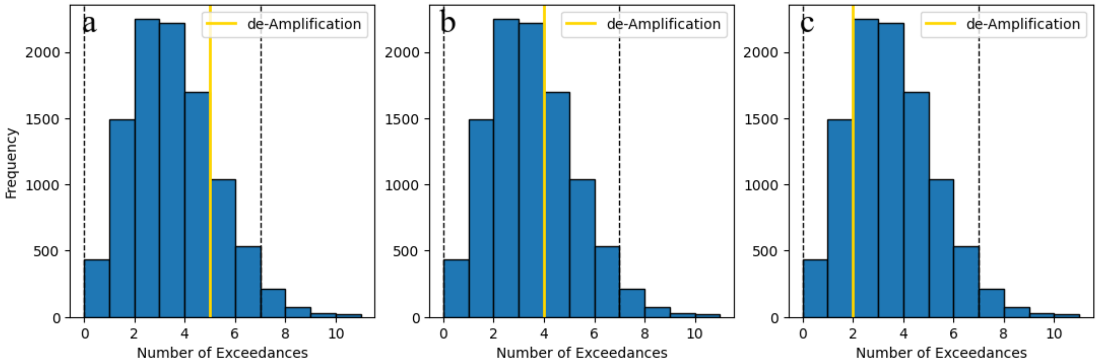

Figure 4-23. The distribution of expected exceeded sites, according to stations lifetimes and the PSHA maps annual probability of exceedance (blue bars). Lower and upper bounds, which correspond to 2.5 and 97.5 percentiles are plotted as black dashed lines. The number of observed exceeded sites due to strong-motion records for SA from 1977 to 2023 are plotted as yellow lines (de-amplification approach) according to the ESHM20. (a) Sa(0.3s), Sa(1.0s), and Sa(3.0s)

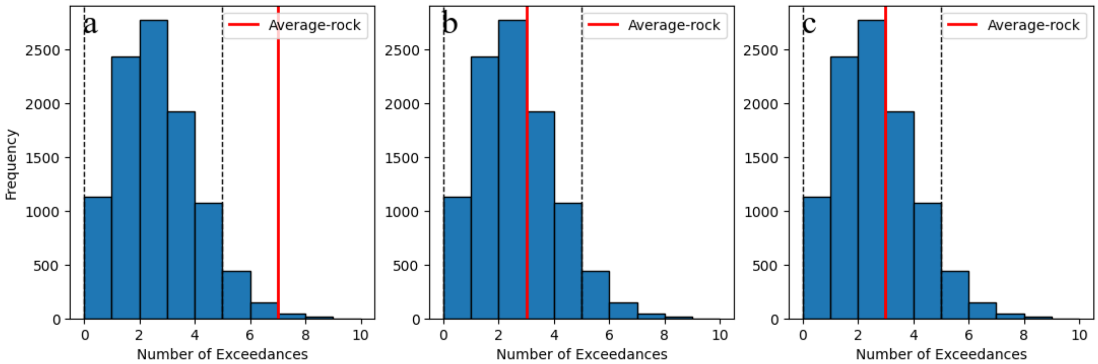

Figure 4-24. The distribution of expected exceeded sites, according to stations lifetimes and the PSHA maps annual probability of exceedance (blue bars). Lower and upper bounds, which correspond to 2.5 and 97.5 percentiles are plotted as black dashed lines. The number of observed exceeded sites due to strong-motion records for SA from 1977 to 2023 are plotted as red lines (average-rock approach) according to the ESHM20. (a) Sa(0.3s), Sa(1.0s), and Sa(3.0s)

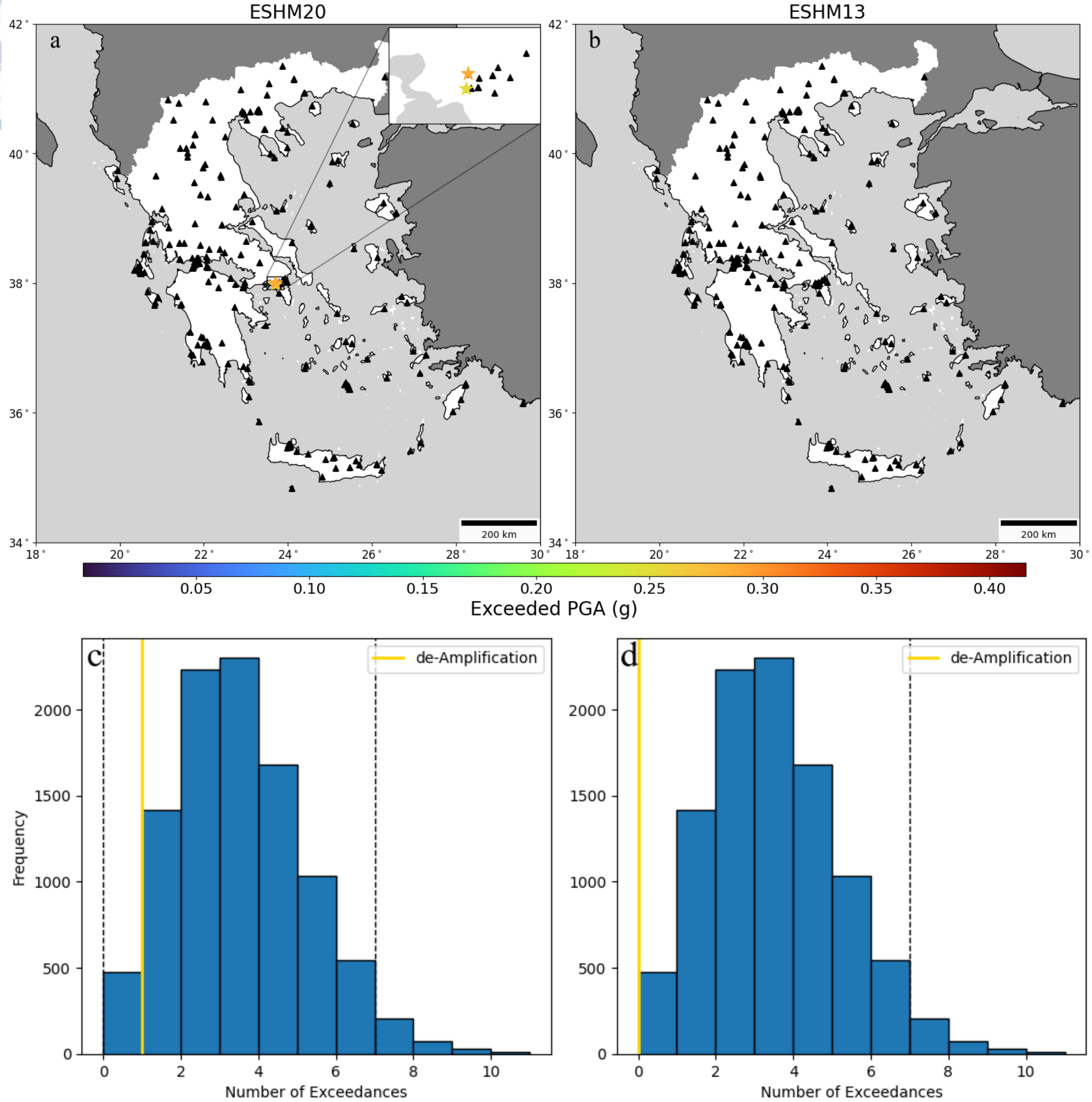

Figure 4-25. Stations (sites) with a maximum RotD50 PGA for the period 1977-2023 that exceeds (a) ESHM20, (b) ESHM13 map thresholds (stars) applying the De-Amplification approach he whole set of stations used in this study are presented as black triangles. The color scale refers to PGA levels. The distribution of expected exceeded sites, according to stations lifetimes and the PSHA maps annual probability of exceedance (blue bars). Lower and upper bounds, which correspond to 2.5 and 97.5 percentiles are plotted as black dashed lines. The number of observed exceeded sites due to strong-motion records for RotD50 PGA from 1977 to 2023 is plotted and as yellow lines (de-amplification approach). (d) ESHM20, (b) ESHM13.

4.3 Macroseismic intensity test

The sites (MDPs) with intensity-inferred PGA that exceed the PSHA maps thresholds are estimated by applying the two different approaches (average-rock and de-amplification), as they were described in this study. In Table 13, the percentage of the sites with intensity-inferred PGA from the three different GMICEs

Table 13. The percentage of the exceeded sites for Greece according to the four PSHA maps using PGA estimated by macroseismic intensity data from historical earthquakes from 1204 to 1897. The differentiation depending on the GMICE used for the conversion intensity-to-PGA is given. The effect of GMICEs uncertainty on the estimation of exceedance sites is also given.

		ESHM20			ESHM13			EAK2000			GSHAP		
		T	W	C	T	W	C	T	W	C	T	W	C
Average-Rock	**Exceeded sites (%)**	5.28	38.64	12.04	7.55	43.39	17.29	27.92	64.75	40.43	18.67	52.54	22.83
	"Worst scenario" (+one std)	91.70	75.59	71.91	90.57	75.60	72.84	97.36	90.17	89.20	95.47	83.05	80.25
	"Best scenario" (-one std)	0.00	1.36	0.00	0.00	1.70	0.00	0.00	22.03	1.54	0.00	6.10	0.30
De-Amplification	**Exceeded sites (%)**	0.29	30.70	9.95	0.58	33.50	9.95	30.05	61.38	38.43	3.18	45.53	17.60
	"Worst scenario" (+one std)	86.13	72.38	68.75	83.82	73.66	69.91	95.38	85.93	81.48	91.62	79.80	75.00
	"Best scenario" (-one std)	0.00	0.51	0.00	0.00	1.02	0.00	0.00	12.79	0.00	0.00	2.56	0.23

T: Tselentis & Danciu 2008; W: Worden et al. 2012; C: Caprio et al. 2015; PSHA: Probabilistic seismic hazard assessment; ESHM20: European Seismic Hazard Model 2020; ESHM13: European Seismic Hazard Model 2013; EAK2000: National seismic hazard map of Greece; GSHAP: Global Seismic Hazard Assessment Program; PGA: Peak ground acceleration; GMICE: Ground motion intensity conversion equation; std: Standard deviation

(Tselentis & Danciu, 2008, Worden et al., 2012, and Caprio et al., 2015) that is above the PSHAs thresholds due to historical earthquakes from 1204 to 1897 is given. As it is clear, there is considerable variation between the three different GMICEs, especially for the Worden et al. (2012) GMICE, which produced PGAs -and therefore exceeded sites- consistently higher than the other two GMICEs. Also, the exceeded site variation is significant between the "Worst" and "Best" scenarios, showing the crucial effect of GMICEs uncertainty. The effect of GMICEs uncertainty can range from 0% exceeded sites for the "Best scenario" to 97% for the "Worst scenario" in some cases; thus, the estimation of the exceeded sites is uncertain enough for the results of some GMICEs.

The difference between the Worden et al. (2012) GMICE and the other two GMICEs exists because the first tends to estimate higher PGAs in comparison with the other two. It should be noted that the Worden et al. (2012) GMICE takes into account the effect of the magnitude and distance-to-rupture. Thus, it is logical that there are differences in the results in relation to those of the other two GMICEs. Also, the Worden et al. (2012) GMICE necessarily contains uncertainty of the magnitude and depth estimation, as well as the use of hypocentral distance instead of the distance-to-rupture. Generally, testing PSHA map against macroseismic intensity data from historical earthquakes is a quite challenging process as there are a lot of uncertainties in the calculations, from earthquake location and magnitude estimation to intensity estimation and conversion to PGA. Figure 4-26 and Figure 4-27 show the effect of GMICEs uncertainty on exceeded sites estimation. As we mentioned before and can be obvious from these Figures, this effect is significant. Thus, the results of this method should be treated with caution and reservation.

Apart from the significant variation in the results, the EAK2000 always has the highest percentage of exceeded sites, the GSHAP and the ESHM13 follow, and the PSHA model with the lowest percentage is the ESHM20. Based on equation 1, the probability of exceedance for a PSHA map with a return period of 475 years and an observation period of 693 years (from 1204 to 1897) is 76.75%. However, a comparison between the expected rate of exceedance and this given by the macroseismic intensity data from historical earthquakes could not be done, as the considered dataset of historical earthquakes is not complete (Cito et al., 2024). Nevertheless, a computation of the number of sites that experienced at least one exceedance due to the 48 historical earthquakes could be done.

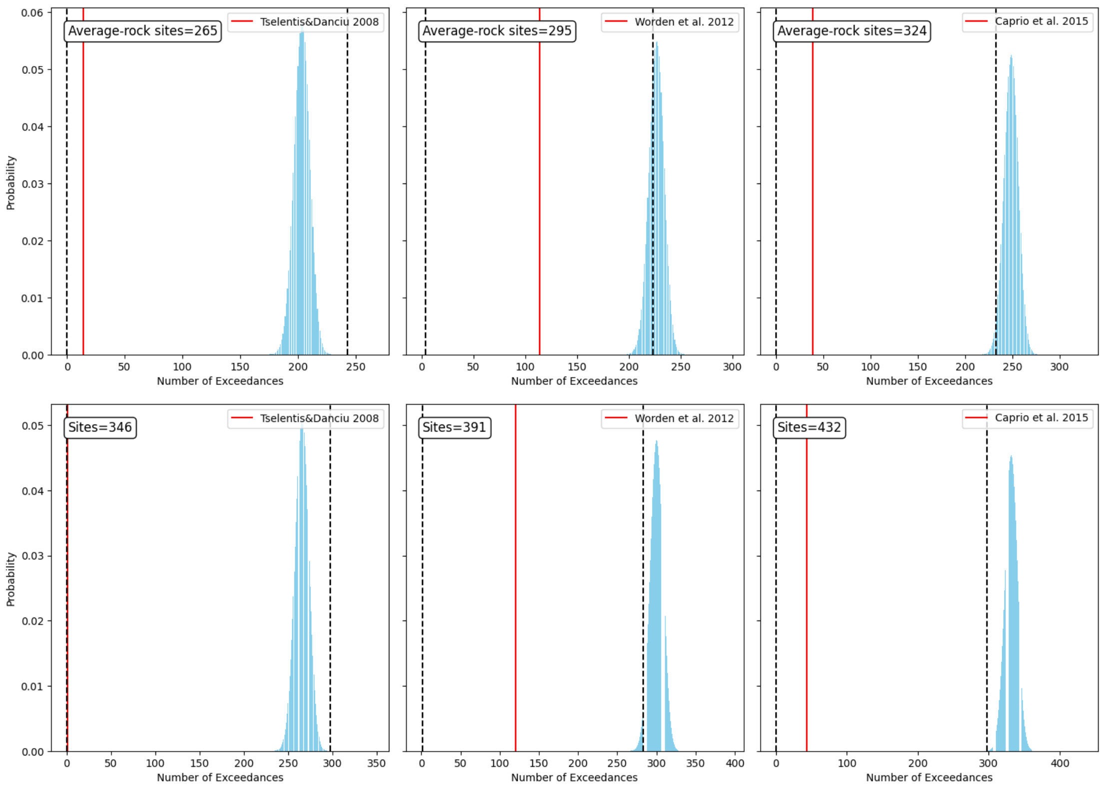

Figure 4-26. The 76.75% probability distribution for a PSHA map with a return period of 475 years and an observation period of 693 years (blue bars). With red lines, the number of observed exceeded sites, due to the strong-shaking produced by the 48 considered historical earthquakes from 1204 to 1897, according to the ESHM20 for the three different GMICEs and the two different approaches. The effect of GMICEs uncertainty on the estimation of exceedance sites is also given (black dashed line). (top) the average-rock approach, (bottom) the de-amplification approach.

Thus, indicatively, the distribution of the 76.75% probability of exceedance was calculated and presented in Figure 4-26 and Figure 4-27 along with the results for the ESHM20 and EAK2000, respectively. The corresponding Figures for the ESHM13 and GSHAP are given in the appendix (Fig. A-13 and Fig. A-14). According to these Figures, the EAK2000 is closer to the expected target; however, as mentioned before, no comparison between the expected and empirical numbers of exceedance can be done. A completed data set might lead to a significantly different number of exceeded sites, so this test only concerns the number of sites that experienced at least one exceedance due to these 48 considered historical earthquakes and nothing more.

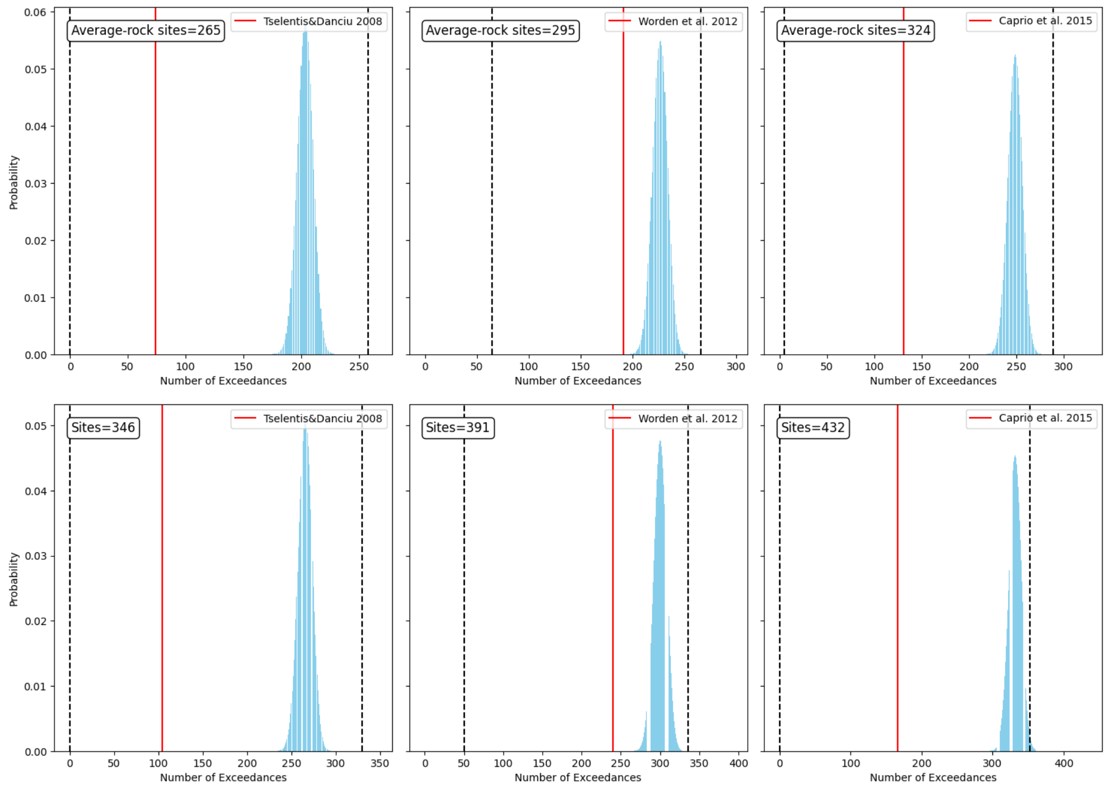

Figure 4-27. The 76.75% probability distribution for a PSHA map with a return period of 475 years and an observation period of 693 years (blue bars). With red lines, the number of observed exceeded sites, due to the strong-shaking produced by the 48 considered historical earthquakes from 1204 to 1897, according to the EAK2000 for the three different GMICEs and the two different approaches. The effect of GMICEs uncertainty on the estimation of exceedance sites is also given (black dashed line). (top) the average-rock approach, (bottom) the de-amplification approach.

5. Conclusion

Four Probabilistic Seismic Hazard Assessment (PSHA) maps— ESHM20, ESHM13, EAK2000, and GSHAP— were evaluated against empirical data from a) ShakeMap footprints, b) strong-motion records, and c) macroseismic intensity data pertaining to historical earthquakes in Greece. For each PSHA map, we calculated the fractional exceedance area, defined as the proportion of sites where Peak Ground Acceleration (PGA), Spectral Acceleration at 0.3s (Sa[0.3s]), 1.0s (Sa[1.0s]), and 3.0s (Sa[3.0s]) exceeded values predicted by the respective PSHA models. Additionally, we generated hazard ratio maps by dividing observed Intensity Measures (*IM*) from ShakeMap by predicted values for each site.

Two distinct methodologies were implemented to address site conditions. First, we conducted analyses for sites with a shear wave velocity (VS30) equal to or exceeding 400 m/s, aligning with an average-rock approach, which considers sites with a generalized category of rock without specific mechanical properties, given the scarcity of true rock sites ($VS30 \geq 800m/s$) in Greece as per Eurocode 8 classification. Second, we applied a de-amplification approach, adjusting the *IMs* from ShakeMaps using amplification factors proposed by Borcherdt (1994) to approximate rock-site conditions. Results from the de-amplification approach indicated smaller exceedance areas and hazard ratios relative to the average-rock approach. Given the significant differences in ground motion characteristics between sites with VS30 values of 400 m/s and 800 m/s, we deemed the de-amplification approach to be more reliable.

ShakeMaps: We analyzed 602 ShakeMap footprints from January 1973 to January 2023, sourced from the USGS and NOA databases, focusing on earthquakes with magnitudes of 4.5 or higher within Greece and a surrounding 100-kilometer radius. To account for potential earthquakes not represented in the ShakeMap data, we employed the methodology described by Pothon et al. (2020) to identify additional earthquakes from the ANSS catalog (USGS) that might produce *IM* values exceeding those captured by the 602 ShakeMaps. Subsequently, we utilized Ground Motion Prediction Equations (GMPEs) from Boore et al. (2021) to estimate *IMs* from these earthquakes, identifying sites where these estimates exceeded those from the ShakeMap footprints. We excluded these sites from further analyses and recalculated the fractional exceedance areas, incorporating uncertainties associated with the ShakeMap data. These results were compared against expectations derived from the PSHA models with a return period of 475 years and an observation period of 50 years (1973-2023). Overall, all PSHA models displayed a good correlation with the observed data (Fig.

4-7). Notably, ESHM13 and ESHM20 tended to overestimate the *IMs* reported by ShakeMap, while GSHAP yielded exceedance areas that closely aligned with the predicted targets. Despite EAK2000 exhibiting the highest fractional exceedance area (10.02%), it approached the 10% target most closely when evaluated with the de-amplification approach.

In terms of the spatial distribution of exceedance areas, all PSHA models exhibited similar patterns, often associated with the same seismic events. Nevertheless, significant discrepancies were observed between the expected and observed values across different PSHA models (Fig. 4-1). Specifically, ESHM13 demonstrated a tendency to overpredict Spectral Acceleration, particularly at Sa(0.3s) and Sa(3.0s), while ESHM20 provided a better fit, especially for Sa(1.0s), closely approximating the predicted target (Fig. 4-8).

The evaluation was conducted across large urban areas and regions of specific interest. Notably, while EAK2000 displayed a strong fit at a national level, analyses for urban centers like Athens, Thessaloniki, and Lefkada revealed considerable exceedance areas and hazard ratios. This highlights that local ground shaking levels may be significantly impactful, although the overall PSHA map still meets the 10% target. This does not imply that EAK2000 underestimates seismic hazards; rather, it indicates the necessity for targeted studies in regions adjacent to major active faults to refine earthquake engineering demands. Furthermore, while ESHM13 had the smallest exceedance area overall, assessments for Lefkada showed that ESHM20 produced lower exceedance areas and hazard ratios, reflecting its conservative approach to regions with heightened seismic activity.

It is critical to note that exceedance at a site does not inherently indicate severe ground shaking. As anticipated, exceedance sites were predominantly located near the epicenters of significant seismic events (Fig. 4-3). However, substantial ground shaking levels (e.g., $PGA \geq 0.2$g or 0.3g) were observed at distances exceeding 30 km from epicenters (Fig. 4-3).

In further evaluations, we compared results from the PSHA maps against those derived from two GMPEs, Boore et al. (2021) and Kotha et al. (2020). We calculated the maximum *IM* assuming rock conditions (VS30 = 800 m/s) for all earthquakes in the ANSS catalog occurring within a 100-kilometer radius of each area of interest. Following this, we employed a similar methodology to analyze ShakeMap footprints. The fractional exceedance areas derived from GMPEs were generally smaller, occasionally approaching zero (Tables 8 and Table 9). However, hazard ratio patterns remained consistent between both ShakeMap and GMPE results. This consistency arises because ShakeMap utilizes multiple GMPEs along with observational data, such as strong motion records and intensity estimates, thus reducing uncertainty compared to single GMPE outputs. Consequently, a single GMPE may overlook specific site characteristics or effects such as directivity.

Strong Motion Records: Subsequently, we evaluated the PSHA maps against strong-motion observations, utilizing a dataset comprising 7,641 records from 650 earthquakes with magnitudes of 4.5 or higher, recorded between 1977 and 2023. This dataset encompasses records from the ESM flat-file and ESM strong-motion database, covering 252 stations across Greece. For each station, we assessed its operational history or calculated it from the available raw record data (without magnitude filtering), correcting for any identified gaps in the data. We then estimated the expected number of exceedances based on the stations' lifetimes and the PSHA maps' annual probability of exceedance. A comparison of the observed distribution of exceeded sites against the expected distribution indicated that observations were largely consistent with ESHM20 and ESHM13. In contrast, GSHAP was found in the 97.5th percentile, while EAK2000 fell outside the expected bounds. For spectral acceleration, ESHM20 aligned well with observations, whereas ESHM13 matched only for Sa(1.0s).

In the ShakeMap analysis, exceedance areas were linked to 58 earthquakes occurring between 1973 and 2023. In the strong-motion analysis, exceedance sites were identified for 17 earthquakes from 1977 to 2023, with 10 of these events also contributing to exceedance areas in the ShakeMap assessment. Both methods exhibited agreement regarding exceedance area locations, particularly for significant ground motion levels, underscoring the utility of ShakeMap data in such analyses, especially given the limitations of strong-motion records over extended observation periods.

Tests for ESHM20 and ESHM13 were also performed on RotD50 (Boore, 2006; Boore, 2010), as these models are valid for this metric. We adjusted ShakeMaps to RotD50 using statistical relationships outlined by Boore and Kishida (2017). While the fractional exceedance area was reduced, the patterns of exceedance remained consistent. In the strong-motion analysis, RotD50 values were calculated where not available, resulting in a reduction in observed exceedances; however, the models still adhered to the 2.5th and 97.5th percentile bounds of the expected exceedance distribution.

Macroseismic Intensity Data: Lastly, we conducted an analysis utilizing macroseismic intensity data from historical earthquakes, incorporating 688 intensity estimations from 48 earthquakes occurring between 1204 and 1897, sourced from the AHEAD database. We converted these intensities into PGA values using three GMICEs: Tselentis and Danciu (2008), Worden et al. (2012), and Caprio et al. (2015). Following this, we determined the exceeded sites according to the four PSHA maps. Results varied among GMICEs; Tselentis and Danciu (2008) and Caprio et al. (2015) yielded similar outcomes, while Worden et al. (2012) produced a greater number of exceeded sites due to its higher estimated PGA values. The EAK2000 PSHA map identified the highest number of exceedances, followed by GSHAP, while ESHM20 recorded the fewest.

The results could not be directly compared to the PSHA maps' 76.75% target for a return period of 475 years and an observation period of 693 years (1204-1987) due to data incompleteness. However, a theoretical probability distribution derived from the 48 historical earthquakes illustrated that all PSHA models yielded fewer exceeded sites, with EAK2000 aligning most closely with the target. It is essential to recognize that a more complete dataset for this 693-year period could significantly alter exceedance numbers. Moreover, this methodology carries considerable uncertainty due to the conversion of intensity to PGA. Alongside GMICE uncertainties, estimating macroseismic intensities involves complex challenges, including uncertainties surrounding earthquake location, magnitude, and depth. Also, the intensity estimations are subjective and include the uncertainty nature of intensity observations and the variability in the human experience of ground shaking (Manea et al., 2024). Thus, these results should be treated with caution.

The results of this study highlight the necessity for a critical evaluation of the PSHA models currently employed in Greece. The variations in fractional exceedance areas derived from different methodologies underscore the influence of site conditions on ground motion predictions. This reinforces the importance of integrating local geological data and site-specific characteristics, and further refinement in site classification methodologies, integrated into PSHA assessments.

Future research should focus on expanding the dataset of historical earthquakes to strengthen the reliability of PSHA models. Incorporating a more comprehensive set of strong-motion records and macroseismic intensities will allow for better validation and calibration of existing models. Additionally, further studies could explore the integration of machine learning techniques to analyze complex seismic data and refine ground motion prediction equations to model local site effects more accurately, particularly in urban environments where infrastructure vulnerability is critical. Moreover, collaborative community efforts could facilitate the sharing of data and methodologies, providing a more unified approach to seismic hazard assessment across Europe.

Bibliography

Albarello, D., & D'Amico, V. (2008). Testing probabilistic seismic hazard estimates by comparison with observations: An example in Italy. *Geophysical Journal International*, *175*(3), 1088–1094. https://doi.org/10.1111/j.1365-246X.2008.03928.x

Albini, P., & Pantosti, D. (2004). The 20 and 27 April 1894 (Locris, Central Greece) Earthquake Sources through Coeval Records on Macroseismic Effects. *Bulletin of the Seismological Society of America*, *94*, 1305–1326. https://doi.org/10.1785/012003174

Albini, P., Locati, M., Rovida, A., & Stucchi, M. (2013). European Archive of Historical Earthquake Data (AHEAD). *Istituto Nazionale di Geofisica e Vulcanologia (INGV)*. https://doi.org/10.6092/ingv.it-ahead

Allen, T. I., & Wald, D. J. (2007). Topographic slope as a proxy for seismic site conditions and amplification. *Bulletin of the Seismological Society of America*, *97*. https://doi.org/10.1785/0120060267

Allen, T. I., Ghasemi, H., & Griffin, J. D. (2023). Exploring Australian hazard map exceedance using an Atlas of historical ShakeMaps. *Earthquake Spectra*, *39*(2), 985–1006. https://doi.org/10.1177/87552930231151977

Allen, T. I., Wald, D. J., Earle, P. S., Marano, K. D., Hotovec, A. J., Lin, K., & Hearne, M. G. (2009). An Atlas of ShakeMaps and population exposure catalog for earthquake loss modeling. *Bulletin of Earthquake Engineering*, *7*(3), 701–718. https://doi.org/10.1007/s10518-009-9120-y

Baker, J. (2008). An introduction to Probabilistic Seismic Hazard Analysis (PSHA).

Banitsiotou, I., Tsapanos, T., Margaris, B., & Hatzidimitriou, P. (2004). Estimation of the seismic hazard parameters for various sites in Greece using a probabilistic approach. *Natural Hazards and Earth System Sciences*, *4*. https://doi.org/10.5194/nhess-4-399-2004

Båth, M. (1965). Lateral inhomogeneities of the upper mantle. *Tectonophysics*, *2*(6), 483–514.

Benetatos, C., Kiratzi, A., Roumelioti, Z., Stavrakakis, G., Drakatos, G., & Latoussakis, I. (2005). The 14 August 2003 Lefkada Island (Greece) earthquake: Focal mechanisms of the mainshock and of the aftershock sequence. *Journal of Seismology*, *9*, 171–190. https://doi.org/10.1007/s10950-005-7092-1

Boore, D. (2006). Orientation-independent measures of ground motion. *Bulletin of the Seismological Society of America*, *96*, 1502–1511. https://doi.org/10.1785/0120050209

Boore, D. (2010). Orientation-independent, nongeometric-mean measures of seismic intensity from two horizontal components of motion. *Bulletin of The Seismological Society of America - BULL SEISMOL SOC AMER*, *100*, 1830–1835. https://doi.org/10.1785/0120090400

Boore, D., & Kishida, T. (2017). Relations between some horizontal-component ground-motion intensity measures used in practice. *Bulletin of the Seismological Society of America*, *107*. https://doi.org/10.1785/0120160250

Boore, D., Stewart, J., Skarlatoudis, A., Seyhan, E., Margaris, B., Theodoulidis, N., Scordilis, E., Kalogeras, I., Klimis, N., & Melis, N. (2021). A Ground-Motion Prediction Model for Shallow Crustal Earthquakes in Greece. *Bulletin of the Seismological Society of America*, *111*. https://doi.org/10.1785/0120200270

Borcherdt, R. (1994). Estimates of Site-Dependent Response Spectra for Design (Methodology and Justification). *Earthquake Spectra - EARTHQ SPECTRA*, *10*. https://doi.org/10.1193/1.1585791

Caprio, M., Tarigan, B., Worden, C., Wiemer, S., & Wald, D. (2015). Ground Motion to Intensity Conversion Equations (GMICEs): A Global Relationship and Evaluation of Regional Dependency. *Bulletin of the Seismological Society of America*, *105*. https://doi.org/10.1785/0120140286

CEN. (2004). *Eurocode 8: Design Provisions for Earthquake Resistance of Structures, Part 1.1: General Rules, Seismic Actions and Rules for Buildings, EN1998-1* [Preprint].

Chiou, B. S.-J., & Youngs, R. R. (2008). *Chiou and Youngs PEER-NGA empirical ground motion model for the average horizontal component of peak acceleration, peak velocity, and pseudo-spectral acceleration for spectral periods of 0.01 to 10 seconds* (Final Report) (Submitted to PEER). Pacific Earthquake Engineering Research Center (PEER).

Chousianitis, K., Sboras, S., Mouslopoulou, V., Chouliaras, G., & Hristopulos, D. (2024). The Upper Crustal Deformation Field of Greece Inferred From GPS Data and Its Correlation With Earthquake Occurrence. *Journal of Geophysical Research: Solid Earth*, *129*. https://doi.org/10.1029/2023JB028004

Cito, P., Vitale, A., & Iervolino, I. (2024). Territorial exceedance of probabilistic seismic hazard from ShakeMap data. *Scientific Reports*, *14*, 4840. https://doi.org/https://doi.org/10.1038/s41598-024-55415-9

Danciu, L., Nandan, S., Reyes, C., Basili, R., Weatherill, G., Beauval, C., Rovida, A., Vilanova, S., Sesetyan, K., Bard, P.-Y., Cotton, F., Wiemer, S., & Giardini, D. (2021). The 2020 update of the European Seismic Hazard Model: Model Overview. (001). https://doi.org/10.12686/a15

Earthquake Planning and Protection Organization. (2003). *Greek seismic code*.

Engineering Strong Motion Database. (2024a). Event Search [Accessed: 2024-07-07]. https://esm-db.eu/#/event/search

Engineering Strong Motion Database. (2024b). MasterStationList [Accessed: 2024-07-07]. https://esm-db.eu//esmws/shakemap/1/masterstationlist.txt

Ganas, A., Oikonomou, I. A., & Tsimi, C. (2013). Noafaults: A digital database for active faults in Greece. *Bulletin of the Geological Society of Greece*, *47*(2), 518–530. https://doi.org/10.12681/bgsg.11079

Gardner, J., & Knopoff, L. (1974). Is the sequence of earthquakes in southern California, with aftershocks removed, Poissonian? *Bulletin of the Seismological Society of America*, *64*(465), 1363–1367.

Giardini, D., Grünthal, G., Shedlock, K. M., & Zhang, P. (1999). The GSHAP Global Seismic Hazard Map. *Annali di Geofisica*, *42*(6), 1225–1228.

Giardini, D., Wössner, J., & Danciu, L. (2014). Mapping Europe's Seismic Hazard. *Eos, Transactions American Geophysical Union*, *95*(29), 261–262. https://doi.org/https://doi.org/10.1002/2014EO290001

Graizer, V., & Kalkan, E. (2016). Summary of the GK15 Ground-Motion Prediction Equation for Horizontal PGA and 5% Damped PSA from Shallow Crustal Continental Earthquakes. *Bulletin of the Seismological Society of America*, *106*(2), 687–707. https://doi.org/10.1785/0120150194

Grünthal, G., Bosse, C., Sellami, S., D, M.-R., & D, G. (1999). Compilation of the GSHAP regional seismic hazard for Europe, Africa and the Middle East. *Annals of Geophysics*, *42*. https://doi.org/10.4401/ag-3782

International Federation of Digital Seismograph Networks. (2024). FDSN Networks [Accessed: 2024-07-07]. https://www.fdsn.org/networks/

Jordahl, K., den Bossche, J. V., Fleischmann, M., Wasserman, J., McBride, J., Gerard, J., Tratner, J., Perry, M., Badaracco, A. G., Farmer, C., Hjelle, G. A., Snow, A. D., Cochran, M., Gillies, S., Culbertson, L., Bartos, M., Eubank, N., maxalbert, Bilogur, A., . . . Leblanc, F. (2020). *geopandas/geopandas: v0.8.1* (Version v0.8.1). Zenodo. https://doi.org/10.5281/zenodo.3946761

Kaklamanos, J., Baise, L., & Boore, D. (2011). Estimating Unknown Input Parameters when Implementing the NGA Ground-Motion Prediction Equations in Engineering Practice. *Earthquake Spectra*, *27*, 1219–1235. https://doi.org/10.1193/1.3650372

Karakaisis, G., Papazachos, C., & Scordilis, E. (2010). Seismic sources and main seismic faults in the Aegean and surrounding area. *Bulletin of the Geological Society of Greece*, *43*, 2026–2042. https://doi.org/10.12681/bgsg.11393

Kassaras, I., Kapetanidis, V., Ganas, A., Tzanis, A., Kosma, C., Karakonstantis, A., Valkaniotis, S., Chailas, S., Kouskouna, V., & Papadimitriou, P. (2020). The New Seismotectonic Atlas of Greece (v1.0) and Its Implementation. *Geosciences*, *10*(11). https://doi.org/10.3390/geosciences10110447

Kaviris, G., Zymvragakis, A., Bonatis, P., Sakkas, G., Kouskouna, V., & Voulgaris, N. (2022). Probabilistic Seismic Hazard Assessment for the Broader Messinia (SW Greece) Region. *Pure and Applied Geophysics*, *179*. https://doi.org/10.1007/s00024-022-02950-z

Kiratzi, A., & Louvari, E. (2003). Focal mechanisms of shallow earthquakes in the Aegean Sea and the surrounding lands determined by waveform modelling: A new database. *Journal of Geodynamics*, *36*, 251–274. https://doi.org/10.1016/S0264-3707(03)00050-4

Kotha, S. R., Weatherill, G., Bindi, D., & Cotton, F. (2020). A regionally-adaptable ground-motion model for shallow crustal earthquakes in Europe. *Bulletin of Earthquake Engineering*, *18*(9), 4091–4125. https://doi.org/10.1007/s10518-020-00869-1

Lanzano, G., Luzi, L., Russo, E., Felicetta, C., D'Amico, M. C., Sgobba, S., & Pacor, F. (2018). Engineering Strong Motion Database (ESM) flatfile. https://doi.org/10.13127/esm/flatfile.1.0

Manea, E. F., Danciu, L., Cioflan, C. O., Toma-Danila, D., & Gerstenberger, M. (2024). Testing the 2020 European Seismic Hazard Model (ESHM20) against observations from Romania. *Natural Hazards and Earth System Sciences Discussions*, *2024*, 1–18. https://doi.org/10.5194/nhess-2023-232

McCue, K. (1999). Seismic hazard mapping in Australia, the Southwest Pacific and Southeast Asia. *Annali di Geofisica*, *42*. https://doi.org/10.4401/ag-3776

Mignan, A., & Chouliaras, G. (2014). Fifty Years of Seismic Network Performance in Greece (1964–2013): Spatiotemporal Evolution of the Completeness Magnitude. *Seismological Research Letters*, *85*, 657–667. https://doi.org/10.1785/0220130209

Musson, R., Grünthal, G., & Stucchi, M. (2009). The comparison of macroseismic intensity scales. *Journal of Seismology*, *14*, 413–428. https://doi.org/10.1007/s10950-009-9172-0

National Observatory of Athens. (2024). ShakeMaps [Accessed: 2024-07-07]. https://accelnet.gein.noa.gr/shakemaps/

Papazachos, C., Papaioannou, C., Papastamatiou, D., Margaris, B., & Theodoulidis, N. (1990). On the reliability of different methods of seismic hazard assessment in Greece. *Natural Hazards*, *3*, 141–151. https://doi.org/10.1007/BF00140428

Pitilakis, K., Riga, E., & Roumelioti, Z. (2016). The urgent need for an improvement of the Greek seismic code based on a new seismic hazard map for Europe and a new site classification system.

Pothon, A., Gueguen, P., Buisine, S., & Bard, P.-Y. (2020). Comparing Probabilistic Seismic Hazard Maps with ShakeMap Footprints for Indonesia. *Seismological Research Letters*, *91*. https://doi.org/10.1785/0220190171

Rey, J., Beauval, C., & Douglas, J. (2018). Do French macroseismic intensity observations agree with expectations from the European Seismic Hazard Model 2013? *Journal of Seismology*, *22*. https://doi.org/10.1007/s10950-017-9724-7

Rovida, A., & Antonucci, A. (2021). EPICA - European PreInstrumental Earthquake CAtalogue, version 1.1 [Dataset]. *Istituto Nazionale di Geofisica e Vulcanologia (INGV)*. https://doi.org/10.13127/epica.1.1

Rovida, A., Antonucci, A., & Locati, M. (2022). The European Preinstrumental Earthquake Catalogue EPICA, the 1000–1899 catalogue for the European Seismic Hazard Model 2020. *Earth System Science Data*. https://doi.org/10.5194/essd-14-5213-2022

Sakellariou, N., Kouskouna, V., & Makropoulos, K. C. (2010). *Macroseismic Intensities in Central-Southern Peloponnese during the 19th century* (Internal Report) (Macroseismic Data Points available in the Hellenic Macroseismic Database of the University of Athens). N&K University of Athens, Greece.

Shedlock, K., & Tanner, J. (1999). Seismic hazard map of the western hemisphere. *Annals of Geophysics*, *42*. https://doi.org/10.4401/ag-3779

Slejko, D., Rebez, A., Santulin, M., Garcia-Pelaez, J., Sandron, D., Tamaro, A., Civile, D., Volpi, V., Caputo, R., Ceramicola, S., Chatzipetros, A., Daja, S., Fabris, P., Geletti, R., Karvelis, P., Moratto, L., Papazachos, C., Pavlides, S., Rapti, D., . . . Zuliani, D. (2021). Seismic hazard for the Trans Adriatic Pipeline (TAP). Part 1: Probabilistic seismic hazard analysis along the pipeline. *Bulletin of Earthquake Engineering*, *19*(9), 3349–3388. https://doi.org/10.1007/s10518-021-01111-2

Slejko, D., Santulin, M., Garcia Pelaez, J., Papoulia, J., Daskalaki, E., Fasulaka, C., Fokaefs, A., Ilinski, D., Mascle, J., Makris, J., Nicolich, R., Papadopoulos, G., Tsampas, A., & Wardell, N. (2010). Preliminary seismic hazard assessments for the area of Pylos and surrounding region (SW Peloponnese). *Bollettino di Geofisica Teorica ed Applicata*, *51*, 163–186.

Sotiriadis, D., & Margaris, B. (2023). Evaluation of the predictive performance of regional and global ground motion predictive equations against Greek strong motion data. *Soil Dynamics and Earthquake Engineering*, *165*, 107656. https://doi.org/10.1016/j.soildyn.2022.107656

Sotiriadis, D., Margaris, B., Klimis, N., & Dokas, I. M. (2023). Seismic Hazard in Greece: A Comparative Study for the Region of East Macedonia and Thrace. *GeoHazards*, *4*(3), 239–266. https://doi.org/10.3390/geohazards4030014

Stirling, M., & Gerstenberger, M. (2010). Ground motion–based testing of seismic hazard models in New Zealand. *Bulletin of the Seismological Society of America*, *100*, 1407–1414.

Stylianou, E., G., M., Kouskouna, V., & Papoulia, J. (2016). Seismic Hazard Assessment in the North Aegean Trough based on a New Seismogenic Zonation. *Bulletin of the Geological Society of Greece*, *Volume L*. https://doi.org/10.12681/bgsg.38198

Tasan, H., Beauval, C., Helmstetter, A., Sandikkaya, A., & Guéguen, P. (2014). Testing probabilistic seismic hazard estimates against accelerometric data in two countries: France and Turkey. *Geophysical Journal International*, *198*(3), 1554–1571. https://doi.org/10.1093/gji/ggu191

Tsapanos, T., Mäntyniemi, P., & Kijko, A. (2009). A probabilistic seismic hazard assessment for Greece and the surrounding region including site-specific considerations. *Annals of Geophysics*, *47*. https://doi.org/10.4401/ag-3367

Tselentis, A., & Danciu, L. (2010). Probabilistic seismic hazard assessment in Greece – Part 1: Engineering ground motion parameters. *Natural Hazards and Earth System Sciences*, *10*. https://doi.org/10.5194/nhess-10-25-2010

Tselentis, A., & Danciu, L. (2008). Empirical Relationships between Modified Mercalli Intensity and Engineering Ground-Motion Parameters in Greece. *Bulletin of The Seismological Society of America - BULL SEISMOL SOC AMER*, *98*, 1863–1875. https://doi.org/10.1785/0120070172

U.S. Geological Survey. (2024a). Comprehensive Earthquake Catalog (ComCat) [Accessed: 2024-07-07]. https://earthquake.usgs.gov/data/comcat/

U.S. Geological Survey. (2024b). ShakeMap Data [Accessed: 2024-07-07]. https://earthquake.usgs.gov/data/shakemap/

U.S. Geological Survey. (2024c). VS30 Database [Accessed: 2024-07-07]. https://earthquake.usgs.gov/data/vs30/

Vamvakaris, D., Papazachos, C., Papaioannou, C., Scordilis, E., & Karakaisis, G. (2017). SEISMIC HAZARD ASSESSMENT IN THE BROADER AEGEAN AREA USING TIME-INDEPENDENT SEISMICITY MODELS BASED ON SYNTHETIC EARTHQUAKE CATALOGS. *Bulletin of the Geological Society of Greece*, *50*, 1463. https://doi.org/10.12681/bgsg.11859

Vavlas, N., Kiratzi, A., Margaris, B., & Karakaisis, G. (2019). Probabilistic Seismic Hazard Assessment (PSHA) for Lesvos Island Using the Logic Tree Approach. *Bulletin of the Geological Society of Greece*, *55*(1), 109–136. https://doi.org/10.12681/bgsg.20705

Woessner, J., Danciu, L., Giardini, D., Crowley, H., Cotton, F., Grünthal, G., Valensise, G., Arvidsson, R., Basili, R., Demircioglu, M. B., Hiemer, S., Meletti, C., Musson, R. W., Rovida, A. N., Sesetyan, K., Stucchi, M., & Consortium, T. S. (2015). The 2013 European Seismic Hazard Model: Key components and results. *Bulletin of Earthquake Engineering*, *13*(12), 3553–3596. https://doi.org/10.1007/s10518-015-9795-1

Worden, C., Thompson, E., Hearne, M., & Wald, D. (2020). ShakeMap Manual Online: Technical Manual, User's Guide, and Software Guide. https://doi.org/10.5066/F7D21VPQ

Worden, C., Gerstenberger, M., Rhoades, D., & Wald, D. (2012). Probabilistic Relationships between Ground-Motion Parameters and Modified Mercalli Intensity in California. *The Bulletin of the Seismological Society of America*, *102*, 204–221. https://doi.org/10.1785/0120110156

Zhang, P., Yang, Z.-X., Gupta, H., Bhatia, S., & Shedlock, K. (1999). Global Seismic Hazard Assessment Program (GSHAP) in continental Asia. *Annali di Geofisica*, *42*, 1167–1190. https://doi.org/10.4401/ag-3778

APPENDIX

A.1 Figures

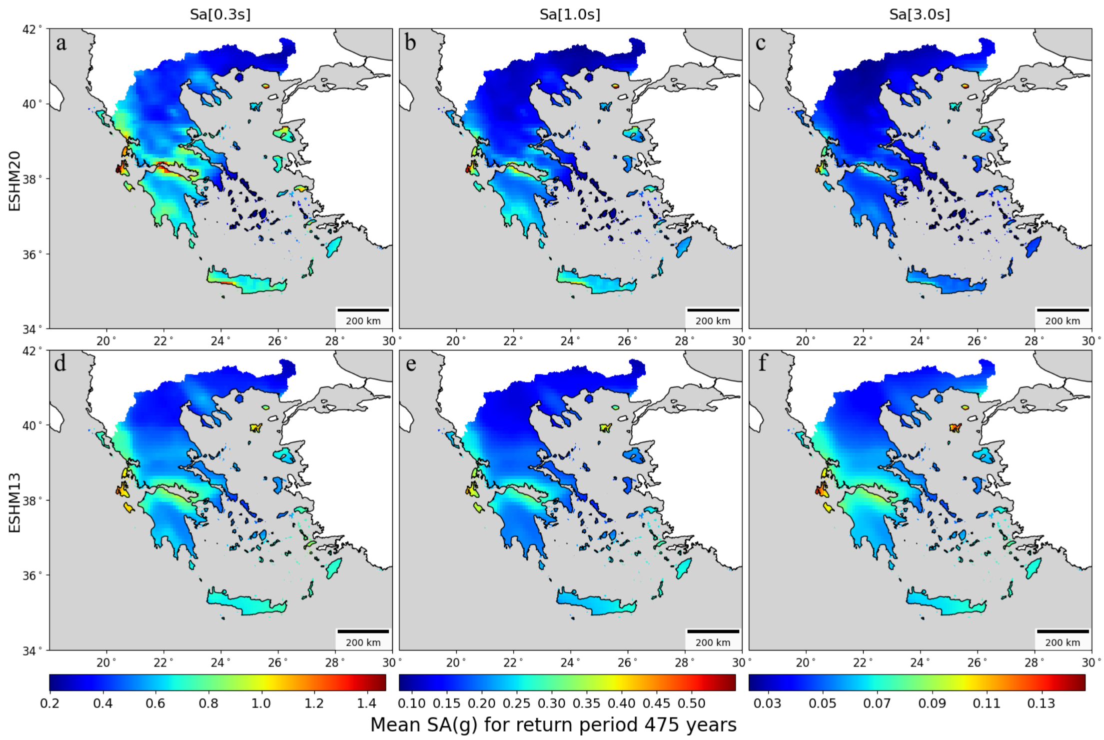

Figure A-1. (a,b,c) the ESHM20 and (d,e,f) ESHM13 seismic hazard maps for SA. The maps show the mean SA for the return period of 475 years. (a,d) Sa(0.3s), (b,e) Sa(1.0s), and (c,f) Sa(3.0s).

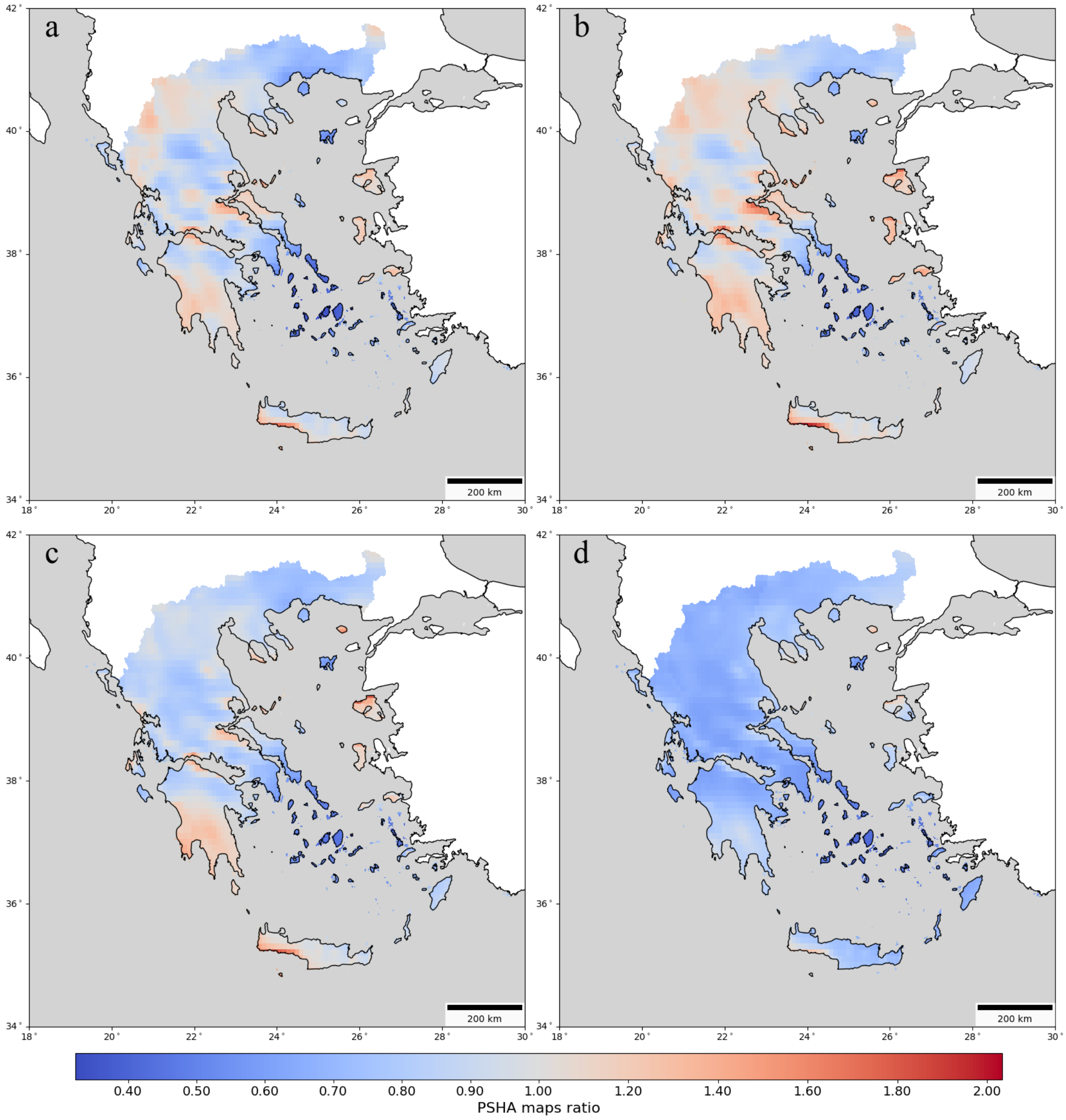

Figure A-2. The ratio of the ESHM13 (a) PGA, (b) Sa(0.3s), (c)Sa(1.0s), and (d) Sa(3.0s) to ESHM20. Values over 1.0 show the sites at which the ESHM13 maps underestimate the hazard predicted by ESHM20.

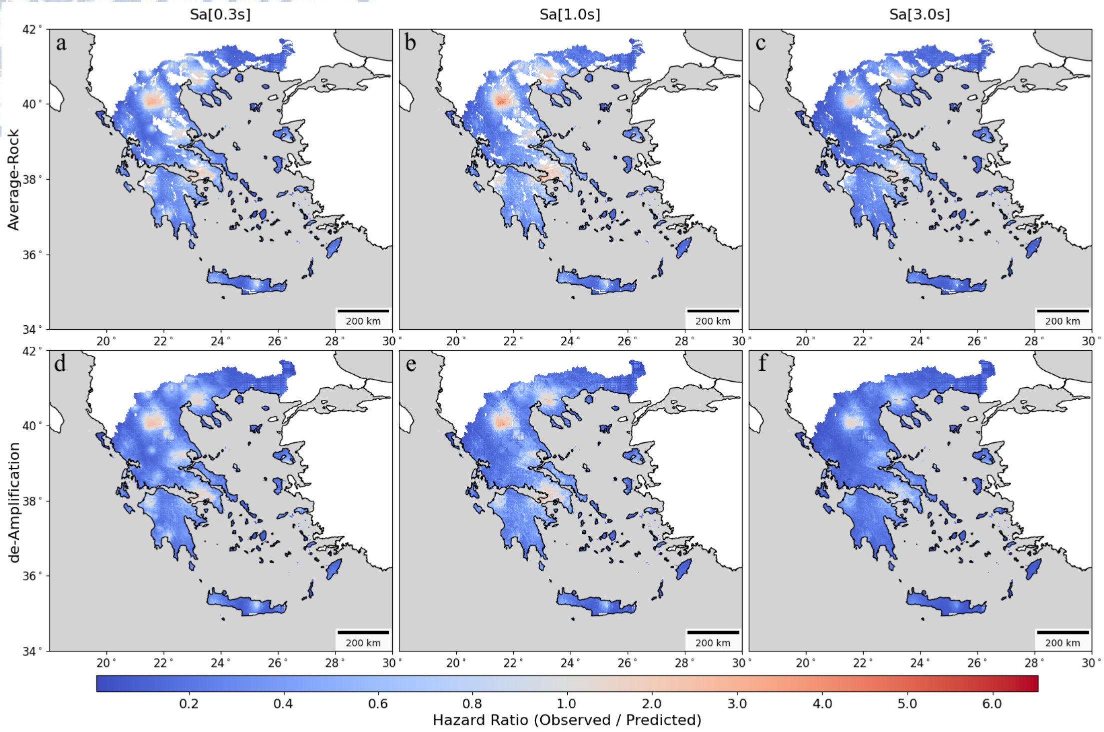

Figure A-3. Hazard Ratio of the 1973-2023 ShakeMap footprints SA to the estimated SA for 10% probability of exceedance in 50 years. Ratio maps are plotted for the ESHM13. (a,d) Sa(0.3s), (b,e) Sa(1.0s), (c,f) Sa(3.0s). (a,b,c) illustrate the results of average-rock method, and (d,e,f) illustrate the results of de-amplification method. Values greater than 1.00 show where the ShakeMap footprints SA exceeds the PSHA thresholds.

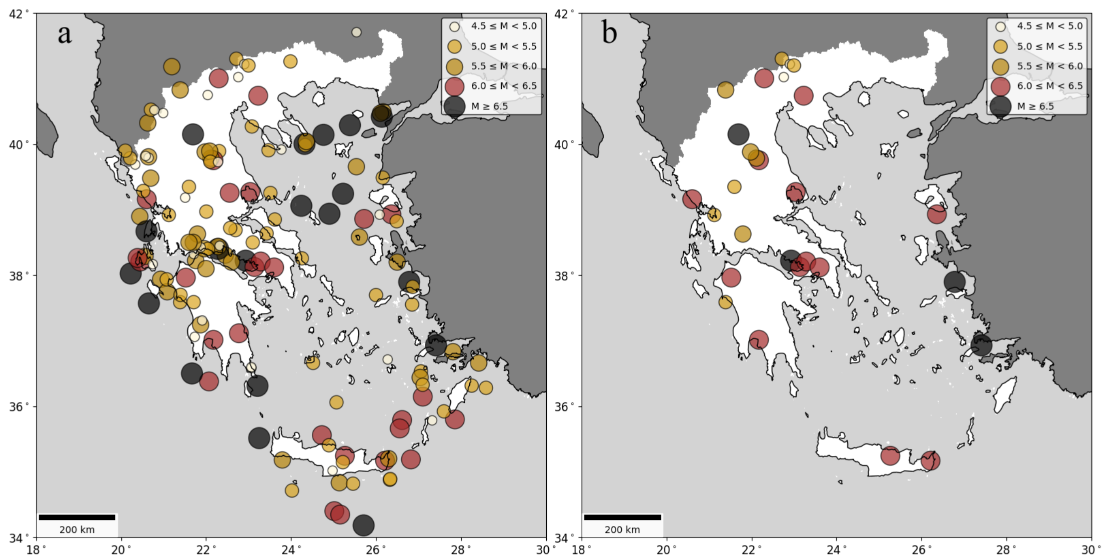

Figure A-4. (a) Location and magnitude of all earthquake events for Greece and the 100-kilometer surrounding area processed by ShakeMap from 1973 to 2023, and they have produced the maximum historical Sa(0.3s). (b) Location and magnitude of earthquake events that have produced a Sa(0.3s) greater than PSHA maps thresholds for both approaches (average-rock or de-amplification).

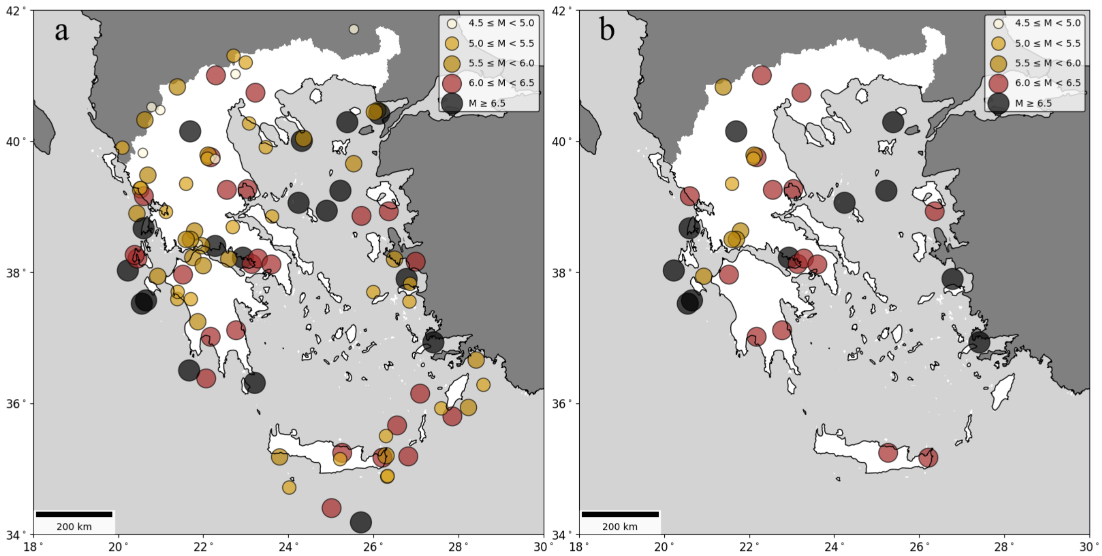

Figure A-5. (a) Location and magnitude of all earthquake events for Greece and the 100-kilometer surrounding area processed by ShakeMap from 1973 to 2023, and they have produced the maximum historical Sa(1.0s). (b) Location and magnitude of earthquake events that have produced a Sa(1.0s) greater than PSHA maps thresholds for both approaches (average-rock or de-amplification).

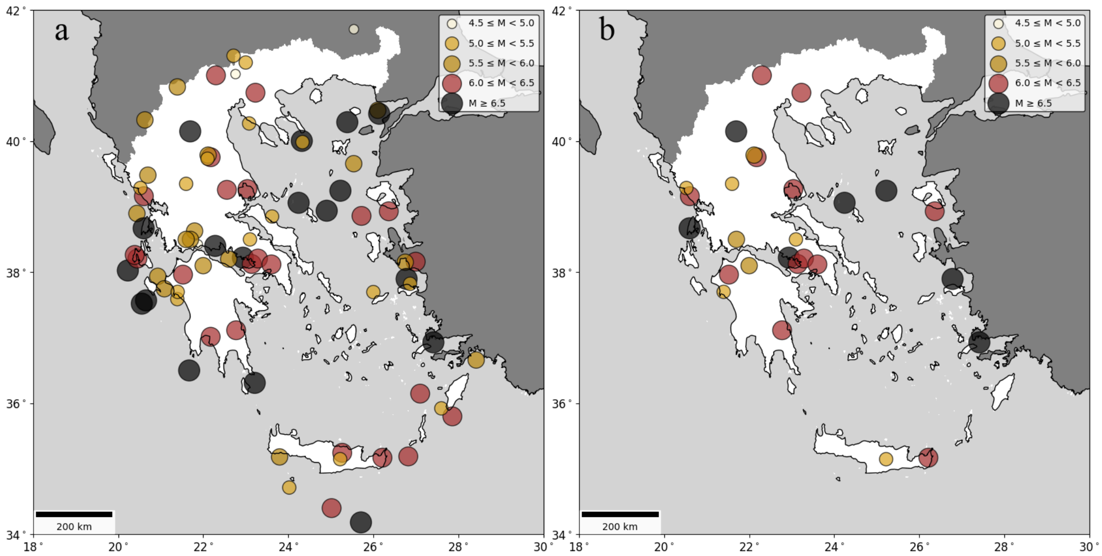

Figure A-6. (a) Location and magnitude of all earthquake events for Greece and the 100-kilometer surrounding area processed by ShakeMap from 1973 to 2023, and they have produced the maximum historical Sa(3.0s). (b) Location and magnitude of earthquake events that have produced a Sa(3.0s) greater than PSHA maps thresholds for both approaches (average-rock or de-amplification).

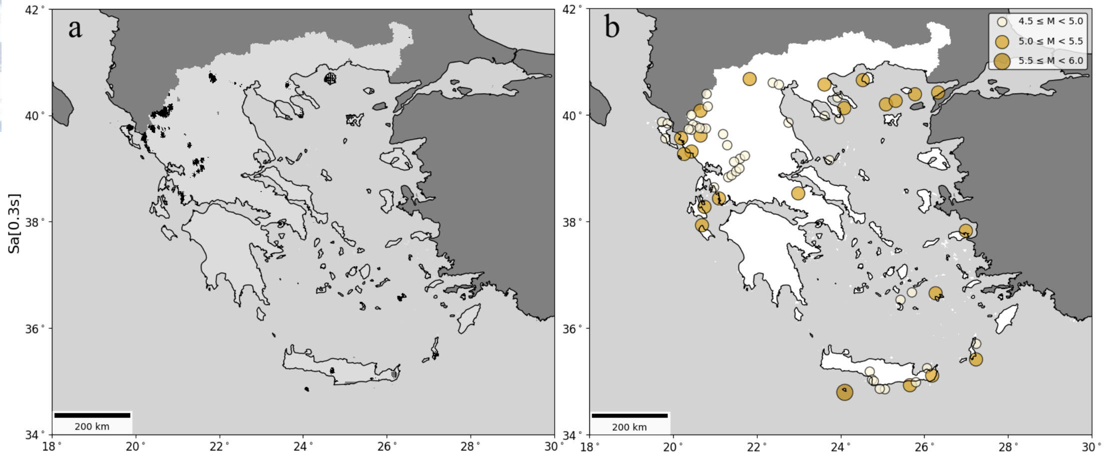

Figure A-7. (a) The total area is illustrated with grey color. The areas with Sa(0.3s) estimated by Boore et al. (2021) GMPE higher than the maximum historical Sa(0.3s) from ShakeMap footprints are illustrated with black color (affected sites). (b) The location and magnitude of earthquake events, which are not modeled by a ShakeMap footprint, producing the Sa(0.3s) estimated by Boore et al. (2021) GMPE higher than the maximum historical Sa(0.3s).

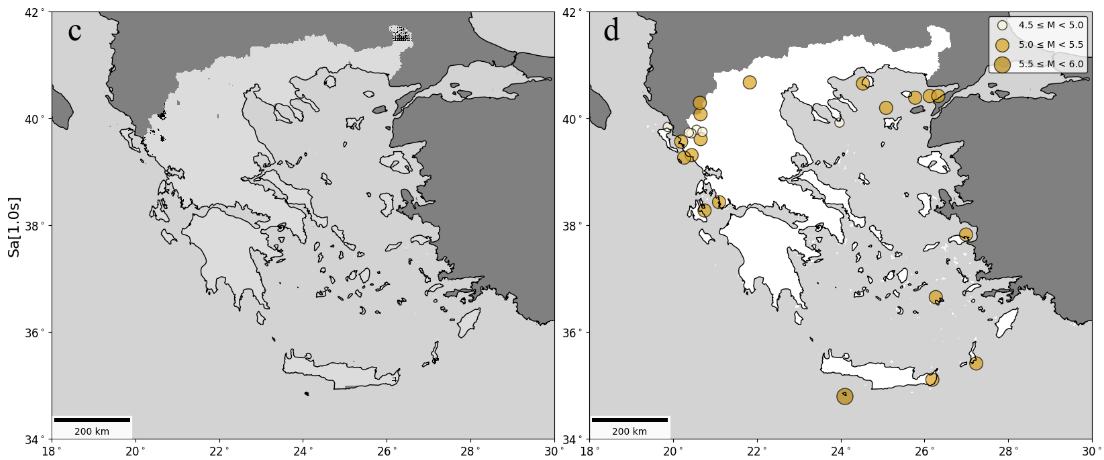

Figure A-8. (a) The total area is illustrated with grey color. The areas with Sa(1.0s) estimated by Boore et al. (2021) GMPE higher than the maximum historical Sa(1.0s) from ShakeMap footprints are illustrated with black color (affected sites). (b) The location and magnitude of earthquake events, which are not modeled by a ShakeMap footprint, producing the Sa(1.0s) estimated by Boore et al. (2021) GMPE higher than the maximum historical Sa(1.0s).

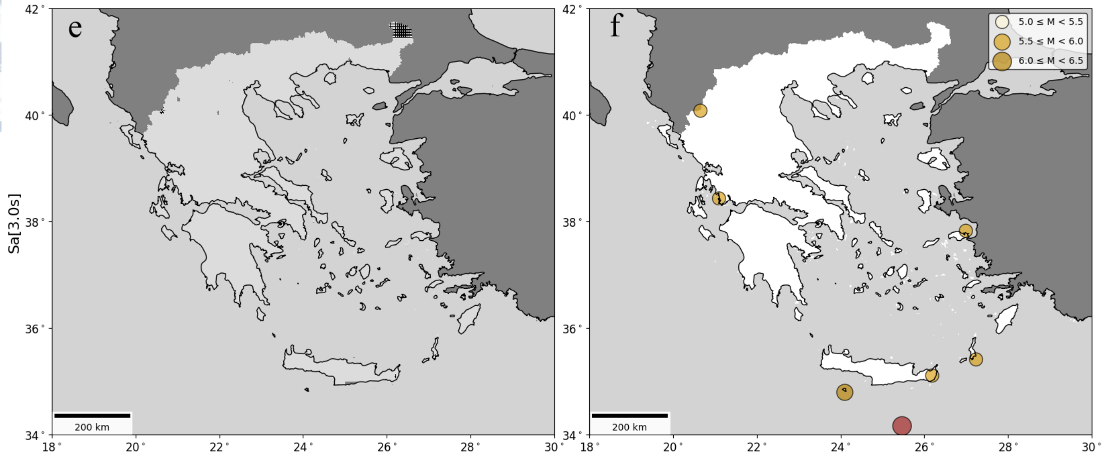

Figure A-9. (a) The total area is illustrated with grey color. The areas with Sa(3.0s) estimated by Boore et al. (2021) GMPE higher than the maximum historical Sa(3.0s) from ShakeMap footprints are illustrated with black color (affected sites). (b) The location and magnitude of earthquake events, which are not modeled by a ShakeMap footprint, producing the Sa(3.0s) estimated by Boore et al. (2021) GMPE higher than the maximum historical Sa(3.0s).

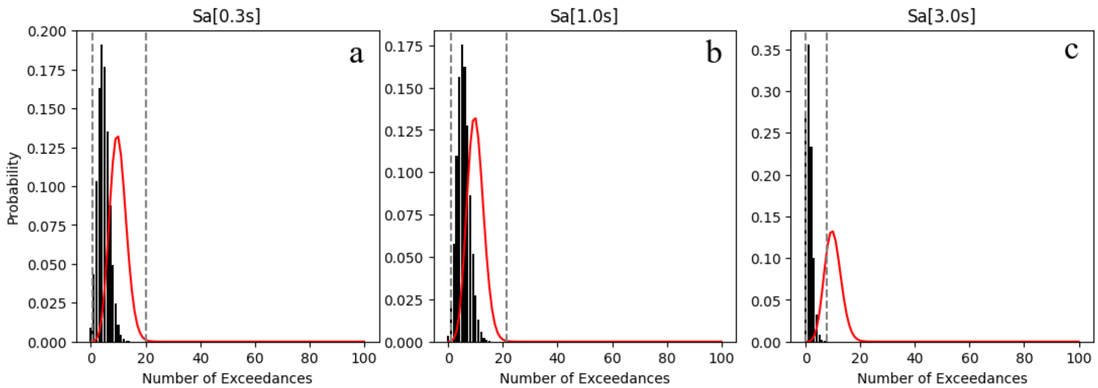

Figure A-10. Binomial distribution of empirical exceedance area for spectral acceleration (black bars) and theoretical exceedance area for the ESHM13 (red line). The affection of ShakeMap uncertainty is given for ± one standard deviation (grey dashed line). (a) Sa(0.3s), (b) Sa(1.0s), and (c) Sa(3.0s).

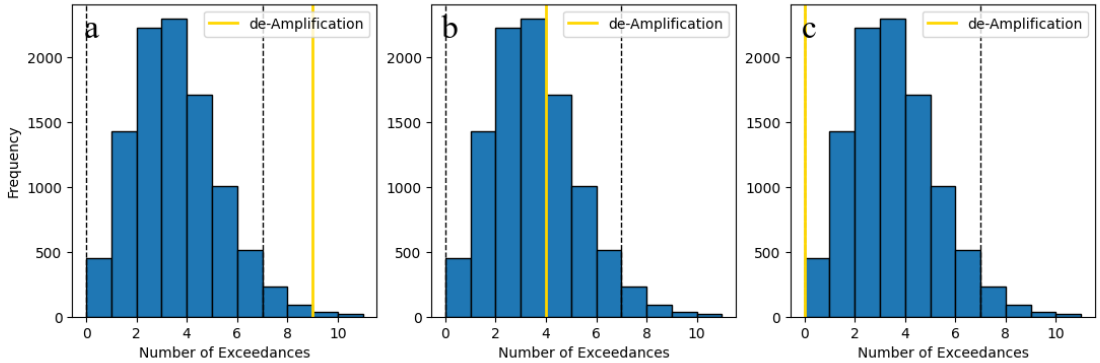

Figure A-11. The distribution of expected exceeded sites, according to stations life time and the PSHA maps annual rate of exceedance (blue bars). Lower and upper bound, which correspond to 2.5 and 97.5 percentile are plotted as black dashed lines. The number of exceeded sites, due to strong-motion records for SA from 1977 to 2023 are plotted as yellow lines (de-amplification approach) according to the ESHM13. (a) Sa(0.3s), Sa(1.0s), and Sa(3.0s)

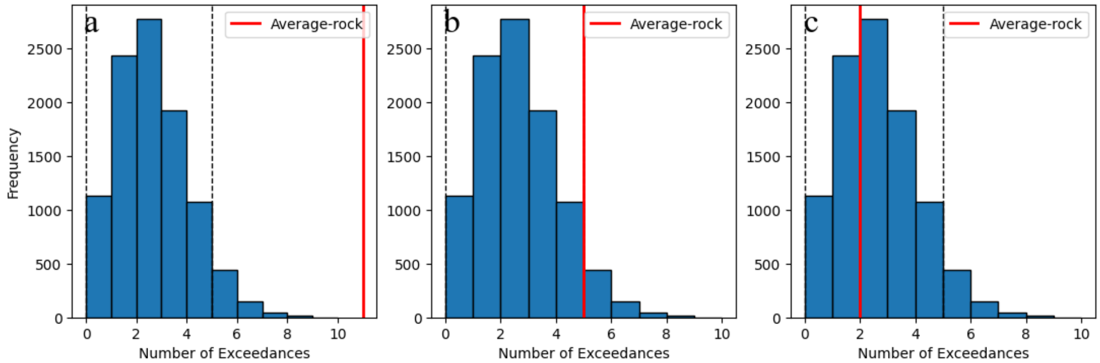

Figure A-12. The distribution of expected exceeded sites, according to stations life time and the PSHA maps annual rate of exceedance (blue bars). Lower and upper bound, which correspond to 2.5 and 97.5 percentile are plotted as black dashed lines. The number of exceeded sites, due to strong-motion records for SA from 1977 to 2023 are plotted as red lines (average-rock approach) according to the ESHM13. (a) Sa(0.3s), Sa(1.0s), and Sa(3.0s)

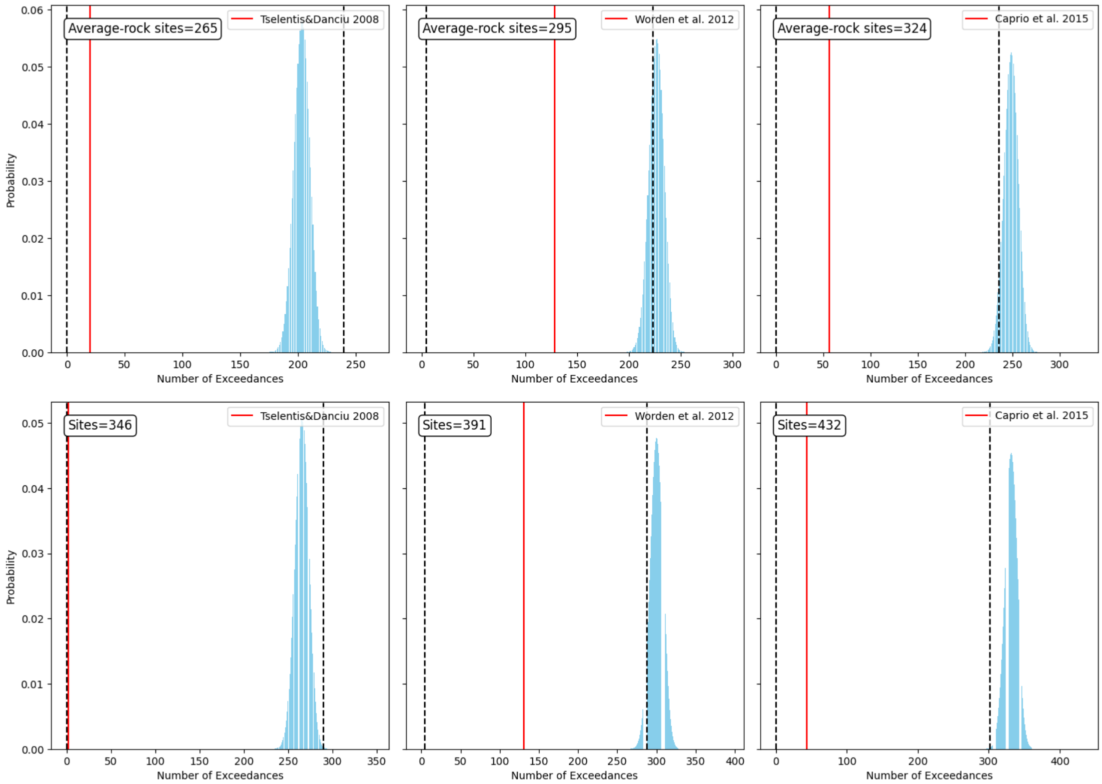

Figure A-13. The 76.75% probability distribution for a PSHA map with return period 475 years and observation period 693 years (blue bars). With red lines the number of exceeded sites, due to the strong-shaking produced by the 48 considered historical earthquakes from 1204 to 1897, according to the ESHM13 for the three different GMICEs and the two different approaches. (top) average-rock approach, (bottom) de-amplification approach. Effect of GMICEs uncertainty on estimated of exceedance sites is also given (black dashed line).

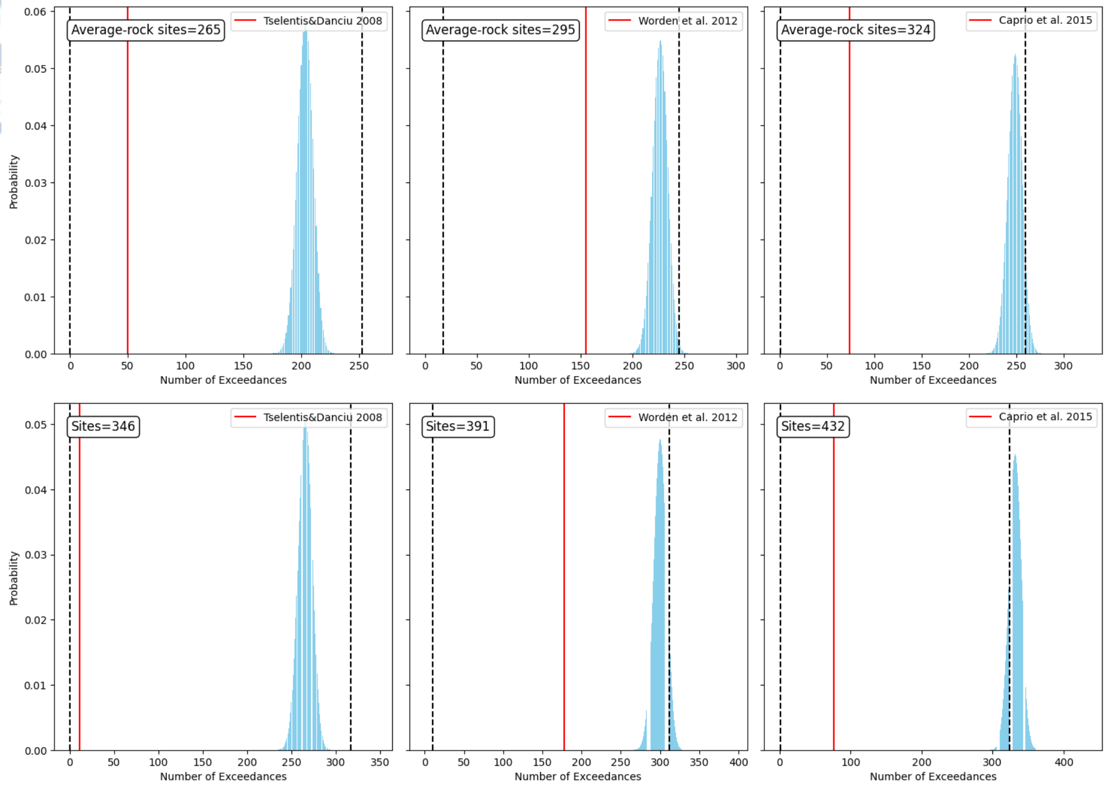

Figure A-14. The 76.75% probability distribution for a PSHA map with return period 475 years and observation period 693 years (blue bars). With red lines the number of exceeded sites, due to the strong-shaking produced by the 48 considered historical earthquakes from 1204 to 1897, according to the GSHAP for the three different GMICEs and the two different approaches. (top) average-rock approach, (bottom) de-amplification approach. Effect of GMICEs uncertainty on estimated of exceedance sites is also given (black dashed line).

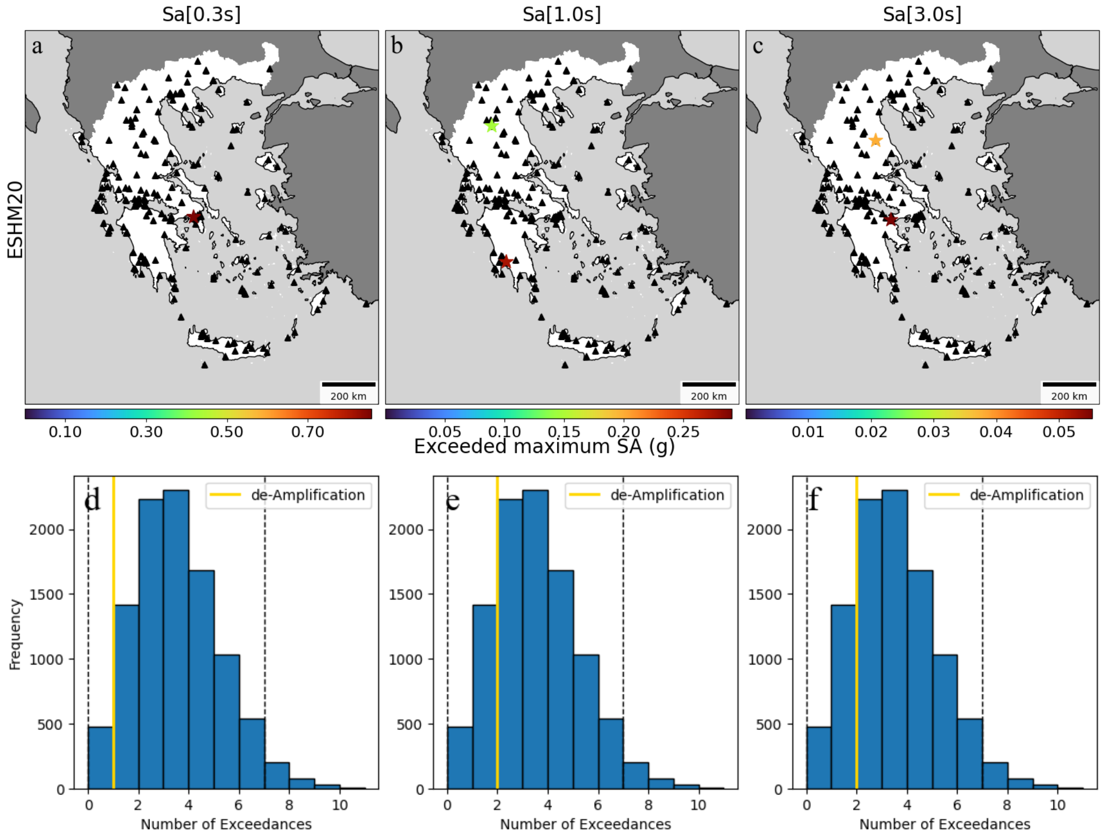

Figure A-15. Stations (sites) with a maximum RotD50 SA for the period 1977-2023 that exceeds (a,b,c) ESHM20 map thresholds (stars) applying the de-amplification approach. The whole set of station used in this study are presented as black triangles. The color scale refers to SA levels. The distribution of expected exceeded sites, according to stations lifetimes and the PSHA maps annual probability of exceedance (blue bars). Lower and upper bounds, which correspond to 2.5 and 97.5 percentiles are plotted as black dashed lines. The number of observed exceeded sites due to strong-motion records for RotD50 SA from 1977 to 2023 are plotted as yellow lines (de-amplification approach) according to the ESHM20.

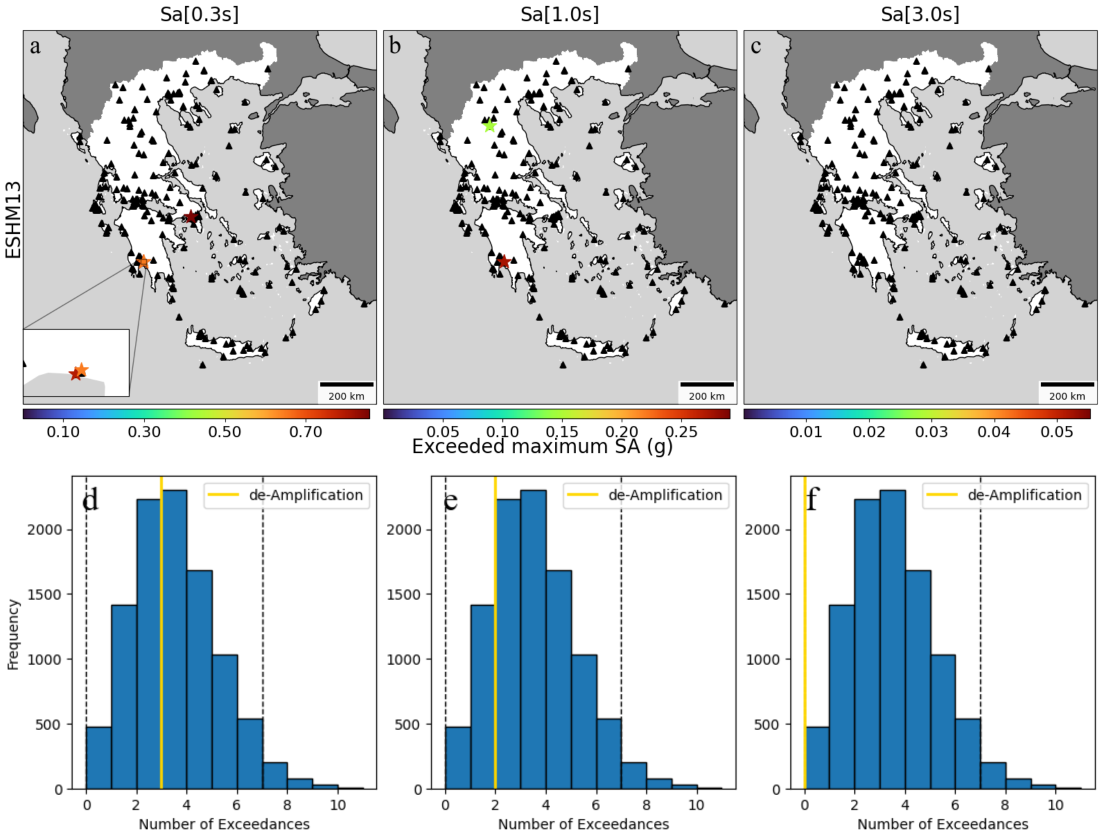

Figure A-16. Stations (sites) with a maximum RotD50 SA for the period 1977-2023 that exceeds (a,b,c) ESHM13 map thresholds (stars) applying the de-amplification approach. The whole set of station used in this study are presented as black triangles. The color scale refers to SA levels. The distribution of expected exceeded sites, according to stations lifetimes and the PSHA maps annual probability of exceedance (blue bars). Lower and upper bounds, which correspond to 2.5 and 97.5 percentiles are plotted as black dashed lines. The number of observed exceeded sites due to strong-motion records for RotD50 SA from 1977 to 2023 are plotted as yellow lines (de-amplification approach) according to the ESHM13.

A.2 Tables

Table A-1. The coordinate windows of the spatial rectangles that were used for each specific area in mainland of Greece.

Regions	Athens	Thessaloniki	Patras	Heraklion	Kozani
max Latitude	38.20	40.75	38.35	35.38	40.50
min Latitude	37.70	40.48	38.15	35.29	40.00
max Longitude	24.10	23.05	21.80	25.20	22.02
min Longitude	23.04	22.75	21.65	25.08	21.47

A.3 Supplement

The Supplement of this study can be found here.